Anatomie postcrânienne de colobinés (Mammalia, Primates) des dépôts plio-pleistocènes du Groupe de l'Omo (Formation de Shungura et d'Usno, campagnes 1967-2018, basse vallée de l'Omo, Éthiopie).

Postcranial anatomy of colobines (Mammalia, Primates) from the Plio-Pleistocene Omo Group deposits (Shungura Formation and Usno Formation, 1967-2018 field campaigns, Lower Omo Valley, Ethiopia)

Colobine postcranials from the Plio-Pleistocene Omo Group

Laurent PALLAS
Laboratoire Paléontologie Évolution Paléoécosystèmes Paléoprimatologie, UMR 7262 PALEVOPRIM, CNRS & Université de Poitiers, 6 rue Michel Brunet, 86073 Poitiers (France)
and
Laboratory of Physical Anthropology, Kyoto University (Japan)
laurent.pallas01@univ-poitiers.fr (corresponding author)

Guillaume DAVER
Laboratoire Paléontologie Évolution Paléoécosystèmes Paléoprimatologie, UMR 7262 PALEVOPRIM, CNRS & Université de Poitiers, 6 rue Michel Brunet, 86073 Poitiers (France)
guillaume.daver@univ-poitiers.fr

Gildas MERCERON
Laboratoire Paléontologie Évolution Paléoécosystèmes Paléoprimatologie, UMR 7262 PALEVOPRIM, CNRS & Université de Poitiers, 6 rue Michel Brunet, 86073 Poitiers (France)
gildas.merceron@univ-poitiers.fr

Jean-Renaud BOISSERIE
Laboratoire Paléontologie Évolution Paléoécosystèmes Paléoprimatologie, UMR 7262 PALEVOPRIM, CNRS & Université de Poitiers, 6 rue Michel Brunet, 86073 Poitiers (France)
and
Centre Français des Études Éthiopiennes, UAR 3132 CFEE, CNRS & Ministère de l'Europe et des affaires étrangères, Addis Ababa, PO BOX 5554 (Ethiopia)
jean.renaud.boisserie@univ-poitiers.fr

RÉSUMÉ

Nos connaissances sur la diversité taxonomique et fonctionnelle de la faune de colobinés fossiles (Colobinae Jerdon, 1867) de la basse vallée de l'Omo sont établies uniquement sur la base de restes crâniodentaires. Nous décrivons ici des spécimens postcrâniens de colobinés fossiles et nous établissons un aperçu approfondi de leur anatomie fonctionnelle et de leur taxonomie. Des comparaisons quantitatives et qualitatives avec des spécimens de colobinés fossiles d'Afrique orientale précédemment décrits nous ont permis d'identifier des morphologies postcraniennes similaires à celles des espèces de grande taille *Paracolobus mutiwa* Leakey, 1982 et *Rhinocolobus turkanaensis* Leakey, 1982 et à une espèce plus petite du genre *Colobus* Illiger, 1811. Nos résultats fonctionnels mettent en évidence chez *Paracolobus mutiwa* une exploitation possible des substrats terrestres et arboricoles et des aptitudes jusque là insoupconnées au grimper au niveau de son membre antérieur. En ce qui concerne *Rhinocolobus, ce travail* confirme grâce à un échantillon de comparison étendu l'anatomie particulière du coude de ce taxon et ses préférences locomotrices pour des substrats arboricoles. Ce travail rapporte également des spécimens de fémur, humérus et tibia présentant des traits arboricoles et similaires en taille et morphologie au genre *Colobus* dans le Membre L de la Formation de Shungura. En apportant de nouvelles données sur la paléocommunauté de colobinés de Shungura, nos résultats contribuent à une meilleure compréhension du contexte biotique qui entoure l'évolution des faunes de mammifères plio-pléistocènes de la Dépression du Turkana et ouvre la voie pour de futures analyses écomorphologiques.

Mots-clés : *Rhinocolobus*, *Paracolobus*, *Colobus*, Turkana, Écomorphologie

ABSTRACT

Our knowledge of the functional and taxonomic diversity of the fossil colobine fauna (Colobinae Jerdon, 1867) from the Lower Omo Valley is based only on craniodental remains. Here we describe postcranial specimens of fossil colobines from the Usno Formation and Shungura Formation, and provide in-depth insights into their functional anatomy and taxonomy. Comparisons with previously described fossil colobine specimens from eastern Africa led us to identify specimens similar to *Paracolobus mutiwa* Leakey, 1982 and *Rhinocolobus turkanaensis* Leakey, 1982. Our results highlight the mixed locomotor substrate preferences of *Paracolobus mutiwa* and add new insights regarding its locomotor behaviors by identifying anatomical characteristics of the forelimb associated with climbing. Postcranial remains reminiscent of *Rhinocolobus* confirm the peculiar elbow morphology of this taxon and its apparent preference for arboreal substrates. We also document femoral, humeral, and tibial specimens with arboreal traits similar in size and morphology to extant *Colobus* Illiger, 1811 in Member L of the Shungura Formation. By providing these new data on the colobine paleocommunity from Shungura, our results contribute to the understanding of the biotic context surrounding Plio-Pleistocene faunas of the Turkana Depression and pave the way for future ecomorphological analyses.

Keywords: *Rhinocolobus*, *Paracolobus*, *Colobus*, Turkana, Ecomorphology

Deleted:

INTRODUCTION

The postcranial morphology of extant African colobus monkeys (i.e., Colobini Jerdon, 1867) differs from that of the cercopithecines (i.e., Cercopithecinae Gray, 1821; Harrison 1989, Benefit 1999), reflecting at least in part their more arboreal locomotor habitus (Kingdon & Groves 2013). The fossil record suggests that the evolutionary history of colobine locomotion was more complex than it may appear from this comparison of living taxa. Early African colobines from lower Upper Miocene deposits display arboreal adaptations (Table 1; Hlusko 2007, Frost *et al.* 2008, Gilbert *et al.* 2010, Nakatsukasa *et al.* 2010). Yet, some early African and Eurasian colobines demonstrate a terrestrial habitus as early as the late Miocene, challenging the hypothesis of colobines being stenotopic primates restricted to an arboreal niche (Table 1; Youlatos *et al.* 2012, Pallas *et al.* 2019). Among the Plio-Pleistocene taxa from the Omo-Turkana Depression (Fig. 1A), *Rhinocolobus turkanaensis* was primarily arboreal and possibly suspensory (Table 1 and Fig. 1B; Jablonski & Leakey 2008a), whereas *Paracolobus mutiwa* has been hypothesized to be more adapted to ground dwelling (Table 1 and Fig.1B; Anderson 2021, Ting 2001). The postcranial anatomy of *Cercopithecoides williamsi* Mollet, 1947 and *Cercopithecoides coronatus* (Broom and Robinson 1950) also indicates frequent use of terrestrial substrates (Table 1, Fig. 1A, and Appendix 2A-B; Birchette 1981, Jablonski & Leakey 2008a). Finally, fossils similar in size and morphology to extant *Colobus guereza* Rüppell, 1835 were described from Pleistocene deposits of the Turkana and Afar Depression (Table 1 and Fig. 1A-B; Jablonski & Leakey 2008a, Frost & Alemseged 2007). Fossil *Colobus* specimens from the Pleistocene sites of Asbole and Okote Member of the Koobi Fora Formation all shows postcranial anatomy consistent with significant use of arboreal substrates. Collectively, Plio-Pleistocene colobine fossil taxa demonstrate significant diversity, both in terms of locomotor substrate preferences and positional behaviors among fossil colobines (Table 1).

The last 20 years have witnessed the publication of numerous studies of early eastern and central African colobines, including associated partial skeletons. These fossils provide a strong comparative dataset on which to base description of new specimens (Frost & Delson 2002, Leakey *et al.* 2003, Hlusko 2006, Frost & Alemseged 2007, Hlukso 2007, Jablonski & Leakey 2008a&b, Gilbert *et al.* 2010, Nakatsukasa *et al.* 2010, Frost 2014, Pallas *et al.* 2019). Despite all these new fossil data, the postcranial anatomy of *P. mutiwa* is currently known from only one single individual (i.e., a male individual provisionally described in Harris *et al.* 1988, and thoroughly described in Anderson 2021), which precludes assessment of the range

Commented [MOU1]: Why are the differences only assumed to reflect locomotor differences? They almost certainly reflect locomotor differences, at least in part. See any functional anatomy study on colobines….e.g., classic papers by Fleagle, 1976; more recnet ones by McGraw et al., Dunham et al., 2015, 2017; etc. etc.

Deleted: a difference assumed to

Deleted: y

Commented [MOU2]: Frost et al. (2022a, b) have pointed out this should be referred to as C. coronatus as the East African material seems conspecific with the South African material described many years before 1982. If you disagree, please state the reasons why somewhere as a possible footnote or other note.

Deleted: *kimeui*

Deleted: Leakey, 1982

Commented [MOU3]: See also Frost (2001 thesis) and recent paper by Brasil et al. (2023) for Middle Awash

of variation for this species. Similarly, the postcranial anatomy of *R. turkanaensis* is represented only by male specimens (i.e., KNM-ER 1542 and KNM-ER 16 in Jablonski & Leakey 2008b). In addition, gaps in colobine evolutionary history remain. While fossil specimens from the Koobi Fora Formation (Upper Burgi, KBS and Okote members) have contributed greatly to the understanding of early colobine paleoecology and paleobiology, little is known before and after this 1.945 Ma - 1.383 Ma time interval (Fig. 1A and Appendix 2; Jablonski & Leakey 2008a and b). In the research presented here, we fill in these two gaps in colobine evolutionary history with postcranial remains from Member C to the upper part of Member G of the Shungura Formation (ca. 2.92 Ma - 1.89 Ma) and from Member L (1.38 Ma - 1.09 Ma; Fig. 1A, B). We also describe several fossil specimens similar in morphology and size to *R. turkanaensis*, *P. mutiwa* and *Colobus* Illiger, 1811, adding new data on the morphological variation (including size and sexual dimorphism) and functional adaptations of these colobines.

Deleted: the

Deleted: the

Deleted: s

Deleted: the

Deleted: the

Fig. 1. – A) Chronostratigraphic distribution of Plio-Pleistocene colobines from eastern Africa, B) chronostratigraphic distribution of Plio-Pleistocene colobines from the Shungura Formation, and C) chronostratigraphic framework of the Shungura Formation. Abbreviations: Fm: Formation, Mb: Member.

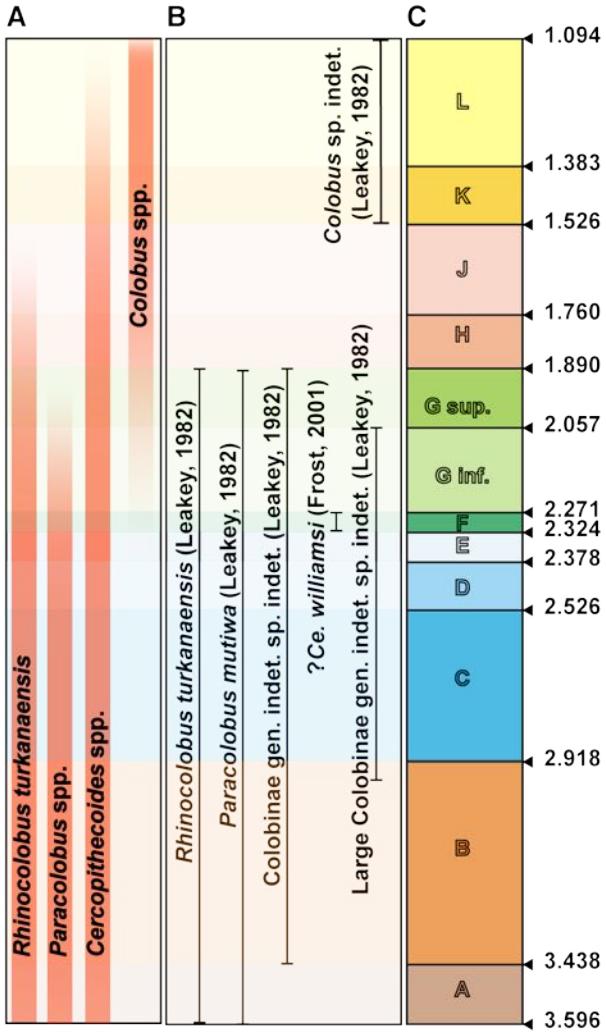

Table 1. – Paleoecological and contextual information regarding the early colobines discussed in this study.

Taxa	Geographical and temporal settings	Anatomical elements documented	Hypothetical locomotion	Accession numbers and references
Microcolobus sp.	Nakali Fm., Kenya.9.9 Ma – 9.8 Ma.	Partial skeleton (KNM-NA 47915 and -NA 47916).	Arboreal substrate preferences (Nakatsukasa *et al.* 2010).	**KNM-NA 47915/16** (Nakatsukasa *et al.* 2010).
Paracolobus enkorikae	Lemudong'o Fm., Kenya. ca. 6 Ma.	Hum. dist.	Arboreal substrate preferences (Hlukso 2007).	**KNM-NK 4470** (Hlukso 2007).
Rhinocolobus turkanaensis & cf. *Rhinocolobus* sp.	Koobi Fora Fm., Kenya. Hadar Fm., Ethiopia. Laetoli Fm., Tanzania.ca. 4 Ma – 1.6 Ma.	Partial skeleton (KNM-ER 1542).Isolated elements: hum. prox. and dist.; uln. prox. and dist.; rad. prox.; tibia prox. and dist., fem. prox. & dist.	Arboreal substrate preferences with leaping, climbing (Harrison 2011, Laird *et al.* 2018), possibly suspensory behaviors (Jablonski & Leakey 2008b).	**KNM-ER 1542**, **KNM-ER 16**, **KNM-ER 5488**, **KNM-ER 45613**, **KNM-ER 45611**, EP-1100/12, LAET 74-247, LAET 76-3870, **A.L. 300-1** (Frost & Delson 2002, Jablonski & Leakey 2008b, Harrison 2011, Laird *et al.* 2018)
P. mutiwa	Nachukui Fm., Kenya.ca. 2.6 Ma.	Partial skeleton (KNM-WT 16827).	Mixed substrate preferences, poor leaping abilities (Ting 2001; Frost and Delson, 2002; Anderson, 2021)	**KNM-WT 16827** (Anderson 2021, Ting 2001)
P. chemeroni	Chemeron Fm., Kenya.ca. 3.0 Ma – 2.5 Ma.	Partial skeleton (KNM-BC 3).	Mixed substrate preferences with prominent climbing, moderate leaping and possibly arm-swinging behaviors (Birchette 1982, Ting 2001)	**KNM-BC 3** (Birchette 1982, Ting 2001)
Kuseracolobus hafu	Assa Issie Fm., Ethiopia.ca. 3.8 Ma – 4.4Ma.	Partial skeleton (ASI-VP 2/59).	Arboreal substrate preferences (Hlusko 2006)	**ASI-VP 2/59b&c** (casts) (Hlusko 2006)
K. aramisi	Middle Awash Research Area, Ethiopia.ca. 4 Ma – 5 Ma.	Isolated elements: hum. dist., astr. dist.	Arboreal substrate preferences (Frost *et al.* 2007, White *et al.* 2009)	DID-VP-1/78, AMW-VP-1/76, KUS-VP-1/43, (Frost *et al.* 2007, White *et al.* 2009)
Cercopithecoides coronatus	Koobi Fora Fm., Kenya.[1]ca. 2 Ma.	Partial skeleton (KNM-ER 176). Isolated element: hum. dist.	Terrestrial substrate preferences, adaptations of the forelimb to manual foraging (Frost & Delson 2002, Jablonski & Leakey 2008b)	**KNM-ER 176**, **A.L. 577-1** (Frost & Delson, 2002, Jablonski & Leakey 2008b)

Formatted: Highlight

Commented [MOU4]: Note that Frost et al. (2022) in the colobines book state that the fossils from Laetoli are more likely to be Kuseracolobus than Rhinocolobus, and this is also in the SI of ther Frost et al. (2022b) PNAS biochronology paper. I wonder if these should really be listed in the hypodigm here ? And if this affects the distribution in Fig. 1, that might need to be adjusted slightly as well.

Deleted: 1

Commented [MOU5]: Note that coronatus is synonomized with C. coronatus. See Frost et al. (2022a, b) in the PNAS paper and colobine book.

Deleted: *kimeui*

Table 1 (following). – Paleoecological and contextual information regarding the early colobines discussed in this study.

Taxa	Geographical and temporal settings	Anatomical elements documented	Hypothetical locomotion	Accession numbers and references
Ce. williamsi	Koobi Fora Fm., Kenya.[1]ca. 2 Ma.	Partial skeleton (KNM-ER 4420).	Terrestrial substrate preferences (Jablonski & Leakey 2008b)	**KNM-ER 4420** (Jablonski & Leakey 2008b)
Ce. meaveae	Hadar Fm., Ethiopia.ca. 3 Ma.	Partial skeleton (AL 2-64).	Terrestrial substrate preferences (Frost & Delson 2002)	**A.L. 2-64**, A.L. 222-14 (Frost & Delson 2002)
Ce. bruneti	Toros-Menalla, Chad.ca. 7 Ma.	Partial skeleton unassociated (TM 266 03-100). Isolated element: fem.	Mixed-substrate preferences (Pallas *et al.* 2019)	**TM 266 03-100, TM 266-03-307** (Pallas *et al.* 2019)
Co. freedmani	Koobi Fora Fm., Kenya.ca. 2 Ma[1].	Partial skeleton. Isolated elements: hum. dist.	Arboreal substrate preferences (Jablonski & Leakey 2008a)	**KNM-ER 5896**, **KNM-ER 857**, **KNM-ER 841**, **KNM-ER 71** (Jablonski & Leakey 2008a)
Co. sp.	Asbole, Ethiopia.ca. 600 ka.	Partial skeleton. Isolated elements: uln. prox., rad. prox., fem. prox., hum. dist. and prox.	Arboreal substrate preferences (Frost & Alemseged 2007)	**ASB-42A**, **ASB-254**, **ASB-210**, **ASB-137**, **ASB-129**, **ASB-91**, **ASB-233-18** (Frost & Alemseged 2007)
Cercopithecidae indet.[2]	Lemudong'o Fm., Kenya.ca. 6 Ma.	Isolated element: hum. dist.	Arboreal substrate preferences (Hlusko 2007).	**KNM-NK 41028, KNM-NK 41169, KNM-NK 41413** (Hlukso 2007)
Cercopithecidae indet.	Konso Fm., Ethiopia.ca. 1.45 Ma.	Isolated element: hum. prox.	NA.	**KGA 4-418** (Frost 2014)

Bold specimens were studied by the first author and integrated in the analysis.
[1] Dates given for the associated partial skeleton (Jablonski *et al.* 2008a, 2008b).
[2] Fossil specimens from Lemudong'o are stated as possibly being conspecific with *P. enkorikae* (Hlusko 2007).

Deleted: *meavae*

Commented [MOU6]: Add specimens from Andalee Frost (2001) and new Middle Awash specimens from Brasil et al. (2023) ?

Deleted: Datation

THE SHUNGURA FORMATION AND USNO FORMATION

The Shungura Formation is divided in twelve geologic members (Fig. 1C; Heinzelin 1983). Apart from members E and H, each member is stratigraphically delineated by tuffs dated by radiochronology or magnetostratigraphy, with unit delineation based on lithological content (Fig. 1C and Appendix 2C; Brown & Heinzelin 1983, Feibel *et al.* 1989, McDougall & Brown 2008, McDougall *et al.* 2012, Kidane *et al.* 2014). The Usno Formation is located northeast of Shungura. Most of the fossil vertebrates from Usno derives from the White Sands and Brown Sands localities and are stratigraphically placed in the U-12-2 and U-12-3 horizons (Heinzelin 1983). These horizons correlate with the units B-1 and B-2 of the Shungura Formation (Heinzelin 1983).

The Omo Group deposits in the Lower Omo Valley record a sedimentological sequence spanning roughly 2.90 million years, providing an incredible window into the evolutionary history of vertebrates in eastern Africa (Howell & Coppens 1974, Boisserie *et al.* 2008, 2010). The Shungura time interval (ca. 3.75 Ma - ca. 1.09 Ma; Fig. 1C) documents significant paleoecological, paleoenvironmental and phyletic changes (e.g., in hominins, the emergence of the genera *Homo* Linnaeus, 1758 and *Paranthropus* Broom, 1938) that occurred in the context of climatic fluctuations (Bobe & Leakey, 2009; Maslin & Trauth, 2009; Reed & Russak, 2009). Renewed fieldwork by the Omo Group Research Expedition (OGRE) has brought forth new contextual and integrative data regarding paleoenvironmental changes and ecological dynamics of Plio-Pleistocene landscapes and faunas (Bibi *et al.* 2012, Souron *et al.* 2012, Blondel *et al.* 2018, Martin et al. 2018, Rowan *et al.* 2018). At Shungura and Usno, these biotic and abiotic events are embedded in a calibrated and accurate temporal framework. Among the biotic evidence are numerous well-preserved postcranial colobine specimens.

Deleted: primates

THE FOSSIL COLOBINES FROM USNO AND SHUNGURA

The Usno and Shungura formations have yielded abundant cercopithecid remains (e.g., relative abundance of up to 53 % in Member C among specimens collected in the OGRE fieldwork according to Boisserie *et al.* 2010). Although colobines are less well represented compared to cercopithecines, this assemblage nonetheless reveals a diversity of colobine taxa (Fig. 1B). Two large morphs (i.e., *P. mutiwa* and *R. turkanaensis*) were described at Shungura and Usno based on isolated cranial, dental and gnathic specimens (Leakey 1987). The taxonomic status of smaller craniodental morphs has remained uncertain (i.e., *Colobus* sp. indet. and Colobinae gen. indet. sp. indet. according to Leakey 1987).

Deleted: a

Knowledge regarding the taxonomy and paleoecology of the colobines from the Usno and Shungura deposits is, to date, primarily derived from analyses of the craniodental remains.

No complete analysis of the fossil colobine postcrania from the Omo has yet been published. Following the results obtained on the craniodental data, we expect to find postcranial specimens similar in size and morphology to *R. turkanaensis*, *P. mutiwa* and *Colobus*. We also expect these specimens to show morphological adaptations in line with the use of arboreal substrates for *R. turkanaensis* and *Colobus* but terrestrial substrates for *P. mutiwa*.

Here, we describe *n* = 32 postcranial specimens that include forelimb (humerus, ulna and radius) and hindlimb (femur and tibia) remains of fossil colobines in the size range of *P. mutiwa*, *R. turkanaensis* and *Colobus*. Fossils were collected between 2008 and 2016 by the OGRE and between 1967 and 1974 by the IORE (International Omo Research Expedition). We provide tentative taxonomic assignments for some of these postcranial specimens to *R. turkanaensis*, *P. mutiwa* and *Colobus*. Several specimens that do not match with the morphology of the above taxa are also considered in this study. Besides describing fossil specimens, we infer their locomotor substrate preferences and locomotor behaviors based on qualitative and quantitative traits. Specifically, we are assessing the terrestrial substrate preferences of *P. mutiwa*, the arboreal and suspensory behaviors of *R. turkanaensis*, and the arboreal and leaping behaviors of early *Colobus*. These data and analyses provide new information on the paleoecology and functional anatomy of the Plio-Pleistocene colobines from the Turkana Depression.

MATERIALS AND METHODS

PALEONTOLOGICAL SAMPLE

The comparative paleontological sample used in this study spans the last 10 million years of colobine evolutionary history focusing on fossils from eastern and central Africa (Table 1). We describe *n* = 32 postcranial specimens from Member B to Member L of the Shungura Formation and the White Sands and Brown Sands locality of the Usno Formation (Table 2). The spatial localization of the Shungura colobine included in this study can be found in Appendix 3.

Deleted: postcranium

Table 2. – Chronostratigraphical context and anatomical and taxonomical information of the specimens from Shungura and Usno described in this study.

Specimens	Formation	Members and units	Skeletal elements	Taxonomy	Figures
B-818A	Usno	Brown sands locality (B-2)	Uln. prox. (right)	Colobinae gen. indet. and sp. indet.	SOM Figure S13
W 7-477B	Usno	White sands locality (B-2)	Fem. prox. (left)	*Paracolobus* cf. *mutiwa*	Figure 20
P 732-1	Shungura	Mb. B (B-0/B-2)	Ulna. prox. (right)	Colobinae gen. indet. and sp. indet.	SOM Figure S13
OMO 3/O-1968-1410	Shungura	Mb. B (B-12)	Hum. dist. (left)	aff. Colobinae	Figure 11
L 107-4	Shungura	Mb. C (C?)	Uln. prox. (right)	*Paracolobus* cf. *mutiwa*	Figure 17
L 373-3	Shungura	Mb. C (C-1)	Uln. prox. (left)	*Rhinocolobus* cf. *turkanaensis*	Figure 15
L 32-144	Shungura	Mb. C (C-5/C-7)	Uln. prox. (left)	*Paracolobus* cf. *mutiwa*	SOM Figure S13
OMO 18-1967-135	Shungura	Mb. C (C-8)	Hum. dist. (left)	Colobinae gen. indet. and sp. indet	Figure 14
OMO 165-1973-608	Shungura	Mb. C (C-5/C-9)	Hum. dist. (left)	Colobinae gen. indet. and sp. indet.	Figure 14
L 78-10031	Shungura	Mb. C (C-8)	Hum. dist. (left)	*Rhinocolobus* cf. *turkanaensis*	Figure 11
OMO 18-1971-702	Shungura	Mb. C (C-8)	Hum. dist. (left)	Colobinae gen. indet. and sp. indet.	Figure 14
OMO 18/inf-10063	Shungura	Mb. C (C-4/C-8)	Hum. prox. (left)	Colobinae gen. indet. and sp. indet.	Figure 6
L 293-10004	Shungura	Mb. C (C-4)	Uln. prox. (right)	*Paracolobus cf. mutiwa*	Figure 11
OMO 294-10006	Shungura	Mb. C (C-9)	Hum. dist. (right)	aff. Colobinae	Figure 11
L 5/6-41	Shungura	Mb. E (E-3/E-4)	Hum. dist. (left)	*Paracolobus* cf. *mutiwa*	Figure 8
OMO 70-10042	Shungura	Mb. E (E-3)	Hum. dist. and prox. (right)	*Paracolobus* cf. *mutiwa*	Figure 8
OMO 176-10006	Shungura	Mb. E (E-1)	Hum. dist. (left)	*Paracolobus* cf. *mutiwa*	Figure 8
L 236-1a and -1b	Shungura	Mb. E (E-4)	Uln. prox. and rad. prox. (right)	*Paracolobus* cf. *mutiwa*	Figures 17 and 18
OMO 57/4-1972-164	Shungura	Mb. E (E-4)	Ulna prox. (left)	*Rhinocolobus* cf. *turkanaensis*	Figure 15
L 7-15	Shungura	Mb. G (G-4/G-8)	Hum. dist. (right)	*Paracolobus* cf. *mutiwa*	Figure 10

Table 2 (following). – Chronostratigraphical context and anatomical and taxonomical information of the specimens from Shungura and Usno described in this study.

Specimens	Formation	Members and units	Skeletal elements	*Taxonomy*	Figures
OMO 222-1973-2751	Shungura	Mb. G (G-7)	Hum. dist. (left)	*Paracolobus* cf. *mutiwa*	Figure 10
OMO 2-10029	Shungura	Mb. G (G-29)	Rad. prox. (left)	*Rhinocolobus* cf. *turkanaensis*	Figure 18
OMO 75/N-1971-728	Shungura	Mb. G (G-12/G-13)	Fem. prox. (right)	*Rhinocolobus* cf. *turkanaensis*	Figure 20
OMO 50-1973-4450	Shungura	Mb. G (G-3/G-13)	Fem. prox. (right)	*Rhinocolobus* cf. *turkanaensis*	Figure 20
F 500-1	Shungura	Mb. G (G-28)	Hum. (right)	*Rhinocolobus* cf. *turkanaensis*	Figure 10
F 501-1	Shungura	Mb. G (G-27/G-28)	Hum. prox. (left)	Colobinae gen. indet. and sp. indet.	Figure 6
OMO 342-10019	Shungura	Mb. L (L-9)	Fem. prox. (left)	cf. *Colobus* sp. indet.	Figure 23
OMO 342-10335	Shungura	Mb. L (L-9)	Hum. prox. (left)	cf. *Colobus* sp. indet.	Figure 9
OMO 342-10298	Shungura	Mb. L (L-9)	Fem. prox. (left)	cf. *Colobus* sp. indet.	Figure 23
OMO 342-10344	Shungura	Mb. L (L-9)	Fem. prox. (right)	cf. *Colobus* sp. indet.	Figure 23
OMO 342-10052	Shungura	Mb. L (L-9)	Hum. prox. (right)	cf. *Colobus* sp. indet.	Figure 9
OMO 377-10024	Shungura	Mb. L (L-7)	Tib. dist. & prox. (right)	cf. *Colobus* sp. indet.	Figure 24

245

NEONTOLOGICAL SAMPLE

We used a large neontological comparative dataset from European and African museums. This dataset includes *n* = 105 individual skeletons representing *n* = 9 cercopithecid genera (*Colobus* Illiger, 1811; *Nasalis* Geoffroy Saint-Hilaire, 1812; *Papio* Erxleben, 1777; *Piliocolobus* Rochebrune, 1877; *Presbytis* Eschscholtz, 1821; *Procolobus* Rochebrune, 1877; *Pygathrix* Geoffroy Saint-Hilaire, 1812; *Trachypithecus* Reichenbach, 1862; and *Semnopithecus* Desmarest, 1822), including *n* = 18 species (see Table 3). For each sample, informations regarding the sex and provenience (wild, captive or unknown) of the specimens are listed in Table 3. Information regarding the accession numbers of the extant specimens can be found in Appendix 37.

Qualitative comparisons between fossil colobines and extant cercopithecids focused on *n* = 4 extant taxa with known locomotor and postural behaviors (i.e., *Colobus guereza*, *Nasalis larvatus* Wurmb, 1787; *Semnopithecus entellus* Dufresne, 1797; and *Papio hamadryas* Linnaeus, 1758). *Co. guereza* is a predominantly arboreal quadrupedal African colobine that frequently engages in leaping and climbing (Rose 1979, Gebo & Chapman 1995, 2000, Fashing, 2016). *N. larvatus*, an Asian colobine, is also a predominantly arboreal quadruped, with bouts of terrestriality (Matsuda *et al.* 2017, Kawabe & Mano 1972), and that engages in leaping and climbing (Yeager *et al.* 2016). *N. larvatus* also incorporates a significant amount of suspension in its locomotor repertoire compared to *Co. guereza* (Yeager *et al.* 2016, Bismark 2010). *S. entellus* is an Asian colobine with mixed substrate preferences and higher frequencies of quadrupedal ground walking and running compared to *Co. guereza* and *N. larvatus* (Rahman *et al.* 2015). Leaping and climbing are nevertheless documented as part of the locomotor repertoire of *S. entellus* (Ripley 1967, McQuinn 2016). *P. hamadryas* is an African papionin with terrestrial substrate preferences (Swedell & Chowdhury 2016), and although climbing and leaping are included in its locomotor repertoire, these behaviors are observed at much lower frequencies than in *Co. guereza*, *N. larvatus* and *S. entellus* (Swedell & Chowdhury 2016).

Table 3. – Size, provenance, taxonomy and sex of the extant sample of cercopithecids included in this study.

Taxa & Total number of specimens	Repositories	Sex ♂ / ♀/ unknown	Provenience: wild / captive / unknown
Colobus sspp.[1] N = 21	RMCA, MNHN	12 / 7 / 1	15 / 2 / 3
Piliocolobus spp.[2] N = 17	RMCA, MNHN, NMB, UZH-MA	4 / 11 / 2	11 / 6 / 0

Commented [MOU7]: Are these all adults? How was adult status determined (i.e., all epiphyses fused, all epiphyses fused with no lines, some epiphyses fused, M3/m3 eruption, ???). If it is a mixed subadult/adult sample, this needs to be stated and identified in Table 3 with an additional column listing numbers of adult/subadult specimens or perhaps in an appendix somewhere.

Commented [MOU8]: Why only these 4 taxa ? There are data for some of the other taxa you have sampled….for Presbytis/Trachypithecus going back to Fleagle and Piliocolobus/Procolobus I believe McGraw and colleagues have multiple papers looking at locomotor behavior and anatomical correlates. It seems like you should make greater use of the information out there in the literature. I don't understand why only these 4 taxa with no justification.

Commented [MOU9]: Captive specimens are obviously not ideal for a study like this, but I understand that sometimes that's the best you can do. Can you at least confirm that they are non-pathological ? Some comment on the criteria for inclusion in the study for the captive specimens is needed.

Procolobus verus N = 2	MNHN, UZH-MA	1 / 1 / 0	1 / 1 / 0
Nasalis larvatus N = 11	UZH-MA, MNHN, NMB	3 / 6 / 2	7 / 3 / 1
Pygathrix nemaeus N = 7	MNHN, UZH-MA, NMB	2 / 4 / 1	1 / 6 / 0
Semnopithecus sspp.[3] N = 8	MNHN, UZH-MA, NMB, KNM	1 / 3 / 4	7 / 1 / 0
Trachypithecus spp.[4] N = 9	MNHN, UZH-MA, NMB	2 / 3 / 4	6 / 3 / 0
Presbytis spp. N = 2	MNHN, UZH-MA	1 / 1 / 0	2 / 0
Subtotal Colobinae N = 77			
Papio spp.[5] N = 32	MNHN, UZH-MA, NMB, MHNL, NME	14 / 8 / 10	7 / 13 / 12
Total N = 106			

[1] *Colobus angolensis cottoni* (n = 3), *Colobus angolensis ruwenzorii* (n = 1), *Colobus angolensis palliatus* (n = 1), *Colobus angolensis angolensis* (n = 1), *Colobus angolensis* sspp. indet. (n = 1), *Colobus guereza occidentalis* (n = 6), *Colobus guereza guereza* (n = 1), *Colobus guereza caudatus* (n = 2), *Colobus guereza* sspp. indet. (n = 4).

[2] *Piliocolobus rufomitratus langi* (n = 1), *Piliocolobus rufomitratus ellioti* (n = 3), *Piliocolobus rufomitratus foai* (n = 1), *Piliocolobus rufomitratus tholloni* (n = 1), *Piliocolobus rufomitratus oustaleti* (n = 1), *Pilicolobus badius temminckii* (n = 1), *Pilicolobus badius* sspp. indet. (n = 5); *Piliocolobus rufomitratus* ssp. indet. (n = 2); Piliocolobus kirkii (n = 2)

[3] *Semnopithecus entellus* (n = 6), *Semnopithecus* sp. indet. (n = 2)

[4] *Trachypithecus auratus* (n = 2), *Trachypithecus cristatus* (n = 2), *Trachypithecus johnii* (n = 2), *Trachypithecus phayrei* (n = 3).

[5] *Papio anubis* (n = 11), *Papio cynocephalus* (n = 3), *Papio hamadryas* (n = 12), *Papio papio* (n = 4), *P. ursinus* (n = 1), Papio sp. indet. (n = 1).

Minimal number of individuals (MNI) for *Papio* sp. indet. coming from the Egyptian archeological sites: humerus MNI = 6; femur MNI = 12; radius MNI = 4; tibia MNI = 9; ulna MNI = 2; astragalus MNI = 7. Not included in the table count.

MORPHOMETRICS

Linear and angular measurements were collected on the humerus (*n* = 27 measurements; Table 4), ulna (*n* = 14 measurements; Table 5), radius (*n* = 6 measurements; Table 5), and femur (*n* = 13 measurements; Table 6). Only linear measurements were taken for the tibia (*n* = 10 measurements; Table 6). Measurements are shown in Figs 2 - 4. We acquired all the measurements with a Mitutoyo Digimatic Calliper CD-8''CX on original specimens and on a cast replica for *Kuseracolobus hafu* Hlusko, 2006. Angles were measured with ImageJv1.50e from photographs of the original specimens and on a cast replica for *K. hafu*.

303
304
305
306
307
308
309
310 **Table 4. –** Measurement protocol used for humeral specimens (Fig. 2)
311

Abbreviations	Description
HPEML	**Width of the proximal humeral epiphysis.** Distance from the most lateral point of the greater tuberosity to the most medial point of lesser tuberosity.
BGML	**Width of the bicipital groove of the humerus.** Distance from the most anteriorly projected lateral and medial point of the groove.
HHSI	**Height of the humeral head.** Distance from the most distal point of the humeral head to its most proximal point.
HHAP	**Length of the humeral head.** Distance from the most anterior point of the humeral head to its most posterior point.
HHMD	**Width of the humeral head.** Distance from the most medial point to the most lateral point of the humeral head (taken posterior to the tuberosities).
LTSI	**Height of the lesser tuberosity of the humerus.** Distance from the most proximal point of the tuberosity to its most distal point.
LTAP	**Anteroposterior dimension of the lesser tuberosity of the humerus.** Distance from the most posterior to the most anterior point of the lesser tuberosity.
GTSI	**Height of the greater tuberosity of the humerus.** Distance from the most proximal point of the tuberosity to its most distal point.
GTAP	**Anteroposterior dimension of the greater tuberosity of the humerus.** Distance from the most proximal point of the tuberosity to its most distal point.
DJML	**Width of the distal articular surface of the humerus.** Distance from the midpoint of the lateral border of the capitulum to the medial border of the trochlea.
DJML2	**Combined width of the distal articular surface and lateral epicondyle of the humerus.** Distance from the most lateral point of the lateral epicondyle to the medial border of the trochlea.
BIEPIC	**Biepicondylar width of the humerus.**

	Distance from the most lateral point of the lateral epicondyle to the most medial point of the medial epicondyle.
CML	**Width of the capitulum of the humerus.** Distance from the midpoint of the lateral border of the capitulum to its most medial extension.
CSI	**Height of the capitulum of the humerus.** Distance from the most proximal to the most distal point of the capitulum.
HRJML	**Width of the humeroradial joint.** Distance from the midpoint of the lateral border of the capitulum to the adjacent point on the lateral trochlear keel.
TSI	**Maximum height of the medial trochlear keel of the humerus.** Distance from the most proximal point on the medial border of the medial trochlear keel to its most distal point.
TML	**Maximum width of the trochlea of the humerus.** Distance from the medial border of the trochlea to the adjacent point on the lateral trochlear keel.

Table 4 (following). – Measurement protocol used for humeral specimens (Fig. 2)

Abbreviations	Description
OFSI	**Maximum height of the humeral olecranon fossa.** Distance from the most proximal point to the most distal point of the fossa.
OFML	**Maximum width of the humeral olecranon fossa.** Distance from the most medial point to the most lateral point of the fossa.
MPillML	**Minimum breadth of the medial humeral pillar of the humerus.** Taken as mid-height of the pillar.
LPillML	**Minimum breadth of the lateral humeral pillar of the humerus.** Taken as mid-height of the pillar.
DeltML	**Maximum breadth (mediolateral) of the shaft at the level of the deltopectoral crest of the humerus.** Distance from the most lateral point to the most medial point of the shaft (including the enthesis of *m. teres major*).
DeltAP	**Maximum breadth (anteroposterior) of the deltopectoral crest of the humerus.** Distance from the most anterior point to the most posterior point of the crest.
MPMxAP	**Maximum breadth of the medial part of the distal articular surface of the humerus.** Distance from the most anterior point of the capitulum to the most posterior point of the medial humeral pillar.
LPMxAP	**Maximum breadth of the lateral part of the distal articular surface of the humerus.** Distance from the most anterior point of the trochlea to the most posterior point of the lateral humeral pillar.
ZCMinAP	**Minimum breadth of the distal articular surface at the level of zona conoidea**
MEAng (°)	**Angulation of the medial epicondyle of the humerus (in °).** Refer to Pallas *et al.* (2019) for a detailed protocol of acquisition.

Measurements taken from photographs are highlighted in grey.

317 **Table 5. –** Measurement protocol used for the ulnar and radial specimens (Fig. 3)
318

Abbreviations	Description
OPAP	**Maximum length of the olecranon process of the ulna.** Distance from the most posterior point of the olecranon process to its most anterior point.
OPML	**Maximum width of the olecranon process of the ulna.** Distance from the most medial to the most lateral point of the olecranon process (including the cresting of the flexor tubercle and the enthesis of *m. triceps brachii*).
OPSI	**Height of the olecranon process of the ulna.** Distance from the mid-point of the anconeal process to the mid-point of the proximal aspect of the olecranon.
OlecAng	**Angulation of the olecranon of the ulna.** A circle is fitted on the sigmoid notch. This circle passes by the most anterior projection of the anconeal and coronoid processes and at mid-height of the sigmoid notch. Olecranon angulation is the angle between the line that passes to the point of inflexion of the posterior part of the olecranon and a line that materializes the sagittal plane and which passes by the center of the circle.
APAP	**Maximum projection of the anconeal process of the ulna.** Distance from the most anterior point of the anconeal process to the adjacent point posterior to it on the shaft border of the sigmoid notch.
APML	**Maximum width of the anconeal process of the ulna.** Distance from the most medial point to the most lateral point of the anconeal process.
SNAPMh	**Breadth of the shaft posterior to the mid-height of the sigmoid notch of the ulna.** Distance from the most anterior point of the sigmoid notch at its mid-height to the adjacent point posterior to it on the shaft border of the sigmoid notch.
SNDP	**Depth of the sigmoid notch of the ulna.** Distance from the mid-point of sigmoid notch to the center of the circle defined in the OlecAng measurement.
SNSI	**Height of the sigmoid notch of the ulna.** From the lateral border of the coronoid process to the distal margin of the anconeal process.
CPAP	**Maximum projection of the coronoid process of the ulna.** From the most anterior point of the coronoid process to the adjacent point posterior to it on the shaft border of the sigmoid notch.
CPML	**Maximum width of the coronoid process of the ulna.** From the most lateral point of the coronoid process to the point adjacent to it.
CPRNML	**Combined width of the coronoid process and radial notch of the ulna.** From the most lateral point of the coronoid process to the most medial point of the radial notch.
RNAP	**Maximum anteroposterior dimension of the radial notch of the ulna.** From the most posterior point to the most anterior point of the notch.
RNSI	**Height of the radial notch of the ulna.** From the most proximal point of the notch to the most distal point adjacent to it.

319

320 **Table 5 (following). –** Measurement protocol used for the ulnar and radial specimens
321
322

Abbreviations	Description
RaNSl	**Maximum length of the radial neck.** Distance from the most superior point of the bicipital tuberosity to the point adjacent to it on the peripheral articular margin of the head.
RNShA	**Minimum breadth of the radial neck.** This breadth corresponds to the shortest axis of the neck.
RNLgA	**Maximal breadth of the radial neck.** This breadth corresponds to the longest axis of the neck.
BBLA	**Lever arm of *m. biceps brachii*.** Distance from the most distal point of the bicipital tuberosity to the most proximal point adjacent to it on the margin of the radial head.
BPExt	**Maximum breadth at the level of the bicipital tuberosity** Maximum distance from the most lateral to the most medial point of the radius at the level of the bicipital tuberosity.
RHShA	**Radial head shortest axis.** Maximum length of the head along its shortest axis.
RHLgA	**Radial head longest axis.** Maximum length of the head along its longest axis.

323 Measurements taken from photographs are highlighted in grey.

324 **Table 6. –** Measurement protocol used for the femoral and tibial specimens (Fig. 4)

Abbreviations	Protocol
FPEML	**Maximum length of the proximal epiphysis of the femur.** Distance from the most medial point of the femoral head to the most lateral point of the *m. vastus lateralis* tubercle.
FHSI	**Maximum height of the femoral head.** Distance from the most proximal to the most distal point of the femoral head.
FHAP	**Maximum breadth of the femoral head.** Distance from the most anterior to the most posterior point of the femoral head.
FNML	**Maximum length of the femoral neck.** Distance from the mid-length of the trochanteric crest to the adjacent point at mid-height of the femoral neck/femoral head junction.
BNML	**Biomechanical neck length of the femur.** Distance from the most lateral point of the *m. vastus lateralis* tubercle to center of the femoral head (taken in posterior view).
FNSI	**Maximum height of the femoral neck.** Distance from the most proximal to the most distal point at mid-length of the femoral neck.
FNAP	**Maximum breadth of the femoral neck.** Distance from the most anterior to the most posterior point at mid-length of the femoral neck.
FMLLT	**Maximum width at the level of the lesser trochanter of the femur.** Distance from the most medial point of the lesser trochanter to the lateral point adjacent to it.
FBMLLT	**Maximum width below the lesser trochanter of the femur.** Mediolateral dimension of the shaft below the lesser trochanter.
FAPLT	**Maximum breadth at the level of the lesser trochanter of the femur.** Distance from the most posterior point of the lesser trochanter to the most anterior point adjacent to it.
FBAPLT	**Maximum breadth below the lesser trochanter of the femur.** Anteroposterior dimension of the shaft below the lesser trochanter.
NSA	**Collodiaphyseal angle of the femur.** Angle between the line that passes through the diaphyseal mid-breadth at 50 % and 25 % of femoral length and the line that bisects the femoral neck (this line is perpendicular to the neck maximal height).
GTProj	**Proximal projection of the greater trochanter of the femur** Distance defined by two lines perpendicular to the line that passes through the diaphyseal mid-breadth at 50 % and 25 % of femoral length. GTProj is measured between the most proximal point of the femoral head and the most proximal point of the greater trochanter.
TPEML	**Width of the proximal tibial epiphysis** Distance from the most lateral to the most medial point of the proximal epiphysis.

325

Table 6 (following). – Measurement protocol used for the femoral and tibial specimens

Abbreviations	Protocol
MshML	**Mediolateral dimension of the tibial shaft at mid-height**
MshAP	**Anteroposterior dimension of the tibial shaft at mid-height**
DEAP	**Maximum depth of the distal tibial epiphysis.** Distance from the most anterior projection of the epiphysis to its most posterior projection (usually the retromalleolar notch).
DEML	**Maximum breadth of the distal tibial epiphysis.** Distance from the most medial point of the malleolus to the most lateral point of the epiphysis.
MAP	**Maximum anteroposterior length of the tibial malleolus.** Distance from the most anterior to the most posterior point of the malleolus.
MML	**Maximum breadth of the tibial malleolus.** Distance from the most medial point to the most lateral point of the malleolus.
TFMxML	**Maximum width of the distal articular surface of the tibia.** Distance between the most medial and lateral point of the distal tibial articular surface at the level of its anterior margin.
TFMinML	**Minimum width of the distal articular surface of the tibia.** Distance between the most medial and lateral point of the distal tibial articular surface at the level of its posterior margin.
TFMxAP	**Maximum length of the distal articular surface of the tibia.** Distance between the most anterior and posterior point of the distal tibial articular surface.

Measurements taken from photographs are highlighted in grey.

To infer substrate preferences and locomotor behaviors, we used morphometric indices that quantify the shape of articular surfaces or the size and development of entheses. Each morphometric index is associated with a functional rationale presented in Table 7. The formulae used to compute the morphometric indices are also listed in Table 7.

Commented [MOU10]: This is nice, but what are the references for these indices and links between the rationale and specific locomotor behaviors? Many of these indices have been used before and correlated to behaviors by studies in the field. Where possible, you should cite these references rather than just make assumptions about the functional rationale for each of these measurements. Perhaps even more convincingly, you could collect basic behavioral data from the literature and run correlations between these indices and the frequency of behaviors of interest to conclusively document the connection between these indices and certain behaviors. See Arenson et al. (2020) paper for a recent example on extant monkeys and %terrestriality. They were able to clearly demonstrate which indices were most highly correlated with %terrestriality data collected from field studies.

Table 7. – Formulae and functional rationale associated with the morphometric indices

Bone	Name of the index	Formulae	Functional rationale
Humerus	Humeral head shape index	(HHAP/HHMD)*100	Associated with mobility of the glenohumeral joint in the coronal and sagittal planes.
Humerus	Lateral projection of the humeral tuberosities	(HPEML/HHMD)*100	Associated with the development and action of the rotator cuff muscles.
Humerus	Relative projection of the medial epicondyle	[(BIEPIC-DJML2)/DJML]*100	Associated with the development and action of the flexor muscles of the forearm.
Humerus	Distal epiphysis relative anteroposterior dimensions	[(LPMxAP*MPMxAP)/DJML]*100	Associated with mobility of the humeroulnar and humeroradial joints in the coronal and sagittal planes.
Humerus	Distal epiphysis relative anteroposterior dimensions at zona conoidea	(ZCMinAP/DJML) 100	Associated with the capacity to withstand mechanical stresses at the level of the humeroradial joint.
Humerus	Humeral pillars breadth differential	(MPillML/LPillML)*100	Associated with the capacity to withstand mechanical stresses at the level of the humeroradial and humeroulnar joints and with the development and action of *m. brachioradialis*.
Humerus	Relative distal development of the medial trochlear keel	(TSI/DJML)*100	Associated with stability of the humeroulnar joint in the coronal and sagittal planes.
Ulna	Olecranon process relative height	(OPSI/SNSI)*100	Associated with mobility of the humeroulnar joint in the sagittal plane and lever arm length of *m. triceps brachii*.
Ulna	Coronoid and radial notch relative lateral projection	(CPRNML/SNSI)*100	Associated with stability of humeroradial joint in pronated hand posture

339 **Table 7 (following). –** Formulae and functional rationale associated with the morphometric index
340

Bone	Name of the index	Formulae	Functional rationale
Radius	Radial neck relative elongation	(RaNSI/RHShA)*100	Associated with the lever arm length of *m. biceps brachii*.
Radius	Radial head shape	(RHShA/RHLgA)*100	Associated with mobility of the humeroradial joint.
Radius	Radial neck shape	(RNShA/RNLgA)*100	Associated with the capacity to withstand mechanical stresses at the level of the radial neck.
Femur	Relative posterior projection of lesser trochanter	[(FAPLT-FBAPLT)/FHAP]*100	Associated with the lever arm length of *m. illiopsoas*.
Femur	Relative proximal projection of greater trochanter	(GTProj/FHAP)*100	Associated with mobility of the coxofemoral joint in the coronal and sagittal planes as well as with the lever arm length of *m. piriformis* and *m. gluteus medius*.
Femur	Relative biomechanical neck length	(BNNL/FPEML)*100	Associated with mobility of the coxofemoral joint in the coronal and sagittal planes as well as with the lever arm length of *m. vastus lateralis* and *m. gluteus minimus*.
Femur	Femoral neck robustness	(FNSI/FPEML)*100	Associated with the capacity to withstand mechanical stresses at the level of the coxofemoral joint.
Tibia	Shape of the distal tibial epiphysis	(DEML/DEAP)*100	Associated with mobility of the crural joint in the coronal and sagittal planes.
Tibia	Shape of the tibial malleolus	(MAP/MML)*100	Associated with the capacity to withstand mechanical stresses at the level of the crural joint.

341
342

3D DATA ACQUISITION

Surface scans were acquired using a Next Engine UltraHD model 2020i 3D Scanner (NextEngine, Santa Monica, USA) and an Artec Space Spider (Artec 3D, Senningerberg, Luxembourg) on original fossil specimens and on casts. Digital reconstructions of the images obtained were produced using GeomagicStudio13 (3D Systems, Rock Hill, USA). Surfaces generated from the 3D data and transverse cross-sections were obtained using Avizo Standard Edition v7.0 (Thermo Fischer Scientific, Waltham, USA).

BODY MASS ESTIMATION AND GEOMETRIC MEANS

Body masses were inferred from postcranial and dental data (Appendix 38) using the regression equations from Ruff (2003) and Delson *et al.* (2000), respectively. For postcranial data, body masses discussed in the text were drawn only from humeral (proximal and distal) and femoral specimens as these elements are well represented in the Omo colobine sample.

Dental measurements used to calculate body masses for the Omo specimens were taken directly from high-quality dental casts (Appendix 38). Body masses deduced from dental data are from mesio-distal dimensions. We employ only M^{1-2} and M_{1-2} to infer body masses and in the case of complete or partial tooth rows, the mean value of the inferred body mass was used. For consistency and regarding the difficult sex attribution of isolated dental specimens, we utilized the parameters of the 'All' sex equation provided by Delson *et al.* (2000).

To quantitatively assess the size of fossil specimens, a geometric mean comparison with a mixed-sex sample of modern *Colobus* spp. is given. We obtained this comparison by calculating the ratio of the geometric mean of the fossil specimen to the average geometric mean of our mixed-sex sample of extant *Colobus*. Information regarding the variables used to compute the geometric mean can be found in Appendix 38.

To quantitatively assess the extent of sexual dimorphism in putative *Rhinocolobus* and *Paracolobus* specimens, we compared the geometric mean of the postcranial specimens from the Omo to the *R. turkanaensis* male partial skeleton KNM-ER 1542 and to the *P. mutiwa* male partial skeleton KNM-WT 16827. This comparison is obtained with the ratio of the geometric mean of the fossil specimen divided by the geometric mean of KNM-ER 1542 for presumed *R. turkanaensis* specimens, and KNM-WT 16827 for presumed *P. mutiwa* specimens.

The estimation of the amount of sexual dimorphism of *R. turkanaensis* is based on $n = 6$ variables for the geometric mean of distal humeral specimens (CSI, TML, TMinSI, TMaxSI, DJML2 and BiEpicML) and on $n = 7$ variables for the geometric mean of proximal ulnar specimens (SNSI, OPAP, OPSI, APML, APAP, CPML and SNAPMidH).

Deleted: ve

Commented [MOU11]: Fine, but you should at least give information about how many measurements went into the GMean (empirical studies suggest ~12 or more is ideal) and which bones these measurements derive from.

Commented [MOU12]: You then compared these to the GM sexual dimorphism in extant Colobus, correct ? Please clarify here.

The estimation of the level of sexual dimorphism of *P. mutiwa* was based on *n* = 7 variables for the geometric mean of distal humeral specimens (HRJML, CML, CSI, TML, DJML, DJML2 and BiEpicML) and on *n* = 5 variables for proximal ulnar specimens (SNSI, APML, CPML, RNAP and RNSI).

The level of sexual dimorphism of *R. turkanaensis* and *P. mutiwa* was also compared to that of *N. larvatus*, which is among the most sexually dimorphic extant colobines (Yeager *et al.* 2016). We calculated the degree of sexual dimorphism of *N. larvatus* identically to the one of the fossil colobines but the geometric mean calculation was based on *n* = 25 humeral variables (all the linear humeral measurements presented in Table 4).

Commented [MOU13]: This should be moved above when you discuss obtaining a GM. Also, this would appear that you are making a number of different Geometric means from the data available, which is fine. But each of the GMs needs to be calculated for as many of your extant taxa as possible as well so you can have some idea of how well they track dimorphism in extant taxa. If these GM values lead to sexual dimorphism ratios similar to that seen from actual body mass data, then that's great and they can assumed to be accurate, but you need to demonstrate this somewhere first.

Commented [MOU14]: For this to be meaningful, you need to use the exact GMs that you use for the fossil taxa and apply them to the extant taxa, and not just Nasalis, but as many colobines as you have in your sample and definitely need to do it for some African colobines in addition to Nasalis. Again, the more the better.

STATISTICAL ANALYSES

All statistical analyses were performed with R v.3.5.0 (R Core Team 2018) with a level of significance set at 0.05. Sexes were pooled in each analysis due to sample size limitations.

As a prerequisite to statistical tests, homoscedasticity (Bartlett test) and normality (Shapiro-Wilk test) were tested in each extant sample (i.e., Colobinae and *Papio* spp.). More precisely, we tested for each sample the null hypothesis of a homogenous variance and

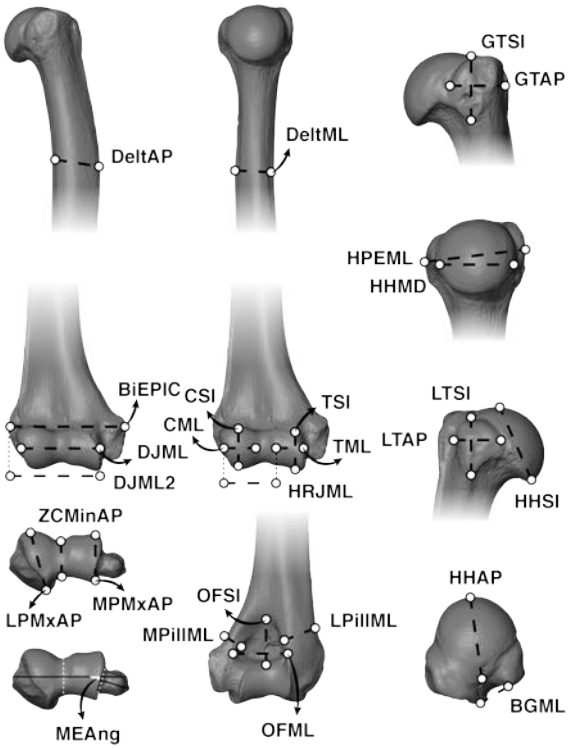

normal distribution of the data. Results of these tests can be found in Appendix 39. Parametric (t-test) or non-parametric (Wilcoxon-Mann-Whitney) tests were then used to assess the level of significance of the differences between *Papio* spp. and extant colobines for each morphometric index.

Fig. 2. – Illustration of the humerus measurement protocol.
Abbreviations: Ant: Anterior, Lat: Lateral, Me: Medial, Prox: Proximal, HPEML: width of the proximal humeral epiphysis, BGML: width of the bicipital groove of the humerus, HHSI: height of the humeral head, HHAP: length of the humeral head, HHMD: width of the humeral head, LTSI: height of the lesser tuberosity of the humerus, LTAP: anteroposterior dimension of the lesser tuberosity of the humerus, GTSI: height of the greater tuberosity of the humerus, GTAP: anteroposterior dimension of the greater tuberosity of the humerus, DJML: width of the distal articular surface of the humerus, DJML2: combined width of the distal articular surface and lateral epicondyle of the humerus, BIEPIC: biepicondylar width of the humerus, CML: width of the capitulum of the humerus, CSI: Height of the capitulum of the humerus, HRJML: width of the humeroradial joint, TSI: maximum height of the medial trochlear keel of the humerus, TML: maximum width of the trochlea of the humerus, OFSI: maximum height of the humeral olecranon fossa, OFML: maximum width of the humeral olecranon fossa, MPillML: maximum breadth of the medial humeral pillar of the humerus, LPillML: minimum breadth of the lateral humeral pillar of the humerus, DeltML: maximum breadth (mediolateral) of the shaft at the level of the deltopectoral crest of the humerus, DeltAP: maximum breadth (anteroposterior) of the deltopectoral crest of the humerus, MPMxAP: Maximum breadth of the medial part of the distal articular surface of the humerus, LPMxAP: Maximum breadth of the lateral part of the distal articular surface of the humerus, ZCMinAP: Minimum breadth of the distal articular surface at the level of zona conoidea, MEAng: Angulation of the medial epicondyle of the humerus.

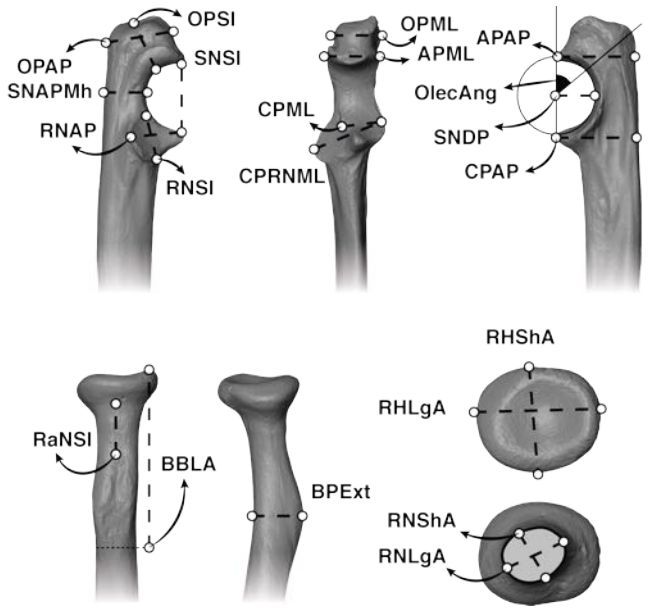

Fig. 3. – Illustration of the ulnar and radial measurement protocols.
Abbreviations: Ant: Anterior, Lat: Lateral, Med: Medial, Prox: Proximal, OPAP: Maximum length of the olecranon process of the ulna, OPML: Maximum width of the olecranon process of the ulna, OPSI: Height of the olecranon process of the ulna, OlecAng: Angulation of the olecranon of the ulna, APAP: Maximum projection of the anconeal process of the ulna, APML: Maximum width of the anconeal process of the ulna, SNAPMh: Breadth of the shaft posterior to the mid-height of the sigmoid notch of the ulna, SNDP: Depth of the sigmoid notch of the ulna, SNSI: Height of the sigmoid notch of the ulna, CPAP: Maximum projection of the coronoid process of the ulna, CPRNML: Combined width of the coronoid process and radial notch of the ulna, RNAP: Maximum anteroposterior dimension of the radial notch the ulna, RNSI: Height of the radial notch of the ulna, RaNSI: Maximum length of the radial neck, RNShA: Minimum breadth of the radial neck, RNLgA: Maximal breadth of the radial neck, BBLA: Lever arm of *m. biceps brachii*, BPExt: Maximum breadth at the level of the bicipital tuberosity, RHShA: radial head shortest axis, RHLgA: Radial head longest axis.

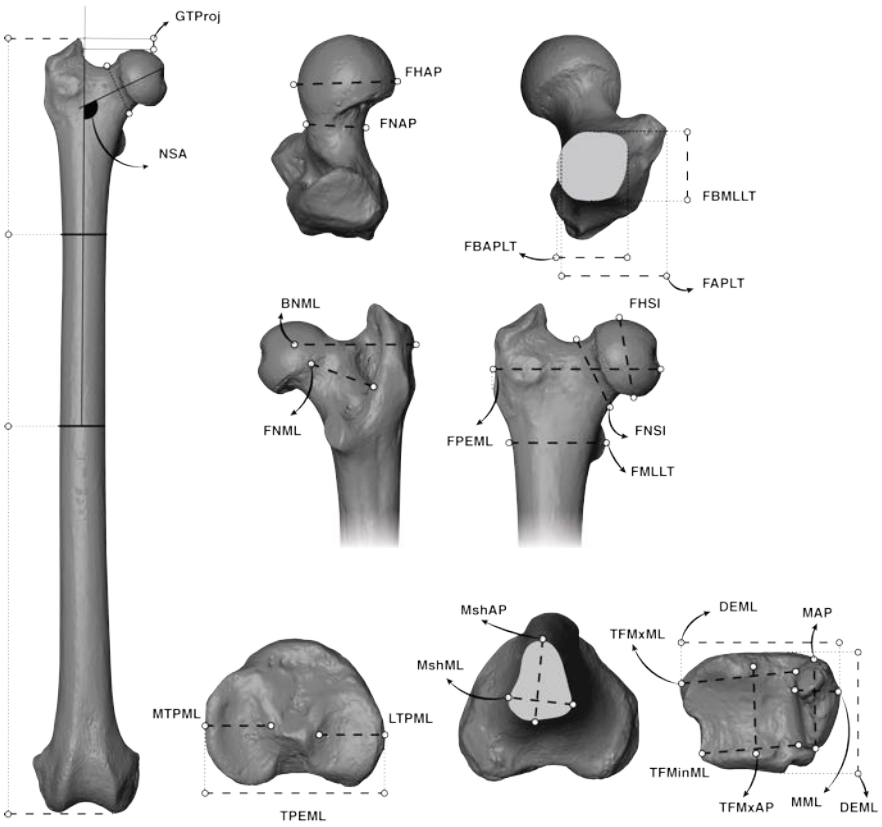

Fig. 4. – Illustration of the femoral and tibial measurement protocols.
Abbreviations: Ant: Anterior, Lat: Lateral, Med: Medial, Prox: Proximal, FPEML: Maximum length of the proximal epiphysis of the femur, FHSI: Maximum height of the femoral head, FHAP: Maximum breadth of the femoral head, FNML: Maximum length of the femoral neck, BNML: Biomechanical neck length of the femur, FNSI: Maximum height of the femoral neck, FNAP: Maximum breadth of the femoral neck, FMLLT: Maximum width at the level of the lesser trochanter of the femur, FBMLLT: Maximum width below the lesser trochanter of the femur, FAPLT: Maximum breadth at the level of the lesser trochanter of the femur, FBAPLT: Maximum breadth below the lesser trochanter of the femur, NSA: Collodiaphyseal angle of the femur, GTProj: Proximal projection of the greater trochanter of the femur, TPEML: Width of the proximal tibial epiphysis, MshML: Mediolateral dimension of the tibial shaft at mid-height, MshAP: Anteroposterior dimension of the tibial shaft at mid-height, DEAP: Maximum depth of the distal tibial epiphysis, DEML: Maximum breadth of the distal epiphysis, MAP:

Maximum anteroposterior length of the tibial malleolus, MML: Maximum breadth of the tibial malleolus, TFMxML: Maximum width of the distal articular surface of the tibia, TFMinML: Minimum width of the distal articular surface of the tibia, TFMxAP: Maximum length of the distal articular surface of the tibia.

ABBREVIATIONS AND ACRONYMS

ABBREVIATIONS

Anatomical parts and orientation

Ant: Anterior, Dent: Dental, Dist: Distal, Hum: Humerus, Fem: Femur, Lat: Lateral, Med: Medial, Prox: Proximal, Post: Posterior, Rad: Radius, Tib: Tibia, Uln: Ulna.

Other abbreviations

Aff: *Species affinis*, Cf: *Confer*, Gen: Genus, Indet: Indeterminate, IORE: International Omo Research Expedition, Fm: Formation, Kg: Kilogram, Mb: Member, MNI: Minimal number of individual, NA: Not available, OGRE: Omo Group Research Expedition, Sh: Shungura, Sp: Species, Spec: Specimen, Us: Usno

INSTITUTIONAL ACRONYMS

A.L.: Afar Locality, AMW: Amba West, ASB: Asbole, BC: Baringo County, CDA: Collodiaphyseal angle, DID: Digiba Dora, ER: East Rudolf, ITA: Intertuberosity angle, KGA: Konso Gardula Area, KNM: Kenya National Museum, KUS: Kuseralee, LAET: Laetoli, MHNL: Museum d'Histoire Naturelle de Lyon (Musée des Confluences), MNHN: Muséum Nationale d'Histoire Naturelle, NA: Nakali, NK: Narok, NMB: Naturhistorisches Museum Basel, NME: National Museum of Ethiopia, RMCA: Royal Museum for Central Africa, TM: Toros-Ménalla, UZH-MA: University of Zurich-Museum of Anthropology, VP: Vertebrate Paleontology, WT: West Turkana

MEASUREMENT ABBREVIATIONS

See Tables 4-6.

RESULTS

SYSTEMATIC PALAEONTOLOGY

Order PRIMATES Linnaeus, 1758

Suborder HAPLORHINI Pocock, 1918
Superfamily CERCOPITHECOIDEA Gray, 1821
Family CERCOPITHECIDAE Gray, 1821
Subfamily COLOBINAE Blyth, 1863

aff. Colobinae
REFERRED MATERIAL. — See Table 2.

Colobinae gen. indet. sp. indet.
REFERRED MATERIAL. — See Table 2.

Genus *Paracolobus* Leakey, 1969
TYPE SPECIES . — *Paracolobus chemeroni* Leakey, 1969
OTHER INCLUDED SPECIES. — *Paracolobus mutiwa* Leakey, 1982, and *Paracolobus enkorikae* Hlusko, 2007.
OCCURENCE IN AFRICA. — The earliest occurrence of the genus is asserted by Late Miocene specimens of *Paracolobus enkorikae* in Lemudong'o (Narok County, Kenya) and the latest occurrence is securely documented by the holotype of *Paracolobus mutiwa* KNM-ER 3843 at ca. 1.87 Ma in the Koobi Fora Formation (Lake Turkana, Kenya).

Paracolobus cf. *mutiwa* (Figs 8; 10; 11; 17; 20 and Appendix 13)
REFERRED MATERIAL. — See Table 2.

Genus *Rhinocolobus* Leakey, 1982
TYPE SPECIES. — *Rhinocolobus turkanaensis* Leakey, 1992
OCCURENCE IN AFRICA. — The earliest and latest occurrences of the genus is asserted by isolated teeth from the Usno Fm. (ca. 3.4 Ma) and KBS Mb. of the Koobi Fora Formation (ca. 1.6 Ma).

Rhinocolobus cf. *turkanaensis* (Figs 11; 15; 18; 20)
REFERRED MATERIAL. — See Table 2.

Genus *Colobus* Illiger, 1811
TYPE SPECIES. — *Colobus polykomos* Zimmerman, 1780

OTHER INCLUDED SPECIES. — *Colobus satanas* Waterhouse, 1838: *Colobus angolensis* Sclater, 1860: *Colobus vellerosus* Geoffroy, 1830: *Colobus guereza* Rüppell, 1835: and *Colobus freedmani* Jablonski & Leakey, 2008.

OCCURENCE IN AFRICA. — The earliest securely attested occurrence of the genus is from the KBS Mb. of the Koobi Formation (ca. 1.9 Ma). The extant distribution of *Colobus* is restricted to the African equatorial zone.

Colobus sp. indet. (Figs 9; 23; 24)

REFERRED MATERIAL. — See Table 2.

A detailed anatomical description of the colobine specimens considered in this study can be found in Appendix 1.

QUALITATIVE AND QUANTITATIVE COMPARATIVE ANATOMY

Comparative anatomy of the humeral proximal epiphyses

Three large proximal humeri are from members C (OMO 18/inf-10063), E (OMO 70-10042) and from the upper part of Member G (F 501-1). They are comparable in absolute size to *R.*

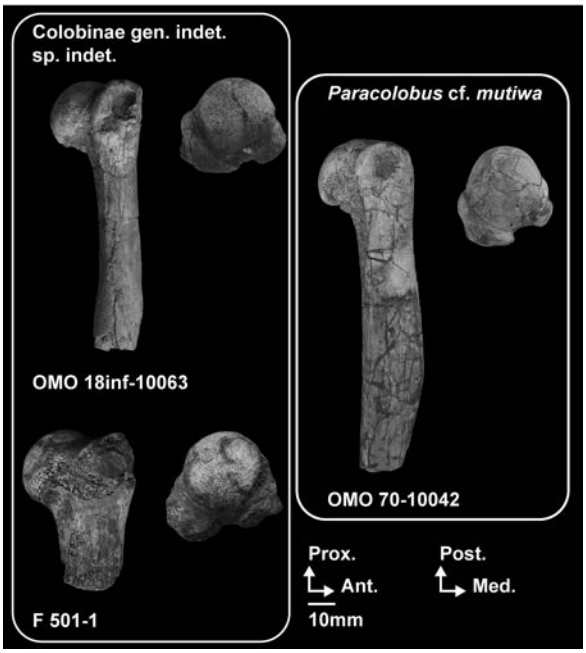

turkanaensis (KNM-ER 1542), *Ce. williamsi*, *Ce. coronatus* and *P. chemeroni* Leakey, 1969 (Table 8 and Appendix 40).

Deleted: *kimeui*

Fig. 5. – Photographs of the proximal humeral anatomy of large fossil colobines from Shungura. Scale: 10 mm. Abbreviations: Ant: Anterior, Lat: Lateral, Post: Posterior, Prox: Proximal.

546 **Table 8. –** Measurements (in mm) of the proximal humeral specimens.
547

	HHSI	HHAP	HHMD	HPEML	GTAP	GTSI	LTAP	LTSI	BGML
OMO 342-10052	12.9	15.9	16.1	19.8	14.5	10.8	9.8		5.7
OMO 342-10335	12.6	16.9	17.2	22.7	16.3	12.6	10.9	12.1	7.5
OMO 18inf-10063	25.7	28.0	~28.6	38.7	27.6	24.2		19.3	~8.3
F 501-1	26.4	30.6	31.0	40.0				~18.8	
OMO 70-10042	24.3	28.0	25.9	32.2	24.1	17.3	16.7	15.6	10.3

548
549

550 F 501-1 and OMO 18/inf-10063 (Fig. 5 and Appendix 4) show typical anatomical traits of
551 the mobile glenohumeral joint of arboreal colobines (Appendix 4): a mediolaterally enlarged
552 humeral head with a well-marked convexity on its anterior and proximal aspects; an obtuse
553 bituberosity angle with tuberosities aligned in the coronal plane and a greater tuberosity that
554 does not extend extensively above the proximal articular surface (Table 9; Rose 1988,
555 Harrison 1989, Gebo & Sargis 1994, Nakatsukasa 1994, Arias-Martorell 2019).

Commented [MOU15]: Really? The greater tuberosity looks above the humeral head in Figure 5. Looks semi-mobile to me, although Fig. 6 does indicate that these are relatively round humeral heads…

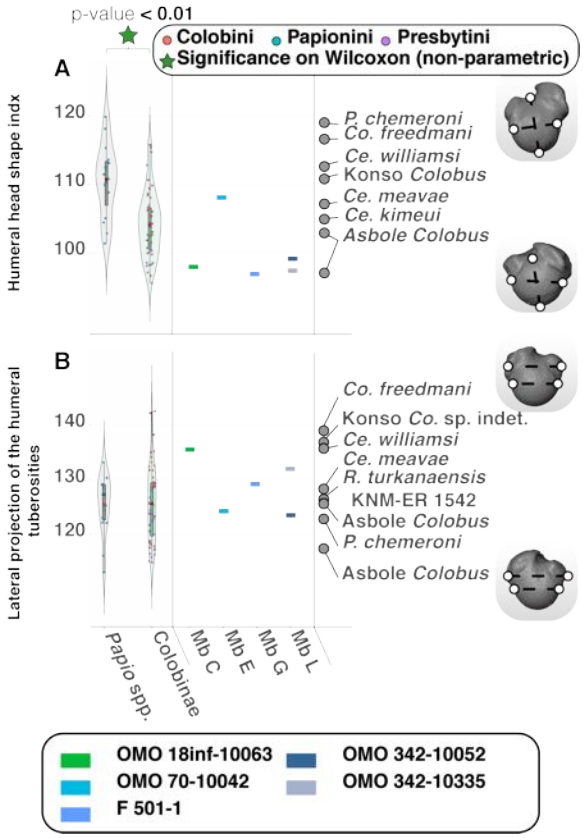

Fig. 6. – Violin plots and boxplots of proximal humeral morphometric indices of extant and extinct colobines, and extant *Papio* spp. Morphologies associated with minimum and maximum values are shown on the margins of the graph. A.) Humeral head shape index in extant colobines (n = 52), *Papio* spp. (n = 16), and fossil colobines, and B.) Lateral humeral tuberosities development index in extant colobines (n = 52), *Papio* spp. (n = 17) and fossil colobines. Means (red diamonds), medians (black rectangles), first quartile and third quartile are plotted. When there are significant differences between taxa ($p < 0.05$), the associated p-values are given.

Table 9. – Qualitative and quantitative (mean, standard deviation and sample size) morphological observations of the proximal humeral morphology of extant cercopithecids and early colobines.

Taxa (in bold, Omo taxa)	Shape of the humeral head	Proximal projection of the greater tuberosity	Morphology of the surgical neck	Intertuberosity angle (ITA) and lateral projection of the tuberosities
[1]Colobinae gen. indet. sp. indet.	**Rounded**	**Moderate**	**Rounded for F 501-1 but elliptical and excavated for OMO 18/inf-10063**	**Obtuse ITA and laterally projected tuberosities**
[2]cf. *Colobus* sp. indet.	**Rounded**	**Low**	**Elliptical and excavated**	**Obtuse ITA and non-projected tuberosities**
[3]*P.* cf. *mutiwa*	**Elliptical**	**Moderate**	**Elliptical and excavated**	**Acute ITA and non-projected tuberosities**
P. chemeroni	Rounded	Moderate	Elliptical	Acute ITA and non-projected tuberosities
P. mutiwa	NA.	NA.	Elliptical and excavated	NA.
Ce. williamsi	Elliptical	Moderate	Elliptical	Acute ITA and laterally projected tuberosities
Ce. meaveae	Elliptical	Moderate	Elliptical	Acute ITA and laterally projected tuberosities
Ce. coronatus	Rounded	Moderate	Elliptical	Obtuse ITA
Ce. bruneti	NA.	NA.	Elliptical	NA.
R. turkanaensis	Rounded	Moderate	Rounded	Obtuse ITA and laterally projected tuberosities
Co. freedmani	Elliptical	Moderate	Elliptical and excavated	Acute ITA and laterally projected tuberosities
Co. sp. indet. Asbole	Rounded	Low	Elliptical and excavated	Obtuse ITA and non-projected tuberosities
Colobus spp.	Rounded (μ = 106.4 ± 4.2, *n* = 16; Figure 6A)	Low	Elliptical and excavated	Obtuse ITA, laterally projected tuberosities (μ = 122.5 ± 4.8, *n* = 16; Figure 6B)
Nasalis larvatus	Rounded (μ = 102.8 ± 3.3, *n* = 6; Figure 6A)	Low	Elliptical with moderate excavation	Obtuse ITA, non-projected tuberosities (μ = 118.5 ± 4.8, *n* = 6; Figure 6B)
Semnopithecus spp.	Elliptical (μ = 101.1 ± 6.7, *n* = 5; Figure 6A)	Moderate	Elliptical with moderate excavation	Acute ITA, laterally projected tuberosities (μ = 122.4 ± 6.9, *n* = 5; Figure 6B)
Papio spp.	Rounded (μ = 110.5 ± 5.4, *n* = 15; Figure 6A)	Marked	Elliptical with moderate excavation	Acute ITA, laterally projected tuberosities (μ = 126.0 ± 5.9, *n* = 16; Figure 6B)

[1]Colobinae gen. indet. sp. indet. include the following specimens: OMO 18inf-10063 and F 501-1.
[2]*P.* cf. *mutiwa* include the following specimens: OMO 70-10042 and OMO 222-1973-2751.
[3]cf. *Colobus* sp. indet. include the following specimens: OMO 342-10335 and OMO 342-10052.

Deleted: *meavae*
Deleted: *kimeui*

Significant differences are detected between extant colobines and *Papio* spp. regarding the relative mediolateral enlargement of the articular surface of the humeral head ($p < 0.01$, Fig. 6A). OMO 18inf-10063 and F 501-1 present index values reflecting a mediolaterally enlarged and spherical humeral head (Fig. 6A and Table 9), as in *Ce. coronatus* (Fig. 6A) and *R. turkanaensis* (specimen KNM-ER 1542 in Fig. 6A, see also Appendix 6). OMO 18inf-10063 and F 501-1, with index values of 97.97 and 98.96, respectively, are outside the range of variation of *Colobus* spp. (μ = 106.4 ± 4.2, Table 9), and *Nasalis larvatus* (μ = 102.8 ± 3.3, Table 9) but are in the range of variation of *Semnopithecus* spp. (μ = 101.1 ± 6.7, Table 9 and Appendix 5).

OMO 70-10042, with an index value of 108.1 (Fig. 6A), departs from the morphological pattern of OMO 18inf-10063 and F 501-1, but is consistent with the anteroposteriorly elongated and hemispherical humeral head seen in *Papio* spp., *P. chemeroni* and *Ce. williamsi* (Fig. 6A, Table 9, Appendixes 5 and 6). Although closer to the mean value of the *Papio* spp. humeral head shape index (μ = 110.5 ± 5.4, Table 9), OMO 70-10042 is nonetheless within the range of variation of *Colobus* spp.

No significant differences are found between extant colobines and *Papio* spp. regarding the lateral projections of the humeral tuberosities (Fig. 6B and Table 9). However, the enlarged and laterally projected tuberosities of OMO 18inf-10063 (index value of 135.47) compared to F 501-1 (index value of 129.13) and OMO 70-10042 (index value of 124.2) are noteworthy (Fig. 6B). OMO 18inf-10063 is outside the range of variation of *Papio* spp., *Colobus* spp., *Nasalis larvatus* and *Semnopithecus* spp. (Table 9).

Two proximal humeral specimens of fossil colobines were recovered from the upper part of Member L (Fig. 7 and Appendix 7). They are similar in size to extant *Pilicolobus* spp. and *Colobus* spp. but also to *Colobus freedmani* Jablonski & Leakey, 2008, *Colobus* sp. indet. from Asbole, and an indeterminate cercopithecid from Konso (Appendix 40).

Deleted: *kimeui*

Commented [MOU16]: The desccription of the basic functional anatomy here is nice, but at some point, you need to describe some features or give some rationale as to why thes specimen should be attributed to P. cf. mutiwa. Why not C. coronatus/ kemeui or C. williamsi for instance ? Why is it most likely to be P. mutiwa ? The Tables are helpful, but it seems like there needs to be some explicit justification for the assignments of these various specimens, and it makes the most sense for it to be included in the Sys Paleo section above, I believe. I think there needs to be some re-organization here....all the information is great, but needs to be presented in a more clearly and taxonomically organized way

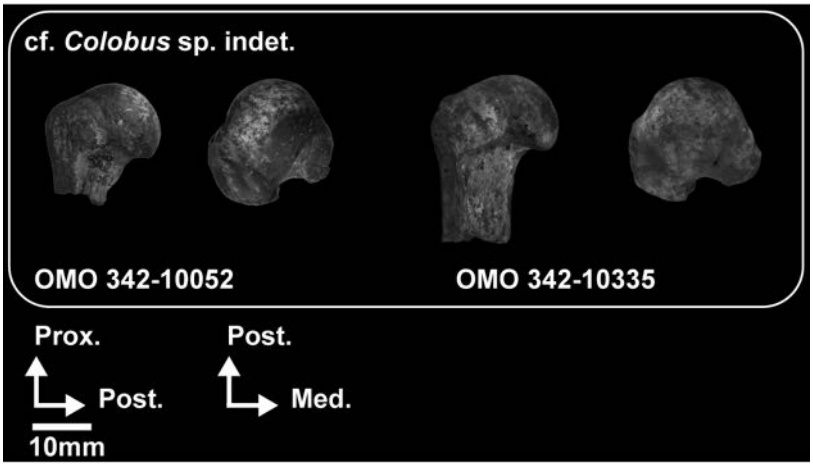

Fig. 7. – Photographs of the proximal humeral anatomy of *Colobus* specimens from Member L. Scale: 10 mm. Abbreviations: Med: Medial, Lat: Lateral, Prox: Proximal, Post: Posterior.

Similar to OMO 18/inf-10063 and F 501-1, the Member L specimens exhibit osteological correlates of a mobile glenohumeral joint (Fig. 6A and Table 9). The Omo specimens from Member L are reminiscent of the *Colobus* sp. from Asbole in humeral head shape morphology, but are quantitatively distinct from the Konso specimen KGA 4-418 and from *Colobus freedmani* (Fig. 6A and B; Appendix 7 and 8). Indeed, with humeral head shape index values of 97.40 for OMO 342-10335 and 99.12 for OMO 342-10052, they are in the range of variation of the Asbole specimens (index values of 97.11 for ASB 129 and 102.91 for ASB 137), *Nasalis larvatus*, and *Semnopithecus* spp. (Table 9). The index value of the lateral projection of the humeral tuberosities of OMO 342-10052 (index value of 123.44) is quite similar to that of the Asbole specimen NME ASB 129 (index value of 117.29) while OMO 342-10335 show a higher index value (index value of 131.99), and hence more developed tuberosities (Fig. 6B). In relative development of the humeral tuberosities, OMO 342-10335 is most similar to the Konso specimen KGA 4-418 (Fig. 6B). The relative lateral development of the humeral tuberosities of OMO 342-10335 and OMO 342-10052 are in the range of variation of *Co. guereza* (μ = 122.5 ± 4.8, Table 9).

Qualitatively, the angle formed by the tuberosities (bituberosity angle following Rose, 1989) is obtuse in F 501-1 and OMO 18inf-10063, similarly to *R. turkanaensis*, *P. mutiwa* and *Ce. coronatus* but unlike *P. chemeroni* and *Ce. williamsi* (Table 9 and Appendix 6). Obtuse intertuberosity angle are also seen in *Co. guereza* and *N. larvatus* (Appendix 5 and Table 9)

Commented [MOU17]: Humeral head is clearly above the greater tuberosity here, this looks like a more mobile shoulder than the other specimens.

Deleted: *kimeui*

Commented [MOU18]: It might be helpful to look at Harrison (1989) here and his classic analysis of Victoriapithecus. I think many of the indices and observations in that paper would be relevant here.

while acute intertuberosity angle are more characteristic of *Papio* and *S. entellus* (Appendix 5 and Table 9). The intertuberosity angle is obtuse in OMO 342-10335 and OMO 342-10052 and conforms with the pattern seen in *Co. guereza* and *N. larvatus* (Appendix 5 and Table 9). Obtuse angles are also seen in fossil specimens from Asbole, Konso and *Co. freedmani* (Appendix 8).

In cross-section, the humeral surgical neck of the Omo colobines is variable in shape, as previously documented in extant cercopithecids (Fleagle & Simons 1982a,Rose 1989, Gebo & Sargis 1994, Nakatsukasa 1994). Omo colobines displays either elliptical (OMO 70-10042 in Appendix 9) or rounded (F 501-1 in Appendix 6 and F 500-1 in Appendix 11) cross-sections. The elliptical (anteroposteriorly extended) cross-section of OMO 70-10042 (Appendix 9) is similar to that of *Papio hamadryas* and *Semnopithecus entellus* (Appendix 5). It is also similar to *P. chemeroni*, *Ce. coronatus* and *Ce. williamsi* (Appendix 6). The rounded anterior portion of the cross-sections of F 501-1 and F 500-1 are similar to *R. turkanaensis* KNM-ER 1542 (Appendix 6). The cross-sections of OMO 18inf-10063 and OMO 222-1973-2751 are elliptical, with a long axis set mediolaterally, as in *Colobus guereza* and *Nasalis larvatus*, and closely matching the morphology of *P. mutiwa* (Appendix 6). The small sized specimens from Member L present a cross-sectional shape distinct from the smooth and rounded one of the large specimen F 501-1. The proximal metaphysis of Member L specimens is rather pinched posteriorly and flanked by extensive excavations (Table 9), as seen in OMO 342-10335 and OMO 342-10052 (Appendix 7), for the *m. teres major* medially and presumably *m. deltoideus* and *m. coracobrachialis* laterally (Nakatsukasa 1994, Rose 1989). The morphology of the Member L specimens is reminiscent of *Colobus* (Table 9).

Deleted: *kimeui*

Comparative anatomy of the humeral diaphysis

As can be observed in the cross-sections set at the surgical neck, the deltopectoral crest is well pronounced proximally in the small specimens of the Member L (Fig. 7) and OMO 70-10042 (Fig. 5) whereas it shows a low relief on OMO 18/inf-10063 (Fig. 5), indicating a more distal development of the deltopectoral crest in the latter specimen. The deltopectoral crests of F 500-1 and OMO 222-1973-2751 (Fig. 8) are well preserved and not as pronounced anteroposteriorly as those observed in extant *Papio* spp. and *Ce. williamsi* (Appendix 5 and 6), but are quite similar to that of *P. mutiwa* (Appendix 10 and 11). The distal extension of the deltopectoral crest of F 500-1 and OMO 222-1973-2751 is not as pronounced as that of *Papio* (Table 10 and Appendix 5).

659 The enthesis of the *m. teres major* is well marked in F 500-1 and OMO 222-1973-2751 (Fig.
660 8 and Table 10) but faint in OMO 70-10042 (Fig. 5 and Table 10). A raised crest is seen on the
661 insertion site of the *m. teres major* in *Ce. williamsi*, *R. turkanaensis* and *P. mutiwa* but not in
662 *P. chemeroni* (Appendix 5 and 10). The *m. teres major* enthesis is salient in extant colobines
663 but usually faintly expressed in *Papio* (Table 10 and Appendix 5).

664

665 **Fig. 8**. – Photographs of the humeral anatomy of presumed specimens of *Paracolobus*
666 *mutiwa* and *Rhinocolobus turkanaensis*. Scale: 10 mm. Abbreviations: Ant: Anterior, Lat:
667 Lateral, Med: Medial, Prox: Proximal.

668

669

670 **Table 10. –** Qualitative and quantitative morphological observations of the diaphyseal
671 humeral morphology of extant cercopithecids and early colobines.
672

Taxa (in bold, Omo taxa)	Development of the *m. teres major* enthesis	Diaphyseal elongation	Deltopectoral crest extension	Supracondylar crest development

[1]*R.* cf. *turkanaensis*	**Moderate**	**Moderate**	**Proximally restricted**	**Moderate**
[2]cf. *Colobus* sp. indet.	**NA.**	**NA.**	**Proximally restricted**	**NA.**
[3]*P.* cf. *mutiwa*	**Moderate (OMO 70-10042) to marked (OMO 222-1973-2751)**	**Moderate**	**Proximally restricted**	**Marked**
P. chemeroni	Poor	Marked	Proximally restricted	Poorly developed
P. mutiwa	NA.	Moderate	NA.	Marked
Ce. williamsi	Marked	Reduced	Proximally restricted	Moderate
Ce. meaveae	NA.	NA.	NA.	Poorly developed
Ce. coronatus	NA.	NA.	NA.	Poorly developed
Ce. bruneti	Moderate	Moderate	Proximally restricted	Poorly developed
R. turkanaensis	Marked	NA.	NA.	Poorly developed
Co. freedmani	Poor	Moderate	Proximally restricted	Poorly developed
Co. sp. indet. Asbole	Poor	NA.	Proximally restricted	Poorly developed
Colobus spp.	Moderate to marked	Moderate	Proximally restricted	Poorly developed
Nasalis larvatus	Moderate to marked	Highly elongated	Proximally restricted	Poorly developed
Semnopithecus spp.	Moderate to marked	Moderate	Proximally restricted	Poorly developed
Papio spp.	Poor to moderate	Moderate	Distally extended	Poorly developed

[1]*R.* cf. *turkanaensis* indet. include F 500-1.

[2] cf. *Colobus* sp. indet. include the following specimens: OMO 342-10335 and OMO 342-10052.

[3]*P.* cf. *mutiwa* include the following specimens: OMO 70-10042, OMO 222-1973-2751, OMO 176-10006 and L 7-15.

Deleted: *kimeui*

679 The diaphyses of F 500-1 and OMO 222-1973-2751 (Fig. 8 and Appendix 11) are not as
680 elongated as in arboreal and suspensory species such as *N. larvatus* and *Py. nemaeus* (Table
681 10 and Appendix 5; Birchette 1982, Rose et al. 1992, Schmitt 1998, Su & Jablonski 2009).
682 Indeed, the humeral diaphyseal portion of those large fossil colobines is shortened compared
683 to most extant colobines. Although buttressed, none of the Omo colobines have a shaft as
684 robust and short as that of *Ce. williamsi* or as gracile as that of *P. chemeroni* (Appendix 10).
685 In diaphyseal proportion and robustness, F 500-1 and OMO 222-1973-2751 are similar to *P.*
686 *mutiwa* (Appendix 10 and Table 10).
687 Transverse cross-sections through mid-diaphysis reveal a pinched anterior side in F 500-
688 1 and OMO 222-1973-2751 (Appendix 11) that may be a byproduct of a developed
689 deltopectoral crest proximal to mid-diaphyseal level (Fig. 8). They also differ from the elliptical
690 shape (with a long axis set anteroposteriorly) of cursorial and terrestrial cercopithecids (Gebo
691 & Sargis 1994, Patel *et al.* 2013, Pallas *et al.* 2019).
692 OMO 3/O-1968-1410 has a well-developed deltopectoral crest and an elliptical cross-
693 section at mid-shaft (Fig. 9 and Appendix 12) reminiscent of the condition seen in *Papio*
694 (Appendix 5) but distinct from other Omo specimens.
695

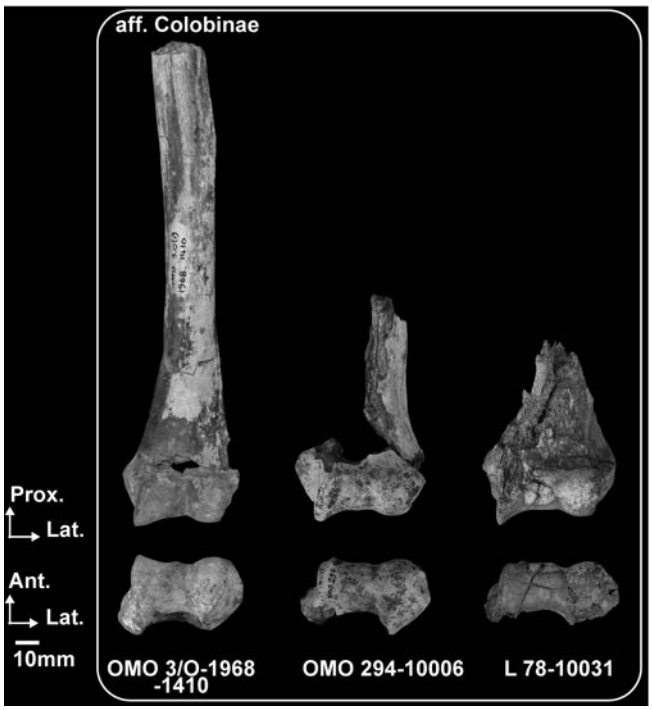

Fig. 9. – Photographs of the humeral anatomy of presumed fossil colobines. Scale: 10 mm. Abbreviations: Ant: Anterior, Lat: Lateral, Med: Medial, Prox: Proximal.

A developed lateral supracondylar crest (insertion site of the *m. brachioradialis*) is present in OMO 222-1973-2751, OMO 70-10042, OMO 176-10006 (Fig. 8, Table 10 and Appendix 9), L 5/6-41 (Appendix 9) and L 7-15 (Fig. 8 and Appendix 11). This enlarged enthesis for the *m. brachioradialis* differs from that of *P. chemeroni*, and *Kuseracolobus hafu* (Appendix 13) but is extremely similar to *P. mutiwa* (Appendix 13). Only a faint lateral supracondylar crest is discernable on F 500-1, OMO 3/O-1968-1410 and OMO 294-10006 (Figs 8; 9). This condition is akin to that of extant *Colobus* and *Nasalis* but contrast with the moderately developed lateral supracondylar crests observed in *Papio* (Table 10 and Appendix 5).

The large, excavated supra-articular fossae seen in OMO 222-1973-2751, OMO 70-10042, OMO 176-10006, L 7-15 (Fig. 8) and L 5/6-41 (Table 11 and Appendix 9) contrast with the weakly excavated coronoid fossae of OMO 3/O-1968-1410 (Fig. 9) and F 500-1 (Fig. 8). While both coronoid and radial fossae are excavated in the formers, there is a substantial depth difference between these fossae in *P. chemeroni*, *K. hafu*, *Co. freedmani*, *Ce. bruneti* Pallas *et al.*, 2019 and *Microcolobus* Benefit and Pickford, 1986 (Table 11, Appendixes 13 and 14. OMO 222-1973-2751, OMO 70-10042, OMO 176-10006, L 7-15 and L 5/6-41 are more similar to *P. mutiwa* and *R. turkanaensis* (Appendix 13) in this respect than to the taxa mentionned above (Table 11). The morphology of the supra-articular fossae of extant *Colobus* and *Nasalis* shows a depth differential in favor of the radial fossa as in OMO 3/O-1968-1410 and F 500-1, whereas both fossae are deep in *Papio* (Table 11 and Appendix 5).

Deleted:

Comparative anatomy of the humeral distal epiphysis

Significant differences are observed between extant colobines and *Papio* spp. regarding the angulation of the medial epicondyle ($p < 0.01$, Fig. 10A), the relative projection of the medial epicondyle ($p < 0.05$, Fig. 10A), the relative anteroposterior dimension of the distal epiphysis ($p < 0.01$, Fig. 10B), and the relative anteroposterior dimension of the zona conoidea ($p < 0.01$, Fig. 10B). Extant colobines also differs from *Papio* spp. in having humeral pillars unequal in width ($p < 0.01$, Fig. 11A), and a moderate distal extension of the medial trochlear keels ($p < 0.01$, Fig. 11B).

OMO 3/O-1968-1410 is similar to terrestrial and semiterrestrial cercopithecids in exhibiting a deep articular surface at the level of zona conoidea (Fig. 10B), a robust medial pillar (Fig. 11A), acutely angled humeral pillars, a retroflexed medial epicondyle (Fig. 10A), and an

anteriorly projecting medial trochlear keel (Table 11). More precisely, OMO 3/O-1968-1410 present a relative depth of the articular surface at the level of zona conoidea of 50.12 and fits outside the range of variation of *Co. guereza*, *N. larvatus* and *S. entellus* but within that of *Papio* (μ = 49.2 ± 3.4, Table 11).

737

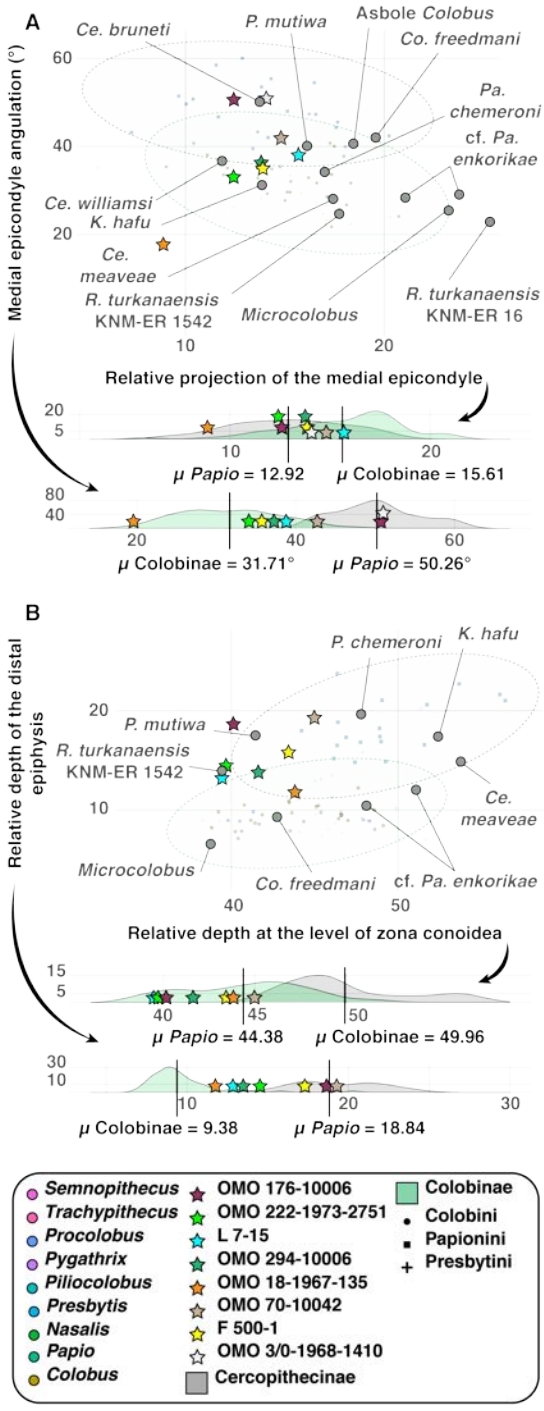
A
Ce. bruneti
P. mutiwa
Asbole Colobus
Co. freedmani
Pa. chemeroni
cf. Pa. enkorikae
Ce. williamsi
K. hafu
Ce. meaveae
R. turkanaensis KNM-ER 1542
Microcolobus
R. turkanaensis KNM-ER 16
Medial epicondyle angulation (°)
Relative projection of the medial epicondyle
μ Papio = 12.92
μ Colobinae = 15.61
μ Colobinae = 31.71°
μ Papio = 50.26°
B
P. chemeroni
K. hafu
P. mutiwa
R. turkanaensis KNM-ER 1542
Ce. meaveae
Microcolobus
Co. freedmani
cf. Pa. enkorikae
Relative depth of the distal epiphysis
Relative depth at the level of zona conoidea
μ Papio = 44.38
μ Colobinae = 49.96
μ Colobinae = 9.38
μ Papio = 18.84
Semnopithecus
Trachypithecus
Procolobus
Pygathrix
Piliocolobus
Presbytis
Nasalis
Papio
Colobus
OMO 176-10006
OMO 222-1973-2751
L 7-15
OMO 294-10006
OMO 18-1967-135
OMO 70-10042
F 500-1
OMO 3/0-1968-1410
Cercopithecinae
Colobinae
Colobini
Papionini
Presbytini

Fig. 10 (previous page). – Scatterplots of distal humeral indices of extant and extinct colobines and extant *Papio* spp. 95 % normal confidence ellipses (given a multivariate normal distribution) are drawn for colobines and *Papio* spp. Kernel density estimates are given for each axis below the scatterplots. A.) Regression of medial epicondyle angulation on the relative projection of the medial epicondyle in extant colobines (*n* = 51), *Papio* spp. (*n* = 19) and fossil colobines. The parameters of the linear model are as follows: R^2= 0.08, y= -0.82x+49.48, and B.) Relative anteroposterior dimensions of the humeral distal articular surface regressed on the relative anteroposterior dimension of the humeral distal articular surface at the zona conoïdea in extant colobines (*n* = 56), *Papio* spp. (*n* = 19) and fossil colobines. The parameters of the linear model are as follows: R^2= 0.20, y= 0.49x-9.93.

Commented [MOU19]: What are the p-values of the regressions ? With r-squared that low, are these even worth reporting ? There doesn't seem to nbe much of a relationship….

750

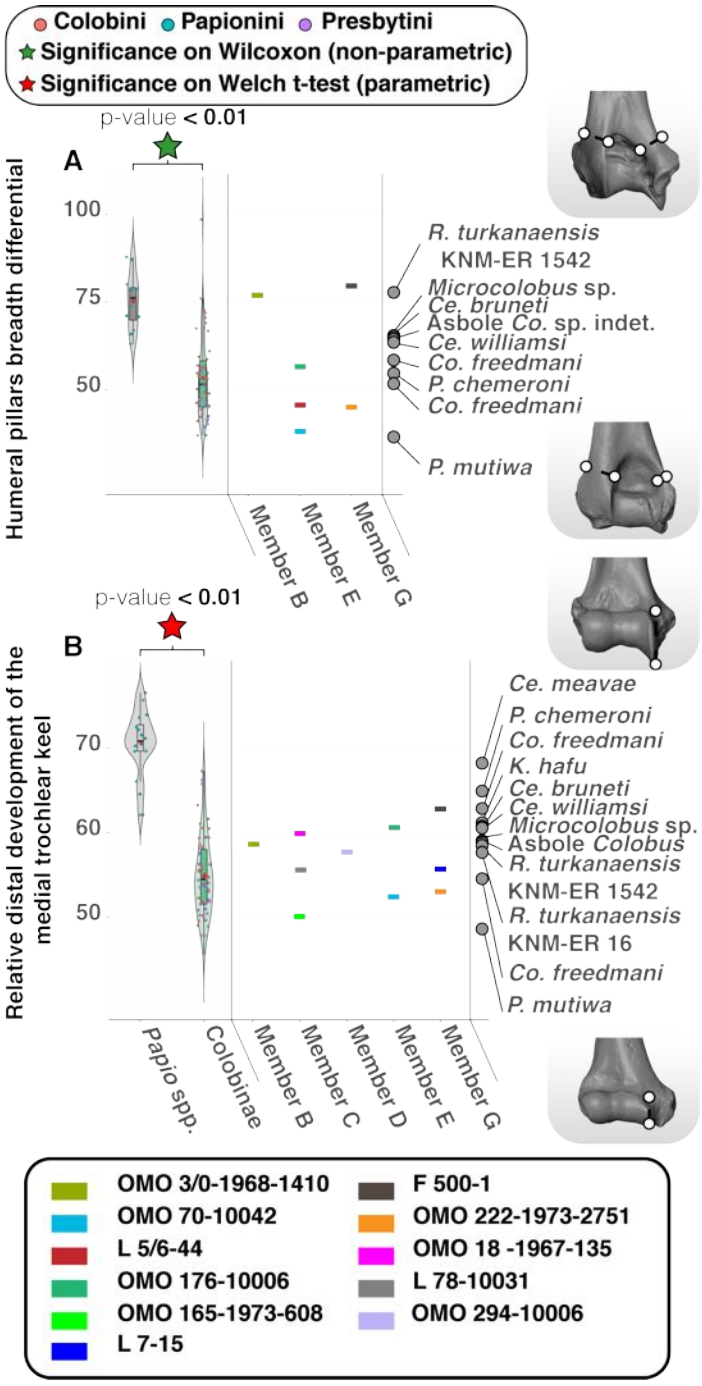
Colobini
Papionini
Presbytini
Significance on Wilcoxon (non-parametric)
Significance on Welch t-test (parametric)
p-value < 0.01
A
Humeral pillars breadth differential
100
75
50
R. turkanaensis
KNM-ER 1542
Microcolobus sp.
Ce. bruneti
Asbole Co. sp. indet.
Ce. williamsi
Co. freedmani
P. chemeroni
Co. freedmani
P. mutiwa
Member B
Member E
Member G
p-value < 0.01
B
Relative distal development of the medial trochlear keel
70
60
50
Ce. meavae
P. chemeroni
Co. freedmani
K. hafu
Ce. bruneti
Ce. williamsi
Microcolobus sp.
Asbole Colobus
R. turkanaensis
KNM-ER 1542
R. turkanaensis
KNM-ER 16
Co. freedmani
P. mutiwa
Papio spp.
Colobinae
Member B
Member C
Member D
Member E
Member G
OMO 3/0-1968-1410
OMO 70-10042
L 5/6-44
OMO 176-10006
OMO 165-1973-608
L 7-15
F 500-1
OMO 222-1973-2751
OMO 18 -1967-135
L 78-10031
OMO 294-10006

Fig. 11 (previous page). – Violin plots and boxplots of distal humeral morphometric indices of extant and extinct colobines and extant *Papio* spp. Morphologies associated with minimum and maximum values are shown on the right of the graph. A*.)* Humeral pillars breadth differential in extant colobines (*n* = 50), *Papio* spp. (*n* = 13), and fossil colobines, and B.) Relative distal development of the medial trochlear keel in extant colobines (*n* = 54), *Papio* spp. (*n* = 17) and fossil colobines. Means (red diamonds), medians (black rectangles), first quartile and third quartile plotted. When there are significant differences between taxa ($p < 0.05$), the associated *p*-values are given.

The relative robustness of its medial pillar (76.82) is also outside the range of variation of *Co. guereza*, *N. larvatus* and *S. entellus* but within that of *Papio* (μ = 75.1 ± 8.0, Table 11). Nevertheless, OMO 3/O-1968-1410 also has a large posterior trochlear articular surface, a poorly distally extended medial trochlear keel (Fig. 11B) and a globular capitulum that demonstrate a morphologically distinct humeroulnar and humeroradial joints compared to *Papio*. The mediolaterally restricted articular surface of OMO 3/O-1968-1410 and its anteroposterior depth at the level of zona conoidea are similar to *Cercopithecoides meaveae* Frost & Delson, 2002 and *K. hafu* but different from those of *Paracolobus mutiwa* and *Rhinocolobus turkanaensis* (Appendix 13).

Deleted: *meavae*

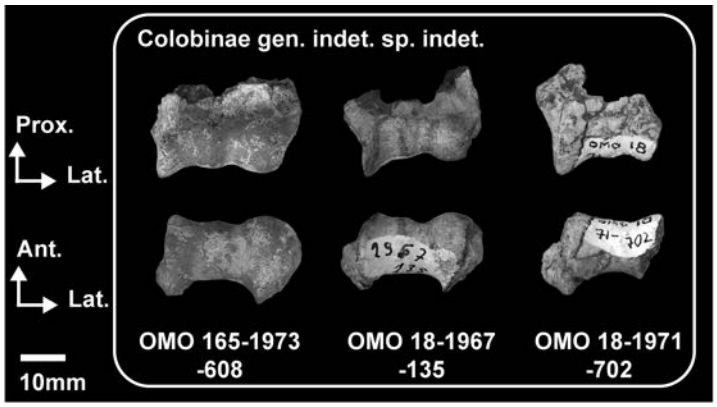

772 **Fig. 12**. – Photographs of the humeral anatomy of medium-sized colobines from Member C.
773 Scale: 10 mm. Abbreviations: Ant: Anterior, Lat: Lateral, Med: Medial, Prox: Proximal.
774
775 Most of the Omo colobines present medial epicondyles facing medially or slightly
776 posteriorly, as seen in extant colobines apart from *S. entellus*. OMO 176-10006 (Fig. 8) and
777 OMO 3/O-1968-1410 (Fig. 9) shows a condition very similar to *Ce. bruneti* and *S. entellus*
778 (Fig. 10A)
779
780

781 **Table 11. –** Qualitative and quantitative morphological observations of the distal humeral morphology of extant cercopithecids and early colobines.
782

Taxa (in bold, Omo taxa)	Coronoid fossa depth	Humeral pillars morphology (angulation and breadth differential)	Trochlea mediolateral enlargement	Medial trochlear keel anterior and distal extension	Anteroposterior (at the level of zona conoidea) depth of the distal articular surface	Shape of the capitulum and depth of the zona conoidea	Angulation and development of the medial epicondyle
[1]*R.* cf. *turkanaensis*	**Shallow**	**Angulated with a poor to moderate breadth differential**	**Moderately enlarged**	**Moderate to marked anterior and distal extensions**	**Shallow articular surface**	**Spherical and deep**	**Medialized and moderately developed**
[2]Colobinae gen. indet. and sp. indet.	**Shallow**	**NA.**	**Weakly enlarged**	**Moderate to marked anterior and distal extensions**	**Deep articular surface**	**Spherical and deep**	**Medialized and weakly developed**
[3]*P.* cf. *mutiwa*	**Deep**	**Angulated with a marked breadth differential**	**Moderate to markedly enlarged**	**Moderate to marked anterior and distal extensions**	**Shallow articular surface**	**Spherical and deep**	**Moderately retroflexed and markedly developed**
P. chemeroni	Shallow	Angulated with a marked breadth differential	Moderately enlarged	Moderate anterior and distal extensions	Deep articular surface	Spherical and deep	Medialized and moderately developed
P. mutiwa	Deep	Angulated with a marked breadth differential	Markedly enlarged	Moderate anterior and distal extensions	Shallow articular surface	Spherical and deep	Moderately retroflexed and markedly developed
Ce. williamsi	NA.	Angulated and possibly with a moderate breadth differential	Weakly enlarged	Marked anterior and distal extensions	Deep articular surface	Flat and shallow	Retroflexed and weakly developed
Ce. meaveae	NA.	Angulated with a marked breadth differential	Weakly enlarged	Marked anterior and distal extensions	Deep articular surface	Flat and shallow	Medialized and weakly developed
Ce. coronatus	NA.	Angulated with a moderate breadth differential	Weakly enlarged	Marked anterior and distal extensions	Deep articular surface	Spherical and deep	Retroflexed and weakly developed
Ce. bruneti	Shallow	Angulated with a poor breadth differential	Weakly enlarged	Marked anterior and distal extensions	Shallow articular surface	NA.	Retroflexed and weakly developed
R. turkanaensis	Shallow	Angulated with a poor breadth differential	Moderate to markedly enlarged	Moderate to marked anterior and distal extensions	Shallow articular surface	Spherical and deep	Medialized and markedly developed
K. hafu	Shallow	Straight with a marked breadth differential	Weakly enlarged	Moderate anterior and distal extensions	Deep articular surface	Spherical and deep	Medialized and weakly developed

Deleted: *meavae*

Deleted: *kimeui*

785 **Table 11 (following). –** Qualitative and quantitative morphological observations of the distal humeral morphology of extant cercopithecids and early colobines.
786

Taxa	Coronoid fossa depth	Humeral pillars morphology (angulation and breadth differential)	Trochlea mediolateral enlargement	Medial trochlear keel anterior and distal extension	Anteroposterior (at the level of zona conoidea) depth of the distal articular surface	Shape of the capitulum and depth of the zona conoidea	Angulation and development of the medial epicondyle
Co. freedmani	Shallow	Angulated with a moderate breadth differential	Markedly enlarged	Marked anterior and distal extensions	Shallow articular surface	Spherical and deep	Moderately retroflexed and markedly developed
Microcolobus sp.	Shallow	Straight with a marked breadth differential	Markedly enlarged	Moderate anterior and distal extensions	Shallow articular surface	Spherical and deep	Medialized and markedly developed
Co. sp. indet. Asbole	Shallow	Angulated with a moderate breadth differential	Markedly enlarged	Moderate anterior and distal extensions	Shallow articular surface	Spherical and deep	Medialized and markedly developed
Colobus spp.	Shallow	Angulated with a moderate to marked breadth differential (μ = 54.6 ± 11.9, *n* = 16; Figure 11A)	Markedly enlarged	Shallow anterior extension, and moderate distal extension (μ = 54.4 ± 4.4, *n* = 16; Figure 11B)	Shallow articular surface (μ = 44.0 ± 3.4, *n* = 16; Figure 10B)	Spherical and deep	Medialized (μ = 32.8 ± 4.4°, *n* = 16; Figure 10A), and markedly developed epicondyle (14.9 ± 2.7, *n* = 16; Figure 10A)
Nasalis larvatus	Shallow	Straight with a marked breadth differential (μ = 41.2 ± 11.9, *n* = 6; Figure 11A)	Weakly enlarged	Shallow anterior extension, and shallow distal extension (μ = 52.0 ± 3.3, *n* = 6; Figure 11B)	Deep articular surface (μ = 46.6 ± 2.8, *n* = 6; Figure 10B)	Spherical and deep	Medialized (μ = 28.3 ± 3.7°, *n* = 6; Figure 10A), and weakly developed epicondyle (μ = 12.6 ± 4.0, *n* = 6; Figure 10A)
Semnopithecus spp.	Shallow	Angulated with a moderate to marked breadth differential (μ = 55.4 ± 6.2, *n* = 5; Figure 11A)	Weakly enlarged	Moderate to marked anterior extension, and moderate to marked distal extension (μ = 66.6 ± 1.3, *n* = 5; Figure 11B)	Deep articular surface (μ = 47.3 ± 2.5, *n* = 5; Figure 10B)	Spherical and shallow	Moderately retroflexed epicondyle (μ = 36.4 ± 7.0°, *n* = 3; Figure 10A), and moderately developed epicondyle (μ = 16.7 ± 1.8, *n* = 3; Figure 10A)
Papio spp.	Deep	Straight with a poor breadth differential (μ = 75.1 ± 8.0, *n* = 12; Figure 11A)	Weakly to moderately enlarged	Marked anterior extension, and marked distal extension (μ = 70.6 ± 3.8, *n* = 16; Figure 11B)	Deep articular surface (μ = 49.2 ± 3.4, *n* = 18; Figure 10B)	Flat and shallow	Retroflexed epicondyle (μ = 49.7 ± 5.3°, *n* = 18; Figure 10A), and weakly developed epicondyle (μ = 13.6 ± 3.3, *n* = 3; Figure 10A)

787 [1]*R.* cf. *turkanaensis* indet. include F 500-1.
788 [2] Colobinae gen. indet. sp. indet. include the following specimens: OMO 165-1973-608, OMO 18-1967-135 and OMO 18-1971-702.
789 [3]*P.* cf. *mutiwa* include the following specimens: OMO 70-10042, OMO 222-1973-2751, OMO 176-10006, L 7-15 and L 5/6-41.

Variation in the size of the medial epicondyle is observed in the Omo colobines. OMO 18-1967-135 (Fig. 12 and Appendix 15) and OMO 176-10006 (Fig. 8 and Appendix 9) illustrate extrema of this range of variation with shortened and well-developed medial epicondyles, respectively. Quantitatively, the shortened medial epicondyle of OMO 18-1967-135 is comparable to *N. larvatus* (Fig. 10A and Appendix 16A), *K. hafu* and *P. chemeroni* while the large medial epicondyle of OMO 176-10006 is reminiscent of the condition seen in extant Colobini and *P. mutiwa* (Fig. 10A and Appendix 16A). In anterior view, the medial epicondyles of OMO 176-10006, OMO 222-1973-2751 and L 7-15 are especially large and show a distinct proximal projection on their superomedial aspects, as also seen in *P. mutiwa* (Fig. 8 and Appendix 13).

The capitular tails of L 7-15 and OMO 222-1973-2751 are large and have distinct lateral projections in anterior view (Figure 8). A particular large capitular tail is also observed in *S. entellus* (Appendix 5).

Despite marked differences in absolute dimensions (Table 12 and Appendix 41), OMO 176-10006 (Fig. 8) and OMO 18-1967-135 (Fig. 12) both have distally extended medial trochlear keels in anterior view (Fig. 11B) and posteriorly projected lateral humeral pillars in inferior view, as also seen frequently in *S. entellus* and *Ce. williamsi* (Appendix 5 and 13), but seldom in *Co. guereza* and *N. larvatus* (Appendix 5). Indeed, with an index value of 60.6, OMO 176-10006 is outside the normal range of variation of *Co. guereza* ($\mu = 54.4 \pm 4.4$, Table 11) but fits with outlying *Co. guereza* specimens of our sample (e.g., the male *Co. guereza* MNHN 1904-1963).

A deep zona conoidea and a globular capitulum are seen in all Omo specimens but OMO 294-10006 (Fig. 9). The zona conoidea is well excavated in *N. larvatus* compared to the shallow zona conoidea of *S. entellus* (Appendix 5), and specimens of the latter taxa match the shallowness of the zona conoidea of OMO 294-10006 (Appendix 5). Relatively shallow zona conoidea are also observed in *Ce. williamsi* and *Ce. meaveae* (Appendix 13 and 14, and Table 11).

Narrow trochleae (i.e., weakly enlarged in Table 11) are observed in OMO 18-1967-135, OMO 18-1971-702 and OMO 165-1973-608 (Fig. 12), and contrasts with the enlarged trochlea of OMO 176-10006, L 7-15 and OMO 222-1973-2751 (Table 11). An enlarged trochlea is seen in *Co. guereza* in contrast with the mediolaterally short trochlea of *N. larvatus* and *S. entellus* (Table 11 and Appendix 5).

Proximally extended olecranon fossae, gracile medial pillars and acutely angled pillars are seen in all Omo specimens but OMO 3/O-1968-1410 (Fig. 9 and Table 11). Gracile (mediolaterally shortened) medial pillars are observed in most extant and early colobines (Fig. 11A and Table 11). *R. turkanaensis* and F 500-1, like OMO 3/O-1968-1410, stand apart from

Deleted: s

Formatted: Indent: First line: 0,5 cm

Deleted: ¶

Deleted:

Deleted: *meavae*

this pattern by having pillars of equal width (i.e., poor pillar breadth differential in Table 11) and a clear buttressing of the medial pillar compared to other colobines (Fig. 11A).

Table 12. – Measurements (in mm) of the distal humeral specimens

Specimens	HRJML	CML	CSI	TML	TSI	DJML	DJML2	BIEPIC	OFSI
OMO 165-1973-608	14.1	10.3	12.3	11.5	14.6	25.9	30.1		
OMO 1967-135	13.7	9.8	10.8	9.4	16.1	23.4	27.7	29.7	
OMO 18-1971-702				11.4	15.5				
OMO 3/0-1968-1410	15.9	11.4	16.4	11.9	16.5	28.1	32.7	36.9	13.3
L 78-10031	~15.3	~11.8	15.3	14.0	~16.9	30.4	37.4	40.8	
OMO 294-10006	15.1	12.3	15.9	13.9	17.1	29.6	~35.4	41.1	
OMO 176-10006	20.1	13.6	18.0	16.8	22.6	37.2	43.0	49.1	19.4
OMO 70-10042	17.1	12.3	16.1	13.8	16.3	31.1	33.5	39.3	15.7
L 5/6-41									18.8
L 7-15	15.8	11.2	14.1	14.0	18.1	32.5	36.4	41.5	17.5
F 500-1	>18.1	>12.3	16.0	14.9	20.7	>32.9	38.2	44.6	14.4
OMO 222-1973-2751	17.3	13.2	16.5	16.7	18.1	34.2	39.3	44.9	16.3

Table 12 (following). – Measurements (in mm) of the distal humeral specimens

Specimens	OFML	LPillML	MPillML	LPMxAP	MPMxAP	ZCMinAP	MEAng (°)	DeltAP	DeltML
OMO 165-1973-608	14.5					15.9			
OMO 1967-135				18.5	16.0	10.3	17.7°		
OMO 18-1971-702									
OMO 3/0-1968-1410		11.1	8.5		23.4	14.1	51.1°	17.8	17.9
L 78-10031						12.8			
OMO 294-10006	~17.3	11.0		24.0	20.7	14.7	36.5°		
OMO 176-10006	18.9	15.0	8.4	25.8	27.1	14.9	50.7°		
OMO 70-10042	16.4	14.6	5.7	21.6	22.4	14.9	42.1°		
L 5/6-41	20.7	~14.8	6.7			14.4			
L 7-15	19.7	13.8	3.8	22.6	>19.1	12.8	38.2°		
F 500-1	19.8	10.1	8.0	23.9	21.8	14.3	35.1°	17.6	22.1
OMO 222-1973-2751	18.4	15.3	6.9	22.4	22.1	13.6	33.2°	19.4	19.4

Comparative anatomy of the ulnar proximal epiphysis and diaphysis

The proximal ulnar and diaphyseal anatomy of the Omo colobines is represented by specimens of various dimensions (Appendix 42) from Usno (B-818A) and Shungura members B (P 732-1), C (L 293-10004, L 107-4, L 32-144 and L 373-3), and E (L 236-1a and OMO 57/4-1972-164).

We found significant differences between *Papio* spp. and extant colobines for the proximal projection of the olecranon process ($p < 0.01$, Fig. 14A), notably with *Nasalis* and *Pygathrix*

showing a shorter olecranon compared to extant baboons and other colobines (Appendix 17). The olecranon process of *Papio* is also significantly more retroflexed than that of extant colobines ($p < 0.01$, Fig. 14B), and the lateral projection of the coronoid and radial notch is significantly more pronounced in *Papio* than in extant colobines ($p < 0.01$, Fig. 14C).

Absolutely (Fig. 13 and Table 13) and relatively (Fig. 14A) short olecranon processes are present in OMO 57/4-1972-164 and L 373-3, similar to the shortened olecranon of the odd-nosed monkeys *Nasalis* and *Pygathrix* (Table 14, Appendix 17B, and see also Su & Jablonski 2009), but distinct from extant baboons and *Co. guereza* (Table 14 and Appendix 18). Indeed, L 373-3 (with an index value of 65.82) and OMO 57/4-1972-164 (with an index value of 75.94) have index values much closer to the range of variation of *N. larvatus* ($\mu = 70.7 \pm 9.7$, Table 14, and Appendix 17B) than that of *Co. guereza* ($\mu = 94.6 \pm 12.0$, Table 14, and Appendix 17B). Shortened olecranon processes are also observed in *Ce. bruneti* (Appendix 19), *P. chemeroni*, *K. hafu* and *R. turkanaensis* (Fig. 14A and Appendix 20). The proximal part of the olecranon of OMO 57/4-1972-164 and L 373-3 is also oriented posteriorly (i.e., retroflexed, see Fig. 14B, Table 14 and Appendix 17A). Whereas the olecranon of *Papio* spp. is significantly more retroflexed than that of extant colobines (Fig. 14B), the olecranon of the suspensory *Nasalis larvatus* and *Pygathrix nemaeus* is more retroflexed than that of the arboreal quadrupeds *Colobus* and *Trachypithecus* (Appendix 17A). Overall, the morphology of the olecranon processes of OMO 57/4-1972-164 and L 373-3 matches that of suspensory colobines by presenting a short and slightly retroflexed olecranon (Table 14, and Appendix 17 and 18).

868 **Table 13. –** Measurements (in mm) of the ulnar specimens

Specimens	SNSI	SNDP	OPAP	OPML	OPSI	OlecAng	APML	APAP	CPML	CPAP	CPRNML	SNAPMh	RNAP	RNSI
B 818c			15.1		15.7		11.0	~18.9				10.7		>8.4
P 732-1	13.1		15.0		13.2							11.3		
L 236-1a	17.2	10.7	19.7	16.9	22.7	50.0°	16.1	27.6	13.4	31.8	26.7	16.7	20.8	13.7
L 293-10004	16.6	9.7	16.5	~11.2	16.2	55.0°	10.6	20.9	8.9	>22.9	16.0	13.0	>14.7	10.1
L 107-4	17.3	10.8	25.2	18.3	25.8	56.7°	16.4	33.6	18.3	35.9	26.2	22.8	20.6	10.7
L 373-3	15.8	10.3	16.9		10.4	61.4°	11.3	19.6	10.0		18.6	11.6	>13.1	10.5
OMO 57/4-1972-164	16.0	9.1	19.0	14.6	12.1	59.2°	15.1	22.2	12.1	24.6	22.3	13.7	17.4	
F 255-8	14.6	9.6	16.0	~9.8	16.1	62.0°	13.0	21.5	10.4	21.2	~19.3	12.5	>15.3	~10.0
L 32-144	15.8	10.0	16.8		>16.1	56.6°	11.8	22.0	11.1	22.0	18.9	13.6	16.8	10.4

869
870
871

872 **Table 14. –** Qualitative and quantitative morphological observations of the ulnar anatomy of extant cercopithecids and early colobines.
873

Taxa (in bold, Omo taxa)	Diaphyseal and olecranon angulations in the sagittal plane	Olecranon process proximal projection	Anconeal process asymmetry	Coronoid articular surface width and orientation	Radial notch subdivision
[1]*R.* cf. *turkanaensis*	**Straight diaphysis, and slight olecranon retroflexion**	**Poor projection**	**Poor**	**Absence of marked differential in width of the articular surface along its length, and poor to moderate distal slanting**	**Absent**
[2]*P.* cf. *mutiwa*	**Straight diaphysis, and straight olecranon**	**Marked projection**	**Moderate**	**Presence of a marked to moderate differential in width of the articular surface along its length, and moderate to marked distal slanting**	**Moderate (L 293-10004) and marked subdivision (L 236-1a)**
P. chemeroni	Straight diaphysis, and straight olecranon	Moderate projection	Poor	Presence of a moderate differential in width of the articular surface along its length, and moderate distal slanting	Absent
P. mutiwa	NA.	NA.	NA.	NA.	Marked subdivision
Ce. williamsi	Curved diaphysis (posterior concavity), and retroflexed olecranon	Poor projection	Marked	Absence of a marked differential in width of the articular surface along its length, and marked distal slanting	Marked subdivision
Ce. meaveae	Retroflexed olecranon	Moderate projection	Moderate	Absence of a marked differential in width of the articular surface along its length, and moderate distal slanting	Moderate subdivision
Ce. coronatus	NA.	NA.	Moderate	NA.	Marked subdivision
Ce. bruneti	Straight diaphysis, and straight olecranon	Poor projection	Moderate	NA.	Moderate subdivision
R. turkanaensis	Straight diaphysis, and straight olecranon	Moderate projection	Poor	Presence of a moderate differential in width of the articular surface along its length, and moderate distal slanting	Absent
Co. freedmani	Curved diaphysis (anterior concavity), and anteflexed olecranon	Marked projection	Poor	Marked differential in width of the articular surface along its length, and poor distal slanting	Absent
Microcolobus sp.	Curved diaphysis (anterior concavity), and anteflexed olecranon	Marked projection	Poor	Moderate differential in width of the articular surface along its length, and poor distal slanting	Absent
Co. sp. indet. Asbole	Curved diaphysis (anterior concavity), and anteflexed olecranon	Marked projection	Poor	Marked differential in width of the articular surface along its length, and poor distal slanting	Moderate subdivision

Deleted: *meavae*

Deleted: *kimeui*

Table 14 (following). – Qualitative and quantitative morphological observations of the ulnar anatomy of extant cercopithecids and early colobines.

Taxa	Diaphyseal and olecranon angulations in the sagittal plane	Olecranon process proximal projection	Anconeal process asymmetry	Coronoid articular surface width and orientation	Radial notch subdivision
Colobus spp.	Curved diaphysis (anterior concavity), and anteflexed olecranon (μ = 38.7 ± 5.0°, *n* = 20; Figure 13B)	Moderate to marked projection (μ = 94.6 ± 12.0, *n* = 19; Figure 13A)	Poor	Marked to moderate differential in width of the articular surface along its length, and poor to moderate distal slanting	Absent to moderate subdivision
Nasalis larvatus	Straight diaphysis, and straight to moderate retroflexion of the olecranon (μ = 48.4 ± 3.4°, *n* = 9; Figure 13B)	Poor projection (μ = 70.7 ± 9.7, *n* = 7; Figure 13A)	Poor	Moderate differential in width of the articular surface along its length, and poor distal slanting	Absent
Semnopithecus spp.	Straight diaphysis, and straight to moderate retroflexion of the olecranon (μ = 50.8 ± 5.5°, *n* = 7; Figure 13B)	Marked projection (μ = 110.7 ± 12.6, *n* = 4; Figure 13A)	Moderate	Marked differential in width of the articular surface along its length, and moderate to marked distal slanting	Moderate to marked subdivision
Papio spp.	Straight to curved diaphysis (posterior concavity), and retroflexed olecranon (μ = 60.3 ± 4.9°, *n* = 30; Figure 13B)	Marked projection (μ = 118.7 ± 11.3, *n* = 12; Figure 13A)	Marked	Marked differential in width of the articular surface along its length, and marked distal slanting	Marked subdivision

[1]*R.* cf. *turkanaensis* indet. include the following specimens: L 373-3 and OMO 57/4-1972-164.

[2]*P.* cf. *mutiwa* include the following specimens: L 107-4, L 236-1a, L 293-10004 and L 32-144.

Long and straight olecranon processes are observed in L 107-4, L 236-1a, and L 293-10004 (Figs 13; 14A; 14B). As such, these specimens are reminiscent of climbers and semiterrestrial primates such as *Semnopithecus entellus* (Appendix 18). Indeed, the relatively long olecranon of L 107-4 (with an index value of 149.13), L 236-1a (with an index value of 131.55) and L 293-10004 (with an index value of 97.89) are closer to *S. entellus* (μ = 110.7 ± 12.6) than to *Co. guereza* and *N. larvatus* (Table 14). The moderate proximal extension and slight retroflexion of the olecranon process of L 32-144 (Appendix 21) is also more consistent with the morphology of L 236-1a and L 293-10004 than that of L 373-3 and OMO 57/4-1972-164 (Fig. 13). None of the Omo colobines have an anteflexed olecranon, contrary to the marked anteflexion of some of their extant (*Trachypithecus* and *Colobus* in Appendix 17 and 19) and fossil counterparts (*Co. freedmani* and *Microcolobus* in Appendix 19). With a straight and moderately long olecranon process, B-818A and P 732-1 (Appendix 21) present an olecranon morphology intermediate between that of L 373-3 and L 107-4 (Fig. 14A).

Fig. 13. – Photographs of the ulnar anatomy of presumed *Rhinocolobus* and *Paracolobus* specimens from Shungura. Scale: 10 mm. Abbreviations: Ant: Anterior, Lat: Lateral, Med: Medial, Prox: Proximal.

None of the Omo colobines show an asymmetry of the anconeal process as pronounced as that of *Papio* and *Cercopithecoides williamsi* (Table 14, Appendix 18 and 20). A substantial elevation of the lateral crest of the anconeal compared to the medial crest of the anconeal is nonetheless visible in L 236-1a and L 107-4. The asymmetry of the anconeal process of L 236-1a and L 107-4 (Fig. 13 and Appendix 22) is more pronounced than that of *P. chemeroni*, *Ce. meaveae* and OMO 57/4-1972-164 (Fig. 13 and Appendix 23).

Deleted: *meavae*

911

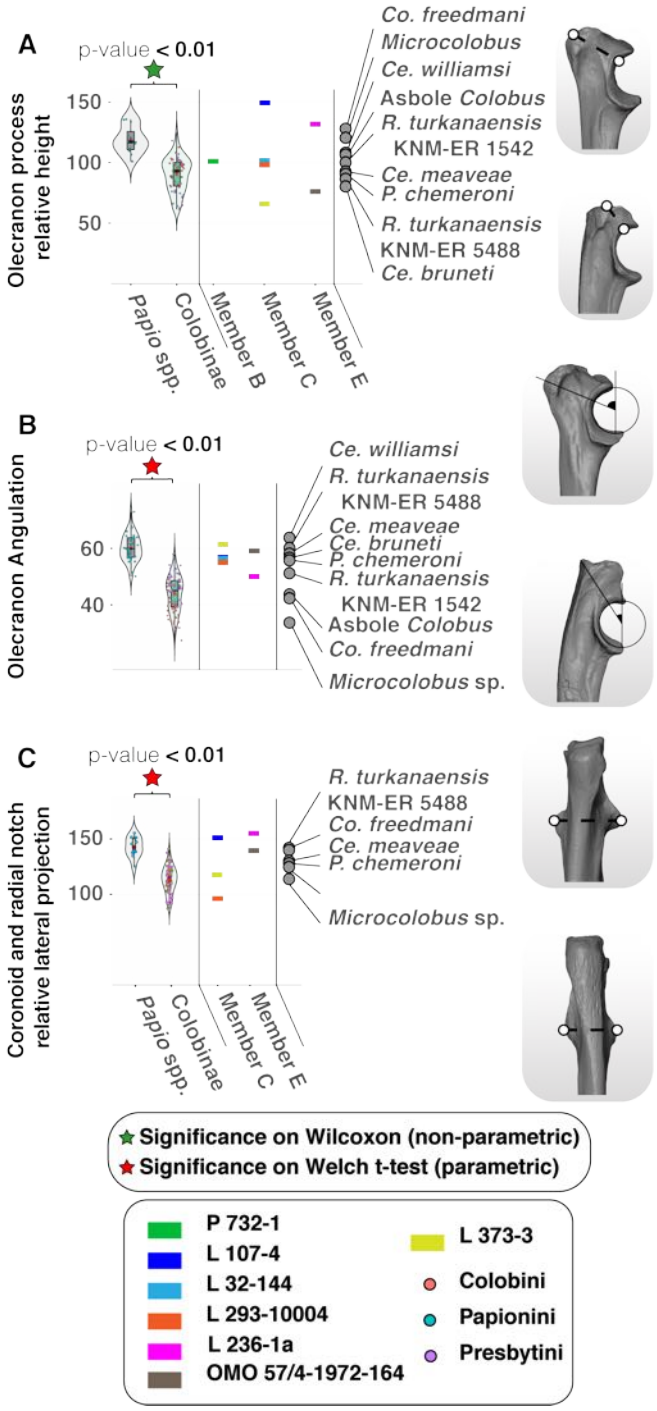
A
p-value < 0.01
Olecranon process relative height
150
100
50
Papio spp.
Colobinae
Member B
Member C
Member E
Co. freedmani
Microcolobus
Ce. williamsi
Asbole Colobus
R. turkanaensis
KNM-ER 1542
Ce. meaveae
P. chemeroni
R. turkanaensis
KNM-ER 5488
Ce. bruneti
B
p-value < 0.01
Olecranon Angulation
60
40
Ce. williamsi
R. turkanaensis
KNM-ER 5488
Ce. meaveae
Ce. bruneti
P. chemeroni
R. turkanaensis
KNM-ER 1542
Asbole Colobus
Co. freedmani
Microcolobus sp.
C
p-value < 0.01
Coronoid and radial notch relative lateral projection
150
100
Papio spp.
Colobinae
Member C
Member E
R. turkanaensis
KNM-ER 5488
Co. freedmani
Ce. meaveae
P. chemeroni
Microcolobus sp.
Significance on Wilcoxon (non-parametric)
Significance on Welch t-test (parametric)
P 732-1
L 107-4
L 32-144
L 293-10004
L 236-1a
OMO 57/4-1972-164
L 373-3
Colobini
Papionini
Presbytini

Fig. 14 (previous page). – Violin plots and boxplots of proximal ulna morphometric indices of extant and extinct colobines and extant *Papio* spp. Morphologies associated with minimum and maximum values are shown on the left of the graph. A.) Relative height of the olecranon process height in extant colobines (n = 55), *Papio* spp. (n = 13) and fossil colobines, B.) Angulation of the olecranon in extant colobines (n = 76), *Papio* spp. (n = 31) and fossil colobines, and C.) Relative expansion of the coronoid and radial notches in extant colobines (n = 54), *Papio* spp. (n = 11) and fossil colobines. Means (red diamonds), medians (black rectangles), first quartile and third quartile are plotted. When there are significant differences between taxa ($p < 0.05$), the associated p-values are given.

Whereas the relief of the anconeal in anterior view is smooth in OMO 57/4-1972-164, *P. chemeroni* and *Ce. meaveae* (Appendix 20), the inferior articular surface of the anconeal is sharply angled in *R. turkanaensis* KNM-ER 1542 (Appendix 20). This marked angulation of the articular surface in anterior view is also seen in the suspensory colobine *N. larvatus* (Appendix 18).

At mid-height of the sigmoid notch, the epiphysis is lengthened anteroposteriorly in L 107-4, L 236-1a and *P. mutiwa* (Appendix 20), but contrast with the lightly built notch of OMO 57/4-1972-164 and L 373-3. The shaft is gracile in *N. larvatus* (Appendix 18), *R. turkanaensis* and *P. chemeroni* (Appendix 20) when compared with L 107-4 (Fig. 13), and *Co. guereza* (Appendix 18).

In L 373-3, the radial notch is large and undivided, whereas moderate (e.g., L 293-10004) to mark subdivisions (e.g., L 236-1a) are seen on other specimens. The marked subdivision of the radial notch of L 236-1a is akin to that of *P. mutiwa* and *Ce. williamsi* (Appendix 20). The undivided notch of L 373-3 is reminiscent of *R. turkanaensis*, *Microcolobus* and *Nasalis larvatus*. In addition, the posterior part of the notch is laterally projected and anteriorly facing in L 236-1 and L 107-4 (Fig. 14C and Appendix 22). Such a projection is also seen in *Papio* spp., *Ce. meaveae*, *R. turkanaensis* and *P. mutiwa* but is not characteristic of extant colobines (Fig. 14C).

The coronoid and anconeal processes of L 107-4 and L 236-1a project anteriorly to a greater extent than that of OMO 57/4-1972-164 and L 373-3. Such projections give a great depth to the sigmoid notch, as also seen in *Co. guereza* and *S. entellus* (Appendix 18) but unlike *N. larvatus* (Appendix 18) and *P. chemeroni* (Appendix 20). None of the Omo colobines and other large Plio-Pleistocene colobines present a more projected anconeal process compared to the coronoid process, as seen in suspensory colobines (see *N. larvatus* in Appendix 18).

Commented [MOU20]: I would argue that this is really capturing the relative LENGTH of the olecranon, not the HEIGHT, which is usaully described in relation to its proximal extension. You would expect colobines (and arboreal quadrupeds more generally) to have a more proximally extended or TALLER olecranon process above the sigmoid notch, even if Papio has a relatively long olecranon because it is retroflexed posteriorly. So I would just change the terms here and it might be nice to add in a measure capturing the proximal extension of the olecranon above the sigmoid notch, i.e., olecranon HEIGHT. The angulation measure is somewhat capturing this, but maybe a height linear measure in the proximal direction would be helpful as well ?

Deleted: *meavae*

Deleted: *meavae*

The posterior portion of the coronoid process is enlarged in L 107-4 (Appendix 22) relative to its anterior portion, as in *P. chemeroni* and *Microcolobus* (Appendix 19 and 20). A more even mediolateral expansion of the coronoid is seen in OMO 57/4-1972-164 (Appendix 23), *R. turkanaensis*, *P. mutiwa* and *Ce. williamsi* (Appendix 20).

The shaft of L 107-4 is curved in the coronal plane, contrasting with the straighter shaft of L 373-3. The coronally curved shaft of L 107-4 is similar to that of *Ce. williamsi* (Appendix 20), but contrast from it by presenting a straight shaft in the sagittal plane (Table 14 and Appendix 20).

We did not observe a pronounced concavity for the attachment sites of the digital flexors and extensors on L 373-3. This morphology contrasts with that of *S. entellus* and *Co. guereza*, but is similar to *N. larvatus* (Appendix 18). A pronounced concavity is visible on the lateral side of the shaft of L 107-4 and is reminiscent of the morphology of *Co. guereza* and *S. entellus* (Appendix 18).

A slit-like depression, extended distally, marks the attachment of the *m. brachialis* in L 373-3. The *m. brachialis* is less excavated and distally extended in the comparatively larger specimen L 107-4 and L 236-1a (Appendix 22 and 23). The shape of the *m. brachialis* enthesis of L 373-3 is more similar to *N. larvatus* and *Co. guereza* than that of *S. entellus* and *Papio* (Appendix 18).

Comparative anatomy of the radial proximal epiphysis and diaphysis

We identified two large-sized radial specimens from the Member E (L 236-1b) and upper part of Member G (OMO 2-10029). Both specimens show well-preserved proximal radial anatomy (Fig. 15) and correspond in absolute dimensions to *Ce. coronatus*, *Ce. williamsi* and *P. chemeroni* (Table 15 and Appendix 43).

A large part of the diaphysis is preserved in OMO 2-10029 (Fig. 15 and Appendix 24). Its well-angulated shaft is similar to extant colobines and differs from the rod-shaped diaphysis of terrestrial cercopithecids and *Ce. williamsi* (Appendix 26 and Table 16). The proximal portion of the shaft of OMO 2-10029 is noticeably more curved than *P. chemeroni* (Appendix 26). The interosseous crest of OMO 2-10029 is weakly developed as in extant colobines and differs from the blade-like morphology seen in *Papio*, *P. mutiwa* and *Ce. williamsi* (Table 16 and Appendix 25 and 26). This is well evidenced by the comparison of the elliptical cross-sectional shape of the mid-diaphysis of OMO 2-10029 (Appendix 24) which contrasts with the fairly triangular shape cross-section of *Papio hamadryas* (Appendix 25).

A significant difference is observed in relative elongation of the radial neck between *Papio* and extant colobines ($p < 0.01$, Fig. 16A). The elongated radial neck of OMO 2-10029 and L

Deleted: s

Deleted: *kimeui*

Deleted:

236-1b matches that of extant colobines and differs from the short neck of extant *Papio* spp. (Fig. 16A).

Specimens OMO 2-10029 and L 236-1a also differ in the morphology of the peripheral articular margin of the radial head. The peripheral margin of the head, particularly its anteromedial part, is markedly beveled in OMO 2-10029 while this bevel is less expressed in L 236-1a (Fig. 15 and Table 16). The beveled margin of the radial head of OMO 2-10029 corresponds well to the morphology of *Ce. coronatus* (Appendix 26) and *N. larvatus* (Appendix 25).

Deleted: *kimeui*

The radial head shape of extant cercopithecids is variable although a more elliptical shape is observed in extant colobines compared to the rounded head of extant *Papio* spp., with a significant difference between both groups ($p < 0.01$, Fig. 16B). None of the Omo colobines have the elliptical head characteristic of *Colobus* spp. (Birchette 1982, Fig. 16B), and are more consistent with the condition typical of *Papio* spp., *Ce. coronatus* and *Ce. williamsi* (Fig. 16B).

Deleted: *kimeui*

The radial neck of extant colobines is elliptical in transverse cross-section and differs significantly from the more rounded neck of extant *Papio* spp. ($p < 0.01$, Fig. 16C). In cross-section, the radial necks of OMO 2-10029 and L 236-1a are more elliptical than those of extant *Papio* spp. and fall on the interquartile range of extant colobines (Fig. 16C).

Fig. 15. – Photographs of the radial anatomy of colobines from Shungura. Abbreviations: Ant: Anterior, Med: Medial, Lat: Lateral, Prox: Proximal, Post: Posterior. Scale: 20 mm.

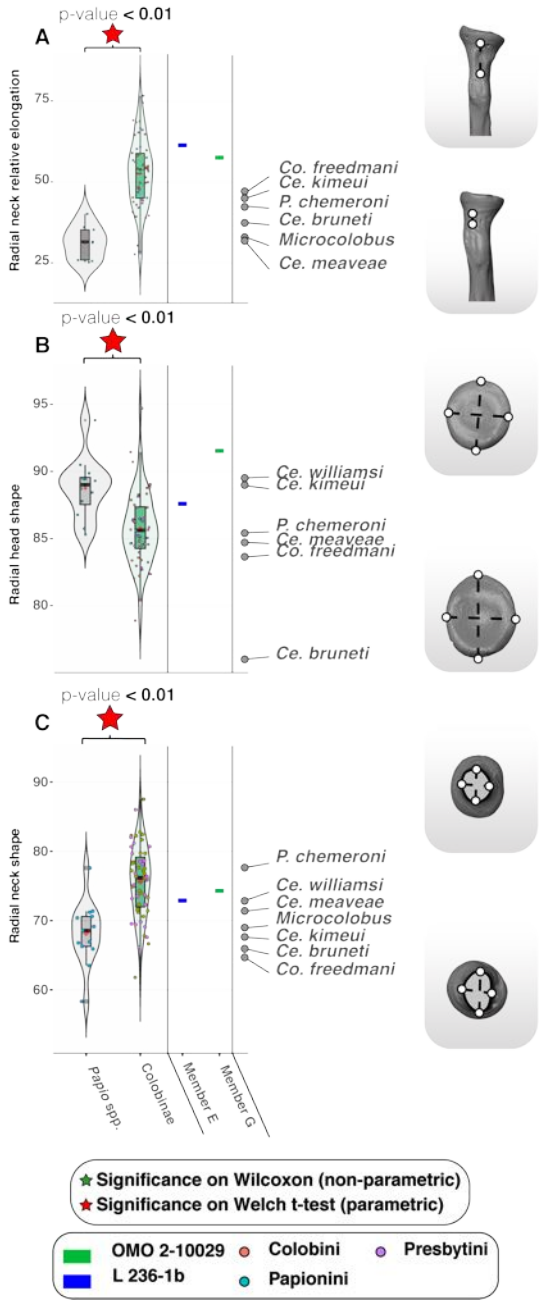
p-value < 0.01
A
Radial neck relative elongation
75
50
25
Co. freedmani
Ce. kimeui
P. chemeroni
Ce. bruneti
Microcolobus
Ce. meaveae
p-value < 0.01
B
Radial head shape
95
90
85
80
Ce. williamsi
Ce. kimeui
P. chemeroni
Ce. meaveae
Co. freedmani
Ce. bruneti
p-value < 0.01
C
Radial neck shape
90
80
70
60
P. chemeroni
Ce. williamsi
Ce. meaveae
Microcolobus
Ce. kimeui
Ce. bruneti
Co. freedmani
Papio spp.
Colobinae
Member E
Member G
Significance on Wilcoxon (non-parametric)
Significance on Welch t-test (parametric)
OMO 2-10029
L 236-1b
Colobini
Papionini
Presbytini

1011

Fig. 16 (previous page). – Violin plots and boxplots of proximal radius morphometric indices of extant and extinct colobines and extant *Papio* spp. Morphologies associated with minimum and maximum values are shown on the right and left of the graphs. A.) Relative elongation of the radial neck in extant colobines (n = 55), *Papio* spp. (n = 10) and fossil colobines, B.) Radial head shape in extant colobines (n = 52), *Papio* spp. (n = 13) and fossil colobines, and C.) Radial neck shape in extant colobines (n = 54), *Papio* spp. (n = 14) and fossil colobines. Means (red diamonds), medians (black rectangles), first quartile and third quartile are plotted. When there are significant differences between taxa ($p < 0.05$), the associated p-values are given.

Table 15. – Measurements (in mm) of the radial specimens

Specimens	RNShA	RNLgA	RaNSI	BPExt	BBLA	RHShA	RHLgA
L 236-1b	10.4	14.3	11.7			19.1	21.0
OMO 2-10029	9.8	13.2	10.7	12.2	36.0	18.3	21.0

Table 16. – Qualitative and quantitative morphological observations of the proximal radius of extant cercopithecids and early colobines.

Taxa (in bold, Omo taxa)	Radial shaft angulation and development of the interosseous crest	Radial head bevel (development and extension)	Radial neck extension
[1]*R.* cf. *turkanaensis*	**Angulated shaft, and poorly developed crest**	**Marked and extensive bevel**	**Long**
[2]*P.* cf. *mutiwa*	**NA.**	**Marked and localized bevel**	**Moderately long**
P. chemeroni	Straight shaft, and moderately developed crest	Marked and localized bevel	Moderately long
P. mutiwa	Straight shaft[3], and well-developed crest	NA.	NA.
Ce. williamsi	NA.	Marked and localized bevel	Short
Ce. meaveae	NA.	Marked and localized bevel	Moderately long
Ce. coronatus	Straight	Marked and extensive bevel	Long
Ce. bruneti	Straight shaft, and poorly developed crest	Marked and localized bevel	Short
Co. freedmani	Angulated shaft, and moderately developed crest	Marked and localized bevel	Moderately long
Microcolobus sp.	Angulated shaft, and well-developed crest	Marked bevel	Short
Colobus spp.	Angulated shaft, and moderate to markedly developed crest	Marked and localized bevel	Moderate to long relative length (μ = 51.7 ± 7.5, n = 18; Figure 16A)
Nasalis larvatus	Angulated shaft, and poorly developed crest	Marked and extensive bevel	Short to moderate relative length (μ = 39.1 ± 8.2, n = 6; Figure 16A)
Semnopithecus spp.	Angulated shaft, and moderately developed crest	Marked and localized bevel	Short to moderate relative length (μ = 48.2 ± 14.9, n = 4; Figure 16A)
Papio spp.	Straight shaft, and well-developed crest	Poorly developed and localized	Short to moderate relative length (μ = 31.3 ± 5.2, n = 9; Figure 16A)

[1]*R.* cf. *turkanaensis* indet. include the following specimens: OMO 2-10029.
[2]*P.* cf. *mutiwa* include the following specimens: L 236-1b.
[3]Observation based only on the anatomy of the proximal portion of the radius of the partial skeleton KNM-WT 1682

Deleted: *meavae*

Deleted: *kimeui*

The radial head of the Omo colobines is obliquely inclined and has a well-defined tubercle on its lateral margins. This morphology is also observed in the extant colobines *S. entellus*, *N. larvatus* and *Co. guereza* (Appendix 26).

The peripheral articular surface proximal to the bicipital tuberosity is poorly extended distally in OMO 2-10029 compared to L 236-1a. The morphology of the radial peripheral

articular surface of L 236-1a, and notably its distal extension, is quite similar to that of *S. entellus* (Appendix 26).

The fovea of the radial head of the Omo colobines are centrally placed but they differ in depth. OMO 2-10029 is distinguished by the greater depth of its fovea (Appendix 24). A globular capitulum with a deep zona conoidea is expected to match the proximal radial anatomy of OMO 2-10029. In sagittal cross-section, the deep fovea and marked anteromedial bevel of the radial head of OMO 2-10029 is most consistent with the radial anatomy of *N. larvatus* than that of *Co. guereza* and *S. entellus* (Appendix 24 and 25).

Comparative anatomy of the proximal femoral epiphysis

Proximal femora are known from Usno (W 7-477B), Lower G (OMO 75/N-1971-728 and OMO 50-1973-728), and several specimens from Member L. OMO 75/N-1971-728, OMO 50-1973-728 and W 7-477B are of similar size (Fig. 17, Table 17 and Appendix 44) while the Member L specimens represent a smaller taxon.

Table 17. – Measurements (in mm) of the femoral specimens

Specimens	FPEML	BNML	NSA(°)	GTProj	FNML	FNSI	FNAP	FHSI	FHAP	FBAPLT	FAPLT
W 7-477b	49.9	39.0	116.2°	5.6	17.5	20.8	17.6	24.2	25.4		
OMO 50-1973-4450	47.8	38.1	110.5°	3.9	17.4	21.8	16.0	25.2	25.1	18.1	24.7
OMO 75/N-1971-728	45.0	36.7	108.0°	3.5	18.5	19.1	14.7	23.2	22.6	18.4	
OMO 342-10019	30.9	24.1	118.7°	0.4	9.2	13.6	10.9	16.1	16.1		
OMO 342-10344	33.9	27.2	118.8°	2.2	9.8	13.6	11.4	16.6	17.0		
OMO 342-10298	34.2	26.7				14.2	~13.0	17.5	16.6		

The femoral head of the large Omo colobines are globular, particularly that of OMO 75/N-1971-729 and OMO 50-1973-728. Extensive encroachment of the femoral head on the neck is visible in OMO 75/N-1971-729 and OMO 50-1973-728 (Table 18 and Appendix 27). Comparatively, clearer delineations between the neck and femoral head are observed in *P. mutiwa*, *Ce. coronatus* and *Ce. williamsi* (Appendix 28). An extension of the femoral head onto the neck is frequently seen in extant colobines but is distinct from the typical morphology of *Papio* (Table 18 and Appendix 29).

Deleted: *kimeui*

Commented [MOU21]: Fair enough, but it's not unusual for many cercopithecines, more broadly, so I don't know if this is a very good taxonomic indicator. For instance, Theropithecus often displays an extension of the articular surface onto the femoral neck. Are these specimens significantly smaller than T. brumpti and/or T. oswaldi of this time period ? And/or to they display other distinctive features ?

1066

1067 **Fig. 17**. – Photographs of the femoral anatomy of colobines from Usno and Shungura.
1068 Abbreviations: Ant: Anterior, Lat: Lateral, Med: Medial, Prox: Proximal, Post: Posterior. Scale:
1069 10 mm.

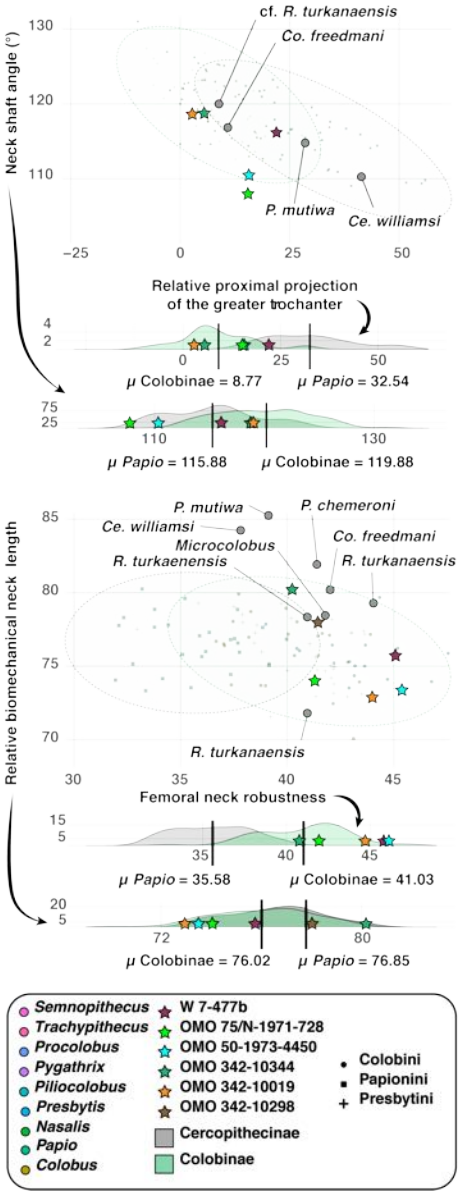

Fig. 18 (previous page). – Scatterplots of proximal femoral indices of extant and extinct colobines and extant *Papio* spp. 95 % normal confidence ellipses (given a multivariate normal

distribution) are drawn for colobines and *Papio* spp. Kernel density estimates are given for each axis below the scatterplots. A.) Regression of the collodiaphyseal angle on the relative projection of the greater trochanter in extant colobines (n = 78), *Papio* spp. (n = 27) and fossil colobines. The parameters of the linear model are as follows: R^2= 0.45, y= -0.23x+121.78, and B.) Regression of the biomechanical neck length on neck robustness in extant colobines (n = 73), *Papio* spp. (n = 27) and fossil colobines. Parameters of the linear model are as follows: R^2= 0.07, y= -0.18x+83.68. When there are significant differences between taxa (p < 0.05), the associated p-values are given.

A significant difference is observed between *Papio* and extant colobines regarding neck-shaft angle, with relatively more acute angle in *Papio* (p < 0.01, Fig. 18A). The collodiaphyseal angle of OMO 75/N-1971-729 and OMO 50-1973-728 is acute, in contrast to most extant colobines (Appendix 29) but similar to *P. mutiwa* and *Ce. williamsi* (Fig. 18A). Indeed, with respective index values of 110.5° and 108°, OMO 50-1973-728 and OMO 75/N-1971-729 are much closer to the mean value of *Papio* (μ = 115.3 ± 4.1°, Table 18) than that of *Co. guereza* (μ = 118.6 ± 3.8°, Table 18).

Extant colobines differ significantly from *Papio* by presenting a robust femoral neck (p < 0.01, Fig. 18B). Although non-significant, we also observed a tendency for colobines to present a shorter neck compared to *Papio* (Fig. 18B). The femoral necks of OMO 75/N-1971-728, OMO 50-1973-728 and W 7-477B are short and robust, as also observed in extant colobines, but unlike *Ce. williamsi* and *Ce. meaveae* (Fig. 18B and Appendix 28). With neck robustness index values superior to 41, OMO 75/N-1971-728, OMO 50-1973-728 and W 7477B are outside the range of variation of extant *Papio* (μ = 35.6 ± 2.3, Table 18) but within the range of variation of *Co. guereza* (μ = 40.0 ± 2.5, Table 18).

The enthesis of the *m. vastus lateralis* of OMO 75/N-1971-729 and OMO 50-1973-4450 is not as laterally projected as that of extant primate leapers (Table 18; Fleagle & Simons, 1995; Cooke & Tallman, 2012) and extant colobines (Appendix 29). In contrast, this enthesis is prominent in both W 7-477B and *P. mutiwa* (Appendix 28), and also comparable in morphology to that of *Co. guereza*, *N. larvatus* and *S. entellus* (Appendix 29).

Commented [MOU22]: What is the p-value here ?

Commented [MOU23]: So is the regression significant ? And even if so, the low r^2 value suggests that these indices are probably unlikely to be connected in any biologically meaningful way, so why even bother with the regression ?

Commented [MOU24]: Shorter neck = more leaping ? See Fleagle (1976, 1977)

Deleted: *meavae*

Table 18. – Qualitative and quantitative morphological observations of the proximal femur of extant cercopithecids and early colobines.

Taxa (in bold, Omo taxa)	Greater trochanter proximal projection	Femoral neck morphology (length, robustness and collodiaphyseal angle [i.e., CDA])	Extension of the femoral head onto the neck and placement of the fovea capitis	Lateral projection of the m. vastus lateralis enthesis	Trochanteric fossa morphology (overall dimension and placement)	Lesser trochanter morphology (placement on the shaft and orientation)
[1]*R.* cf. *turkanensis*	**Moderate proximal projection**	**Short, and robustly built neck with an acute CDA**	**Marked extension of the femoral head onto the neck, and centrally-set fovea capitis**	**Projected**	**Large and proximally-set**	**Distally-set, and medially facing**
[2]*P.* cf. *mutiwa*	**Moderate proximal projection**	**Long, and shallow neck with an acute CDA**	**Moderate extension of the femoral head onto the neck, and eccentrically-set fovea capitis**	**Projected**	**Large and distally-extended**	**Distally-set, and posteriorly facing**
[3]cf. *Colobus* sp. indet.	**Poor to moderate proximal projection**	**Short, and robustly built neck with an acute CDA**	**Moderate extension of the femoral head onto the neck, and centrally-set fovea capitis**	**Projected**	**Short and distally-extended (slit-like)**	**Proximally-set, and medially facing**
P. chemeroni	NA.	Short, and robustly built neck with an acute CDA	Marked extension of the femoral head onto the neck, and centrally-set fovea capitis	Projected	Large and distally-extended	Proximally-set, and medially facing
P. mutiwa	Moderate proximal projection	Moderately long neck, with a robust and acute CDA	Moderate extension of the femoral head onto the neck, and centrally-set fovea capitis	Projected	Large and distally-extended	Distally-set, and medially facing
Ce. williamsi	Marked proximal projection	Long, and shallow neck with an acute CDA	Moderate extension of the femoral head onto the neck, and eccentrically-set fovea capitis	Non-projected	Large and distally-extended	Distally-set, and posteriorly facing
Ce. meaveae	Marked proximal projection	Long, and shallow neck with an acute CDA	NA.	Non-projected	Large and distally-extended	Distally-set, and posteriorly facing
Ce. coronatus	NA.	Long, and shallow neck with an acute CDA	NA.	NA.	NA.	Distally-set, and posteriorly facing
Ce. bruneti	NA.	NA.	NA.	NA.		NA.
R. turkanaensis	NA.	NA.	NA.	NA.	NA.	NA.

Deleted: *meavae*

Deleted: *kimeui*

Table 18 (following). – Qualitative and quantitative morphological observations of the proximal femur of extant cercopithecids and early colobines.

Taxa (in bold, Omo taxa)	Greater trochanter proximal projection	Femoral neck morphology (length, robustness and collodiaphyseal angle [i.e., CDA])	Extension of the femoral head onto the neck and placement of the fovea capitis	Lateral projection of the m. vastus lateralis enthesis	Trochanteric fossa morphology (overall dimension and placement)	Lesser trochanter morphology (placement on the shaft and orientation)
Co. freedmani	Moderate proximal projection	Short, and robustly built neck with an acute CDA	Moderate extension of the femoral head onto the neck, and centrally-set fovea capitis	Projected	Short and distally-extended (slit-like)	Proximally-set, and posteriorly facing
Microcolobus sp.	Poor proximal projection	Short, and robustly built neck with an obtuse CDA	NA.	Projected	Short and distally-extended (slit-like)	NA.
Co. sp. indet. Asbole	Moderate proximal projection	Short, and robustly built neck with an acute CDA	Moderate extension of the femoral head onto the neck, and centrally-set fovea capitis	Projected	Short and distally-extended (slit-like)	Proximally-set, and posteriorly facing
Colobus spp.	Poor to moderate proximal projection (μ = 13.3 ± 8.0, *n* = 25; Figure 18A)	Short to moderately long neck, robustly built neck (μ = 40.0 ± 2.5, *n* = 26; Figure 18B), and acute CDA (μ = 118.6 ± 3.8°, *n* = 25; Figure 18A)	Moderate to marked extension of the femoral head onto the neck, and centrally-set fovea capitis	Projected	Short and distally-extended (slit-like)	Proximally-set, and posteriorly facing (μ = 31.41 ± 5.9, *n* = 19; Figure 19)
Nasalis larvatus	Poor to moderate proximal projection (μ = 14.1 ± 10.0, *n* = 6; Figure 18A)	Short neck, robustly built neck (μ = 41.3 ± 2.1, *n* = 6; Figure 18B), and acute CDA (μ = 118.5 ± 4.1°, *n* = 6; Figure 18A)	Moderate to marked extension of the femoral head onto the neck, and centrally-set fovea capitis	Projected	Short and distally-extended (slit-like)	Proximally-set, and medially facing (μ = 23.24 ± 3.1, *n* = 6; Figure 19)
Semnopithecus spp.	Moderate to marked proximal projection (μ = 18.3 ± 10.1, *n* = 3; Figure 18A)	Long neck, robustly built neck (μ = 39.0 ± 1.8, *n* = 6; Figure 18B), and acute CDA (μ = 116.6 ± 1.5°, *n* = 3; Figure 18A)	Moderate to marked extension of the femoral head onto the neck, and eccentrically-set fovea capitis	Projected	Large and distally-extended	Distally-set, and medially-facing (μ = 28.93 ± 2.8, *n* = 5; Figure 19)
Papio spp.	Marked proximal projection (μ = 32.5 ± 11.3, *n* = 26; Figure 18A)	Long neck, gracile neck (μ = 35.6 ± 2.3, *n* = 26; Figure 18B), and highly acute CDA (μ = 115.3 ± 4.1°, *n* = 26; Figure 18A)	Poor extension of the femoral head onto the neck, and eccentrically-set fovea capitis	Non-projected	Large and distally-extended	Distally-set, and posteriorly facing (μ = 34.40 ± 3.9, *n* = 14; Figure 19)

[1]*R.* cf. *turkanaensis* indet. include the following specimens: OMO 50-1973-4450 and OMO 75/N-1971-728
[2]*P.* cf. *mutiwa* include W 7-477b
[3]cf. *Colobus* sp. indet. include the following specimens: OMO 342-10019, OMO 342-10344, OMO 342-10298
1112

The fovea capitis of OMO 75/N-1971-729 and OMO 50-1973-4450 is located centrally on the femoral head whereas it is placed more eccentrically in W 7-477B (Table 18 and Appendix 30). *P. mutiwa*, *Ce. williamsi* and the presumed *Rhinocolobus* specimen KNM-ER 551 present a centrally placed fovea distinct from that of W 7-477B (Appendix 30). The centrally placed fovea of OMO 75/N-1971-729 and OMO 50-1973-4450 is more comparable to that of *N. larvatus* while W 7-477B is more similar to *Co. guereza* and *S. entellus* (Appendix 29).

Although proximally restricted, the trochanteric fossa of OMO 75/N-1971-729 and OMO 50-1973-4450 is wide, as in *Ce. williamsi*, *P. chemeroni* and *R. turkanaensis* (Table 18 and Appendix 28). In comparison, the fossa of W 7-477B is more restricted mediolaterally. The mediolaterally short fossa of W 7-477B is reminiscent of the morphology of *Co. guereza* while the wide fossa of OMO 75/N-1971-729 and OMO 50-1973-4450 is similar to *N. larvatus* (Appendix 28).

An enlarged enthesis of the ischiofemoral ligament is set on the medial border of the trochanteric fossa of W 7-477B, a morphology also observed in *Co. guereza* (Appendix 29).

A palpable femoral tubercle for the attachment site of the illiofemoral ligament is present in all the large Omo colobines. This enthesis is particularly rugose and enlarged in OMO 50-1973-4450, similarly to *Ce. williamsi* (Appendix 28). Although the illiofemoral tubercle can be salient in extant colobines (see *Se. entellus* and *Co. guereza* in Appendix 29), none of the extant colobines from our comparative dataset matches the size and shape of the illiofemoral tubercle of OMO 50-1973-4450. A pitted area is located proximal to the lesser trochanter in OMO 50-1973-4450, OMO 75/N-1971-729, and W 7-477B along with a well-defined distal portion of the intertrochanteric crest. This combination of character (pitted area and pronounced distal portion of the intertrochanteric crest) is also observed in *P. mutiwa* and in the presumed *Rhinocolobus* femur KNM-ER 551 (Appendix 28).

The proximal aspect of the intertrochanteric crest is more robust in W 7-477B than in OMO 50-1973-4450, OMO 75/N-1973-4450, KNM-ER 551, and *P. mutiwa* (Appendix 28). The quadrate tubercle of W 7-477B is nonetheless poorly developed compared to *P. mutiwa* (Appendix 28).

Extant colobines are significantly distinct from *Papio* by presenting a less proximally extended greater trochanter ($p < 0.01$, Fig. 18B). The proximal projection of the greater trochanter is moderate in OMO 50-1973-4450 and OMO 75/N-1971-728 but pronounced in W 7-477B (Fig. 19A). More precisely, OMO 50-1973-4450, with an index value of 15.70, and OMO 75/N-1971-728, with an index value of 5.50, are close to the mean value of *N. larvatus* ($\mu = 14.1 \pm 10.0°$, Table 18). W 7-477B, with an index value of 22.00, stands between *S. entellus* ($\mu = 18.3$

Commented [MOU25]: These plots show Papio with a taller or more proximally extended trochanter, yes ?

± 10.1°, Table 18) and *Papio* (μ = 32.5 ± 11.3°, Table 18). *Ce. williamsi* is the only colobine that has a projection of the greater trochanter clearly similar to that of *Papio* (Fig. 18A).

The lesser trochanter of *Papio* is significantly more developed and projected posteriorly than that of extant colobines ($p < 0.01$, Fig. 19). The lesser trochanter is oriented medially in W 7-477B, OMO 50-1973-4450 and OMO 75/N-1973-4450 (Figs 17; 19). The Omo colobines

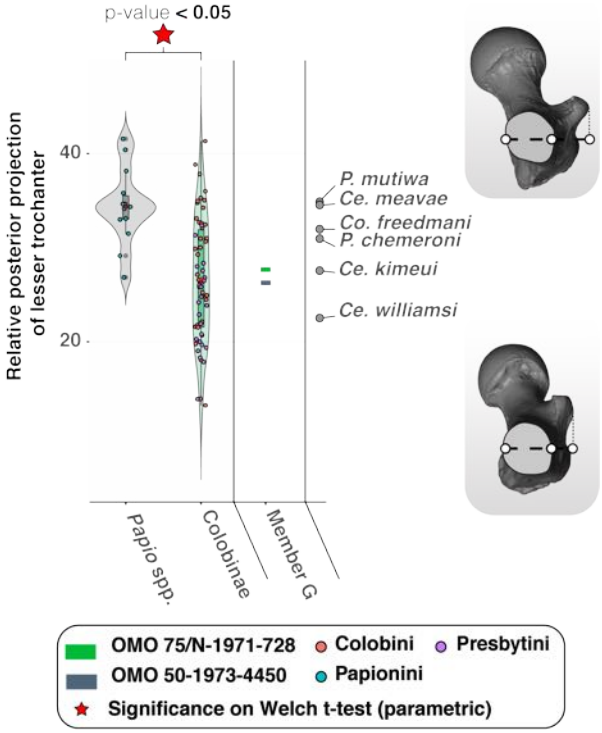

resemble their extant counterparts in this aspect as their lesser trochanter is significantly more medially projected than that of extant *Papio* spp. (Fig. 19). In their degree of projection and development, the lesser trochanters of W 7-477B, OMO 50-1973-4450 and OMO 75/N-1973-4450 are more similar to those of KNM-ER 551 (cf. *Rhinocolobus*) and *P. mutiwa* than those of *Ce. williamsi* and *Ce. meaveae* (Appendix 28). None of the Omo colobines present a lesser trochanter as large and as proximally located as that of *P. chemeroni* (Appendix 29).

Fig. 19. – Violin plots and boxplots of the posterior projection of the lesser trochanter in extant colobines ($n = 55$), *Papio* spp. ($n = 12$) and fossil colobines. Morphologies associated

Deleted:
Deleted: 9
Deleted: *meavae*

with minimum and maximum values are shown on the left of the graph. Means (red diamonds), medians (black rectangles), first quartile and third quartile as well as maximum and minimum values.

Small femoral specimens from Member L (Fig. 20, and Appendix 31 and 44) are reminiscent of extant colobine anatomy by having a short and robust femoral neck, obtuse collodiaphyseal angles, proximally and medially restricted trochanteric fossae, medially oriented lesser trochanters, a centrally placed fovea capitis, enlarged attachment sites for the iliofemoral, ischiofemoral and pubofemoral ligaments, and a laterally projected *m. vastus lateralis* enthesis (Fig. 18A, B, Table 18). Their morphology matches that of *Co. freedmani*, *Microcolobus* and *Colobus* from Asbole (Appendix 32).

Deleted: the

Fig. 20. – Photographs of the femoral anatomy of colobines from Member L. Abbreviations: Ant: Anterior, Med: Medial, Lat: Lateral, Prox: Proximal, Post: Posterior. Scale: 10 mm.

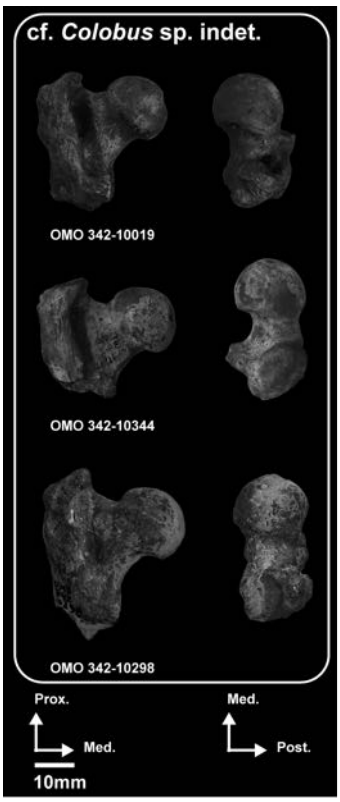

Comparative anatomy of the proximal tibial epiphysis

A complete tibia is known from a specimen from the Member L (OMO 377-10024 in Fig Fig. ure 21) similar in size to extant *Colobus* spp. (Table 19 and Appendix 45).

Fig. 21. – Photographs of the tibial anatomy of a colobine from Member L. Abbreviations: Ant: Anterior, Med: Medial, Lat: Lateral, Prox: Proximal, Post: Posterior. Scale: 10 mm.

The tibial plate of OMO 377-10024 is retroflexed and both condyles are concave, with no difference in depth between them (Appendix 33), as in the similarly sized *Co. freedmani* but unlike the large colobine *R. turkanaensis* (Appendix 34). The proximal tibia of OMO 377-10024 is also characterized by widely spaced, and blunt tibial spines that show virtually no height differential and are connected by a straight, rather than oblique, transverse line as in *Co. freedmani*.

Deleted: well

The tibial tuberosity of OMO 377-10024 is extended distally, as in extant colobines (Appendix 35), although the precise level of distal extension of the cnemial crest is difficult to assess due to missing portions of the shaft proximal to the mid-diaphysis.

The transverse cross-sections of the proximal metaphysis of *Co. guereza* and *S. entellus* are also extended anteroposteriorly and contrast with the more rounded cross-section of *N. larvatus* (Appendix 35). Marked concavities for the insertion of the *m. tibialis anterior* and *m. tibialis posterior* are seen on the proximal diaphysis of OMO 377-10024 (Appendix 33). A particularly enlarged *m. tibialis anterior* enthesis is also visible in *Co. freedmani* (Appendix 34), *Co. guereza* and *S. entellus*, but the *m. tibialis posterior* is nonetheless much less developed in these fossil and extant specimens than that of OMO 377-10024 (Appendix 35).

Table 19. – Measurements (in mm) of the tibia OMO 377-10024

Specimen	TPEML	MTPML	LTPML	MshAP	MshML	DEML	DEAP	MAP	MML	TFMxML	TFMnML
OMO 377-10024	27.6	10.1	11.6	12.4	8.6	17.6	13.7	9.8	5.6	11.4	8.8

Comparative anatomy of the tibial diaphysis

Only the curvature of the shaft distal to the mid-diaphysis is assessable in OMO 377-10024 and the observed pattern is that of a straight diaphysis, similar to that of *Co. freedmani*. The transverse cross-section set at the mid-diaphysis is elliptical, and not as robust as that of *Co. freedmani* nor as triangular as that of *Co. guereza* (Appendix 34 and 35).

Comparative anatomy of the distal tibial diaphysis

The fibular notch of OMO 377-10024 is weakly expressed, as in extant (Appendix 35) and fossil colobines (Appendix 34). OMO 377-10024 also has a a proximodistally elongated depression on the anterior portion of the lateral side of the malleolus, presumably for a developed anterior tibiotalar ligament. No other obvious evidence of a developed ligamentous attachment area is detected on this specimen. Extensive depressions for the anterior tibiotalar ligament are also visible in the *Papio*, *S. entellus* and *N. larvatus* specimens illustrated in Appendix 35.

The large and blunt anterior tibial beak of OMO 377-10024 is not as pronounced as that of the putative *Rhinocolobus* tibia from Laetoli (Laird *et al.* 2018), and that of *N. larvatus* and *Co. guereza* (Appendix 36 and Table 20). When viewed anteriorly, the tibial malleolus of OMO 377-10024 is flared, a feature that may be related to a more angular medial facet of the astragalus. A similarly flared malleolus is observed in *Co. guereza* (Appendix 35).

Table 20. – Qualitative morphological observations of the tibia of extant cercopithecids and early colobines.

Taxa (in bold, Omo taxa)	Deltoid ligaments imprinting	Malleolar morphology (robustness and distal extension)	Development of the anterior process of the tibial distal epiphysis	Shape of the distal epiphysis	Tibial plate depth differential
[1]cf. *Colobus* sp. indet.	**Moderate**	**Gracile malleolus with a poor distal extension**	**Moderate**	**Rectangular-shaped**	**Poor depth differential between the condyles**
P. chemeroni	Moderate	Gracile malleolus with a moderate distal extension	Marked	Rectangular-shaped	Poor depth differential between the condyles
Ce. meaveae	NA.	NA.	Moderate	Rectangular-shaped	Poor depth differential between the condyles
R. turkanaensis	Poor	Robust malleolus with a poor distal extension	Moderate	Rectangular-shaped	Marked depth differential between the condyles
Co. freedmani	Moderate	Robut malleolus with a poor distal extension	Moderate	Rectangular-shaped	Marked depth differential between the condyles
Colobus spp.	Moderate to marked	Gracile malleolus (μ = 196.99 ± 23.8, n = 19; Figure 22A) with a poor distal extension	Moderate to marked	Rectangular-shaped (μ = 128.22 ± 6.93, n = 17; Figure 22B)	Poor depth differential between the condyles
Nasalis larvatus	Moderate to marked	Robust malleolus (μ = 176.90 ± 16.2, n = 7; Figure 22A) with a moderate distal extension	Moderate to marked	Square-shaped (μ = 119.77 ± 4.10, n = 7; Figure 22B)	Marked depth differential between the condyles
Semnopithecus spp.	Moderate to marked	Robust malleolus (μ = 172.60 ± 21.2, n = 4; Figure 22A) with a distal extension	Moderate	Rectangular-shaped (μ = 128.64 ± 1.94, n = 3; Figure 22B)	Moderate depth differential between the condyles
Papio spp.	Marked	Gracile malleolus (μ = 193.22 ± 20.6, n = 26; Figure 22A) with a distal extension	Moderate	Square-shaped (μ = 118.51 ± 5.47, n = 25; Figure 22B)	Moderate depth differential between the condyles

[1]cf. *Colobus* sp. indet. include OMO 377-10024

Deleted:

Deleted: *meavae*

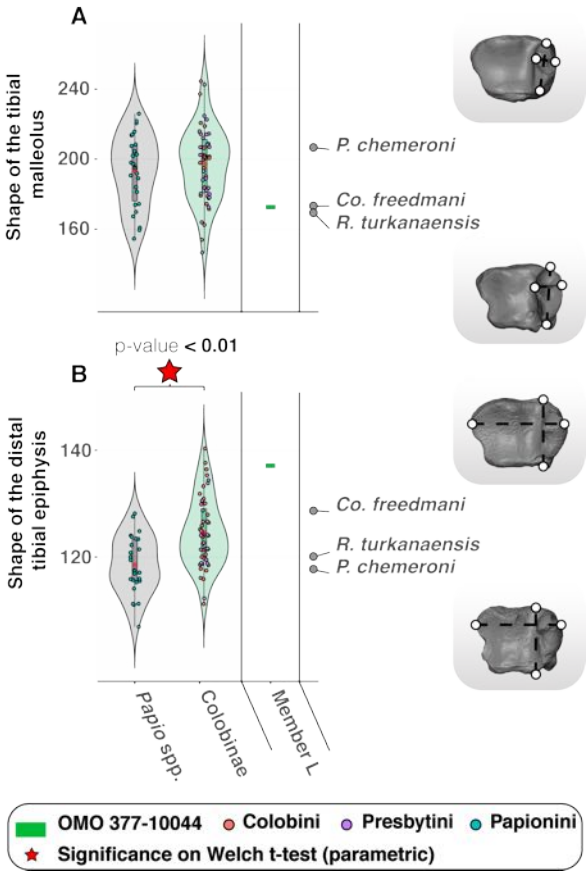

Fig. 22. – Violin plots and boxplots of morphometric indices of distal tibia of extant and extinct colobines and extant *Papio* spp. Morphologies associated with minimum and maximum values are shown on the right of the graph. A.) Shape of the distal tibial epiphysis in extant colobines (n = 48), *Papio* spp. (n = 26) and fossil colobines, and B.) Shape of the tibial medial malleolus in extant colobines (n = 51), *Papio* spp. (n = 27) and fossil colobines. Means (red diamonds), medians (black rectangles), first quartile and third quartile are plotted. When there are significant differences ($p < 0.05$) between taxa, the associated p-values are given.

No significant difference is detected in our extant cercopithecid sample concerning malleolar shape (Fig. 22A), but the malleolar shape index of OMO 377-10024 is nonetheless

in the lowest range of variation of extant colobines. The low index value of OMO 377-10024 demonstrate the robustness of its malleolus (Table 20). High index values are associated with anteroposteriorly elongated and mediolaterally shallow malleoli. With an index value of 172.6, OMO 377-10024 is close to the mean value of *N. larvatus* (μ = 176.90 ± 16.2, Table 20) and *Semnopithecus* spp. (μ = 172.60 ± 21.2, Table 20) but is distinct from the more anteroposteriorly elongated and mediolaterally narrow malleolus of *Colobus* spp. (μ = 196.99 ± 23.8, Table 20 and Appendix 35). The malleolar shape of OMO 377-10024 is quite similar to that of *Co. freedmani* and *R. turkanaensis* but distinct from the more elongated and shallow malleolus of *P. chemeroni* (Appendix 34).

In coronal cross-section, the shape of the tibial astragalar surface is asymmetric in OMO 377-10024, with a higher slope value for the lateral facet compared to the medial facet (Appendix 33). A similar level of asymmetry is observed in *Co. freedmani* and *P. chemeroni* (Appendix 34).

A significant difference is observed between *Papio* and extant colobines regarding the shape of the tibial distal epiphysis ($p < 0.01$, Fig. 22B). With low index values, the epiphysis of *Papio* is square shaped compared to the mediolaterally elongated epiphysis of colobines (Fig. 22B).

The distal epiphysis of OMO 377-10024 is mediolaterally extended, as in extant colobines (Fig. 22B). Precisely, OMO 377-10024, with an index value of 137.10, is closer to the mean value of *Colobus* spp. (μ = 128.22 ± 6.93, Table 20) than *Papio* spp. (μ = 118.51 ± 5.47, Table 20).

The asymmetry (in mediolateral dimension) of the anterior and posterior margins of the astragalar articular surface of OMO 377-10024 (i.e., trochlear wedging) is not as pronounced as that of *Co. freedmani* (Appendix 34), nor as that of *Co. guereza* and *N. larvatus* (Appendix 35).

In transverse cross-section, the shape of the distal metaphysis of OMO 377-10024 is triangular, similar to that of *Co. freedmani* (Appendix 36), and its interosseous crest is not as prominent as that of *R. turkanaensis* (Table 20 and Appendix 36). Compared to extant colobines, the distal metaphysis of OMO 377-10024 is more similar to the triangular shape of *Co. guereza* than to the more elliptical cross-section of *N. larvatus* (Appendix 35).

BODY MASS INFERENCES AND GEOMETRIC SIZE COMPARISONS

Body masses

1282 The inferred body masses of the postcranial specimens described in this study range from
1283 ca. 7.3 kg for the tibia OMO 377-10024 to ca. 34 kg for the distal humerus OMO 176-10006
1284 (Fig. 23).
1285
1286

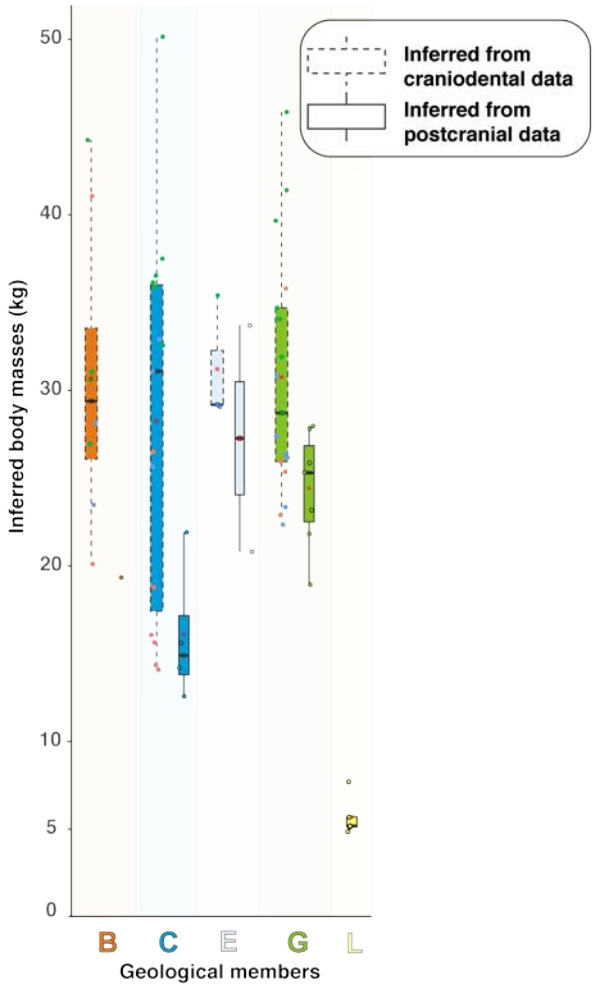

Fig. 23. – Boxplots of inferred body masses of fossil colobines from members B, C, E, G and L of the Shungura Formation.

Body masses inferred from postcranial fossil specimens of members C (OMO 18-1967-135, OMO 18-1973-608 and OMO 165-1973) and L matches that of extant *Piliocolobus* spp. and *Colobus* spp. (Appendix 38). Indeed, *Co. freedmani* and Asbole specimens have inferred

body masses that ranges, on average, from ca. 7 kg to ca. 9 kg (Appendix 38), a range consistent with that of the Member L postcranial specimens (Appendix 38).

Body masses inferred from dental data are consistently higher than postcranial masses (Fig. 23) and ranges from ca. 14 kg for OMO 84-1970-107 (isolated M_2 of a Colobinae indet. from Member C according to Leakey [1987]) to ca. 50 kg for OMO 18-1970-294 (M^1 or M^2 from a *P. mutiwa* specimen from Member C according to Leakey 1987, see also Appendix 38). The presumed body mass of dental specimens of *P. mutiwa* ranges from ca. 27 kg to ca. 50 kg and that of *R. turkanaensis* from ca. 22 kg to ca. 33 kg (Appendix 38).

Geometric mean comparisons

Comparison of geometric means of selected isolated Omo specimens to that of the male partial skeleton *R. turkanaensis* KNM-ER 1542 are made to explore sexual dimorphism within the Omo sample. None of the Omo postcranial specimens morphologically similar to *R. turkanaensis* exceed KNM-ER 1542 in size (Fig. 24).

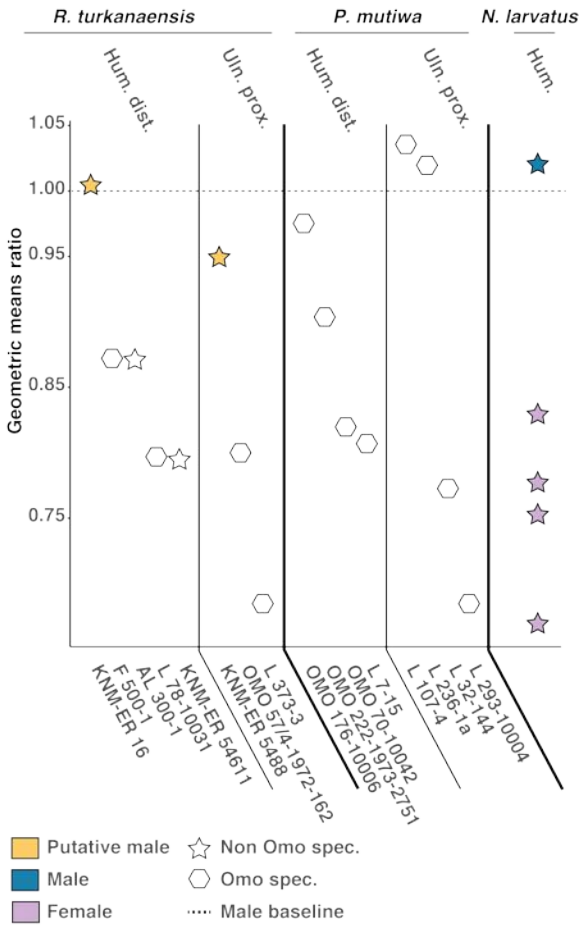

Fig. 24. – Dot plot of geometric mean ratio between fossil specimens and *N. larvatus*. Comparison is made between specimens of unknown sex with fossil male specimens of *P. mutiwa* and *R. turkanaensis*, KNM-WT 16827 and KNM-ER 1542, respectively.

Commented [MOU26]: What do you mean by « male baseline » in this figure ? What are you calculating as a GM ratio ? It is unclear what is going on here. I would think that a GM Sex dimophism ratio in any monkey should be greater than 1 if dividing male GM by female GM. Please clarify what is going on in this plot.

The distal humerus L 78-10031 is small compared to that of the male KNM-ER 1542 but similar in size to the putative *Rhinocolobus* female specimen KNM-ER 54611 (Fig. 24). Similarly, the proximal ulna L 373-3 and OMO 57/4-1972-162 are smaller than those of the male *Rhinocolobus* specimens KNM-ER 5488 and KNM-ER 1542. The size differential of the

specimens attributed here to *R. turkanaensis* does not exceed the size differential observed in the humeral dimensions of a sample of male and female *N. larvatus* (Fig. 24). When compared in geometric mean to the male *P. mutiwa* partial skeleton KNM-WT 16827, the proximal ulna L 107-4 and L 236-1 exceed it in size (Fig. 24). The distal humerus OMO 176-10006 is also close in geometric size to KNM-WT 16827. The distal humerus OMO 70-10042 and L 7-15 and the proximal ulna L 32-144 are smaller than KNM-WT 16827. L 293-10004 (proximal ulna) is the smallest specimen of *P. mutiwa* but its size difference from KNM-WT 16827 does not exceed the size difference observed in the humeral dimensions of an extant sample of *N. larvatus*.

Commented [MOU27]: See my comment above. I have no idea what is going on in this plot. You need to clarify or remind us of what ratio you are using and how you are quantifying dimorphism for each element. It seems like numerous things are being conflated or combined into one « ratio » here. Please clarify.

DISCUSSION

In regard to colobine evolutionary history, the period between the end of the Pliocene and the beginning of the Pleistocene corresponds to a phase of diversification both from a locomotor and taxonomic point of view (Table 1; Birchette 1982, Harris *et al.* 1988, Frost & Delson 2002, Hlusko 2006, Frost *et al.* 2007, Jablonski & Leakey 2008a&b, Gilbert *et al.* 2010, Nakatsukasa *et al.* 2010, Pallas *et al.* 2019). Indeed, at least five large-bodied species belonging to the genera *Cercopithecoides*, *Paracolobus* and *Rhinocolobus* are documented in this time range. Among them, *Cercopithecoides williamsi* and *Cercopithecoides coronatus* are described as primarily terrestrial while *Rhinocolobus turkanaensis* is described as arboreal. *Paracolobus chemeroni* and *Paracolobus mutiwa* show postcranial anatomy indicating less stereotyped substrate preferences compared to *Rhinocolobus* and *Cercopithecoides*. Our study demonstrates that the colobines from Usno and Shungura display body masses ranging from ca. 7 kg to ca. 35 kg, locomotor preferences for mixed and arboreal substrates, and positional behaviors including leaping, climbing and possibly suspension. Overall, this indicates the presence of a functionally and ecomorphologically diverse colobine paleocommunity.

Deleted: the

Deleted: *kimeui*

Deleted: early

For the time interval covered by the Omo Group deposits (ca. 4 Ma to ca. 1 Ma), insights into the locomotor repertoire of Plio-Pleistocene colobines were inferred from the associated partial skeletons of *Paracolobus*, *Rhinocolobus* and *Cercopithecoides*, among others (Table 1). The Shungura and Usno formations include several postcranial specimens in the size range of these genera. Our taxonomic scheme is tentative and needs to be tested in the future by conjoint evaluation of craniodental and postcranial specimens. Nevertheless, the strong morphological similarities of the specimens discussed here with known fossil colobines from eastern Africa raise important points of discussion regarding the functional anatomy, paleoecology, and evolutionary history of Plio-Pleistocene colobines.

Deleted: o

FUNCTIONAL INTERPRETATIONS AND TAXONOMY

Functional interpretations and taxonomy of the humeral specimens

A first humeral morphotype of a medium-sized colobine is found in Member C and is represented by specimens OMO 18-1967-135, OMO 18-1971-702 and OMO 165-1973-608. These specimens have a stabilized humeroulnar and humeroradial joints, both designed to withstand mediolateral joint reaction forces. They also present a medial epicondyle reduced in size, a trait frequently seen in *Nasalis larvatus,* and which may be related to a weak musculature of the digit and carpal flexors. Indeed, the *m. flexor carpi ulnaris,* which inserts on the medial epicondyle, is described by Schultz (1986) as moderately developed in *N. larvatus* compared to the African colobine *Procolobus verus* Van Beneden, 1838. OMO 18-1967-135, OMO 18-1971-702 and OMO 165-1973-608 are notably reminiscent of *Ce. meaveae* and *Paracolobus enkorikae* Hlusko, 2007 from Lemudong'o regarding the above mentioned characteristics (Appendix 14). Pending additional discoveries of postcranial and craniodental specimens, OMO 18-1967-135, OMO 18-1971-702 and OMO 165-1973-608 provide new evidence for the presence of a colobine distinct from *Colobus*, *Paracolobus mutiwa* and *Rhinocolobus turkanaensis* in the Omo.

A second morphotype includes *n* = 5 specimens from members E (OMO 70-10042, OMO 176-10006, and L 5/6-41) and G (L 7-15 and OMO 222-1973-2751). The morphological features shared by these specimens are the following: large entheses for the *mm. teres major* and *brachioradialis*, depth of the radial fossa, large and projected medial epicondyle, developed capitular tails and narrow and medial humeral pillar. Altogether, these features indicate an enhanced climbing ability. The enlarged and distally set enthesis of the *m. teres major* illustrates powerful arm adduction and medial rotation (Fleagle & Simons, 1982a). Also, the enlarged and proximally extended enthesis of the *m. brachioradialis* indicates powerful forearm flexion capabilities (Koukoubis *et al.* 1995, Boland and Spigelman 2008), and is further suggestive of frequent climbing behaviors (Fleagle & McGraw 1999, 2002). Their large medial epicondyles indicate the presence of a developed musculature for the wrist flexors (Lague *et al.* 2019) and its medial projection implies enhanced rotational capabilities of the forearm (Ibáñez-Gimeno *et al.* 2014). In addition, the proximal extension of their medial epicondyles maximizes the lever arm of *m. pronator teres* when the elbow is flexed and the hand supinated (Ibáñez-Gimeno *et al.* 2014). Their enlarged capitular tails are another line of evidence supporting increased stabilization of the humeroradial joint during full elbow flexion (Gebo 1989). Finally, deep supratrochlear fossae also indicate increased elbow flexion capabilities (Fleagle & Simons 1995). This combination of anatomical characters is also

Deleted: *meavae*

Deleted: n

Deleted: the

Deleted:

present on the humeral anatomy of KNM-WT 16827, a partial skeleton attributed to *P. mutiwa*. Given ***i)*** the morphological affinities of the Omo specimens with KNM-WT 16827, ***ii)*** the identification of *P. mutiwa* craniodental specimens in members E and G, ***iii)*** the congruence between craniodental and postcranial body masses inferred from *P. mutiwa* specimens from the Omo, and ***iv)*** the presence of ulnar and femoral morphs referable to *P. mutiwa* in the E and G members (see the following paragraphs), we allocate the above-mentioned specimens in the *P. mutiwa* hypodigm. The specimens from members E and G would represent temporally younger (*i.e.*, *ca.* 240,000 and *ca.* 455,000 years younger, respectively) *P. mutiwa* specimens compared to the partial skeleton from Nachukui (i.e., KNM-WT 16927).

A third morphotype is documented by specimens from members C (L 78-10031; Fig. 6) and G (F 501-1; Fig. 6). These specimens differ from the second morphotype (attributed here to *P. mutiwa*) in having a deeper zona conoidea, a shallower coronoid fossa, a faintly developed enthesis for the *m. brachioradialis*, a mediolaterally narrow trochlea, and absence of proximal extension of the olecranon fossa. These characteristics reflect moderate elbow flexion capabilities and stabilization of the humeroradial joint in various hand posture. Indeed, the excavated zona conoidea and globular capitulum indicate a mobile and stabilized humeroradial joint (Rose 1988, Rose *et al.* 1992, Tallman & Cooke 2016, Takano *et al.* 2018). The narrow trochlea of these specimens also suggests a minor role for the humeroulnar joint in withstanding transarticular forces (Birchette 1982, MacPhee and Meldrum 2006, Takano *et al.* 2018). Found at the upper part of Member G, in unit G-29, the morphology of F 500-1 is similar to that of *R. turkanaensis* specimens from the Upper Burgi Member of Koobi Fora. Interestingly, F 500-1 shares with *R. turkanaensis* an equal breadth of the humeral pillars and differs from *P. mutiwa* and extant colobines in this aspect.

A fourth morphotype is represented by OMO 3/O-1968-1410, a partial humerus from the Member B (Fig. 7), which was previously identified as a colobine by Ciochon (1993) on the basis of a multivariate morphometric analysis. This specimen is in the size range of *Ce. meaveae* in absolute humeral dimensions (Appendix 41). Functionally, the posterior orientation of its medial epicondyle implies a reorientation of the torques of hand and carpal flexors posteriorly compared to the medialized epicondyle of extant and fossil arboreal colobines. Similarly, its deep zona conoidea, robust humeral pillars and anteriorly projected medial trochlear keel help in withstanding high joint reaction forces and stabilizing the elbow in the parasagittal plane during quadrupedal movement on terrestrial substrates (Schmitt 2003). The humeral anatomy of OMO 3/O-1968-1410 also displays evidence of arboreal locomotor substrate preferences. This statement is supported by two characteristics: first, its proximodistally short medial trochlear keel indicates a substantial mobility of the humeroulnar

Deleted: adequacy

Deleted: s

Deleted: *meavae*

joint compared to extant *Papio*. Second, its shallow coronoid fossa is similar to extant arboreal colobines and reflects reduced capabilities for flexion. Taken independently, the above mentionned anatomical characteristics of OMO 3/O-1968-1410 can be found in early colobines, but their combination has not yet been described. More precisely, the anteroposteriorly deep and mediolaterally narrow distal humeral articular surface of OMO 3/O-1968-1410 is most similar to *P. chemeroni*, *K. hafu*, *Ce. meaveae* and *Ce. williamsi* than to *P. mutiwa* and *R. turkanaensis*. However, the Omo specimen can be distinguished from *P. chemeroni*, *K. hafu* and *Ce. meaveae* by its robust medial pillar and retroflexed medial epicondyle and it can also be distinguished from *Ce. williamsi* by its globular capitulum. Given the similarity of OMO 3/O-1968-1410 with several fossil colobines, we support an assignment of this specimen to Colobinae as a working hypothesis, but a precise generic assignment is ruled out pending recovery of additional specimens.

The fifth morphotype is only represented by OMO 294-10006, a specimen discovered at the top of Member C (Appendix 2) and in the size range of OMO 3/O-1968-1410 and *Ce. meaveae* (Appendix 41). This specimen differs from *R. turkanaensis* and *P. mutiwa* in having a mediolaterally restricted distal articular surface, a deep articular surface at the level of zona conoïdea and a less globular capitulum. OMO 294-10006 also differs from *Papio* by presenting a shallow medial trochlear keel, a large posterior trochlear articular surface and a medialized medial epicondyle. This combination of characteristics may reflect a partial terrestrial habitus or phylogenetic inertia with characters inherited from a more colobine terrestrial ancestor. Similar to OMO 3/O-1968-1410, the attribution of OMO 294-10006 to a colobine is regarded here as a working hypothesis.

A sixth morphotype includes two proximal humeral specimens (i.e., OMO 342-10052 and OMO 342-10335) that are smaller compared to *Paracolobus* and *Rhinocolobus*. These specimens were found in Member L and present a mobile glenohumeral joint, as demonstrated by the presence of a wide humeral head articular surface and an obtuse intertuberosity angle. They also exhibit an asymmetric shape of their surgical neck. All, these characteristics are also seen in *Colobus guereza*, *Co. freedmani*, *Colobus* specimens from Asbole, and a taxonomically indeterminate cercopithecid from Konso. The Shungura specimens are also in the size range of the above-mentioned fossil *Colobus* specimens. Altogether, these observations allow specimens OMO 342-10052 and OMO 342-10335 to be provisionally assigned to the genus *Colobus*.

A seventh morphotype includes two proximal humeral specimens (i.e., OMO 18inf-10063 and F 501-1) that show a mediolaterally extended humeral head and well-developed humeral tuberosities. This combination of features is also observed in *R. turkanaensis* and reflects

Deleted: *meavae*

Deleted: *meavae*

Deleted: *meavae*

Commented [MOU28]: Are they outside the size and morphological range of fossil Lophocebus cf. albigena from Koobi Fora ?

mobility of the glenohumeral joint and a longer lever arm for the rotator cuff muscules. OMO 18inf-10063 differs from F 501-1 in having an elliptical and mediolaterally extended surgical neck compared to the more rounded surgical neck of the latter specimen. The anteroposteriorly compressed surgical neck of OMO 18inf-10063 is also observed in *P. mutiwa* KNM-WT 16827, *P.* cf. *mutiwa* OMO 222-1973-2751, and *Co. guereza* and may be related to a developed musculature of the *m. triceps brachii*, *m. brachialis* and *m. teres major* on the upper part of the humeral shaft. Such a well-developed musculature is in agreement with the functional interpretation of the elbow of *P. mutiwa* KNM-WT 16827 and *P.* cf. *mutiwa* from the Omo. OMO 18inf-10063 differs from *P.* cf. *mutiwa* specimen OMO 70-10042, however, by showing more proximally developed humeral tuberosities and a mediolaterally expanded humeral head. These features suggest that OMO 18inf-10063 illustrates a more mobile glenohumeral joint compared to OMO 70-10042, but given the small number of proximal humeral specimens of large colobines identified here (n = 3) compared to distal humeral specimens (n = 12), any taxonomic distinctions based on the proximal humerus shape would be considered tentative. Similarly, while F 501-1 is phenetically similar to *R. turkanaensis* KNM-ER 1542 in exhibiting a rounded surgical neck, more data are needed to understand the range of variation in surgical neck shape among extant colobines. In conclusion, we assign OMO 18inf-10063 and F 501-1 to large Colobinae gen. indet. and sp. indet., pending further analysis on the glenohumeral joint of large Plio-Pleistocene colobines.

Deleted:

Functional interpretations and taxonomy of the ulnar specimens

Distinct ulnar morphologies are observed in specimens from members C (*i.e.*, L 293-10004, L 373-3, L 107-4 and L 32-144) and E (*i.e.*, L 236-1a & OMO 57/4-1972-164).

A first ulnar morphotype, represented by L 373-3 and OMO 57/4-1972-164, is characterized by a marked reduction of the olecranon process and a wide, undivided radial notch. Short olecranon processes are related to pronounced extension abilities at the elbow (Su & Jablonski, 2009) while the undivided radial notch suggests increased rotational abilities of the forearm (Rose 1983, 1988, Gebo & Sargis 1994). The proximal part of their olecranon is also slightly retroflexed to increase the lever arm of the *m. triceps brachii* during elbow extension postures (Drapeau 2004). Moreover, the anterior expansion of the coronoid process of OMO 57/4-1972-164 would have facilitated stress dissipation in elbow extension postures. The distally extended enthesis of the *m. brachialis* of L 373-3 also indicates powerful and frequent forearm flexion (Rose *et al.* 1996). Altogether, these features are consistent with frequent use of the elbow in extended postures, perhaps during suspension behaviors, extended-elbow climbing or overhead food retrieval. Interestingly, overhead food retrieval is

more common in *Piliocolobus badius* Kerr, 1792 than in the sympatric *Colobus polykomos* Zimmerman, 1780 in the Taï Forest (Dunham *et al.* 2016).

Overall, the morphology of L 373-3 and OMO 57/4-1972-164 is congruent with that of *R. turkanaensis.* When compared to previously described postcranial specimens, their reduced size rules out any assignment to a male individual. However, the size differences between the specimens does not exceed the level observed in *N. larvatus* (Fig. 24). Given our observations and analyses, L 373-3 and OMO 57/4-1972-164 might represent the first described ulnae of *R. turkanaensis* females.

A second ulnar morphotype, represented by L 107-4, L 32-144, L 293-10004 and L 236-1a, has a proximally extended olecranon process, an anteroposteriorly buttressed sigmoid notch with anteriorly projecting anconeal and coronoid processes, asymmetrical margins of the anconeal, an enlarged posterior aspect of the coronoid process, a laterally projected radial notch, a moderate distal inclination of the coronoid, a complete or partial subdivision of the radial notch, and a poorly extended enthesis for the *m. brachialis*. The proximal extension of their olecranon would have increased the leverage of the *m. triceps brachii*, allowing for powerful extension of the elbow (Harrison 1989, Fleagle & Simons 1995). The anteroposterior buttressing of their sigmoid notch indicates that the ulnar side of their elbow was adapted to withstand substantial compressive transarticular stresses. Similarly, the anteriorly protruding anconeal and coronoid processes and the asymmetrical anconeal margins support the view of a stabilized elbow against transversely directed stresses (Birchette 1982; Rose 1983; Schmitt 2003; MacPhee & Meldrum, 2006). The wide posterior portion of the articular surface of the coronoid process indicates an ability to withstand significant transarticular stress in a flexed or semi-flexed elbow posture (Takano *et al.* 2018). The lateral projection of their radial notches will also have increased joint stability in pronated hand postures, as observed in large terrestrial cercopithecids (Richmond *et al.* 1998). In addition, the partially or fully subdivided radial notches of these specimens indicate reduced rotational capabilities of the forearm (Rose 1988; Harrison 1989; Gebo & Sargis, 1994), especially compared to the first morphotype (e.g., L 373-3). The distally inclined medial portion of their coronoid processes would also likely have accommodated a salient humeral medial trochlear keel, further enhancing elbow stabilization in a fashion typical to that of terrestrial cercopithecids (Schmitt 2003). Conclusively, the morphological features exhibited by L 107-4, L 32-144, L 293-10004 and L 236-1a point to a stable humeroulnar joint, primarily loaded in a flexion posture. Such adaptations corroborate slow and cautious climbing with a flexed elbow and quadrupedal walking on arboreal substrates. These specimens are provisionally allocated to *Paracolobus mutiwa* given their ***i)*** similar size and anatomy compared to the partial skeleton of *P. mutiwa*

Deleted: assignation

Deleted:

Deleted: specimens

KNM-WT 16827, ***ii)*** the presence of similar-sized craniodental specimens of *P. mutiwa* in members C and E, and ***iii)*** by their chronological setting regarding the partial skeleton KNM-WT 16827 as the Omo specimens are ca. 240,000 years and ca. 110,000 years older than KNM-WT 16827.

Functional interpretations and taxonomy of the radial specimens.

We demonstrated in the previous section that the ulnar anatomy of L 236-1a corresponds to that presented by the partial skeleton of *P. mutiwa* KNM-WT 16827 (SI.27). The proximal ulna L 236-1a is associated with a proximal radius (L 236-1b) that is hence also provisionally assigned to *P. mutiwa*. Unfortunately, only a few preserved portions of L 236-1b are commonly shared with KNM-WT 16827, which prevents extensive comparative work. L 236-1a present a distal extension of the peripheral articular margin, just above its bicipital tuberosity, which differs from the other radius assignable to a large colobine, OMO 2-10029 (see below), and functionally indicates of a close packing of the proximal radioulnar joint in a pronated hand posture in L 236-1, similar to terrestrial cercopithecids.

A second morphotype, represented by the sub-complete radius OMO 2-10029, is morphologically distinct from *Paracolobus.* spp., *Cercopithecoides.* spp., and L 236-1a by the following combination of anatomical characteristics: an angulated shaft with a poorly developed interosseous crest, an elongated neck, a deep fovea and a tilted head with a marked beveled surface on its medial margin. The angulated shaft of OMO 2-10029 is diagnostic of increased rotational capabilities of the forearm (Ibáñez-Gimeno *et al.* 2014). Its smooth interosseous crest suggests a weakly developed musculature of the *m. flexor pollicis longus* and *m. abductor pollicis longus*, and perhaps a poor reliance on manipulative behaviors (Fleagle & McGraw 2002). The elongated radial neck of OMO 2-10029 indicates the presence of a powerful lever arm for the *m. biceps brachii*, which differs from the reduced lever arm observed in terrestrial cercopithecids (Birchette 1982, Harrison 1989, Rose *et al.* 1992). Its deep radial fovea would have ensured stability of the humeroradial joint in various hand postures, as in arboreal colobines. The presence of a bevel on the anteromedial portion of its radial head is characteristic of a stabilized humeroradial joint in a pronated posture while its extension on the perimeter of the head indicates joint stability in forearm rotation (Rose *et al.* 1992, Patel 2005). The inclination of the radial head of OMO 2-10029 is also linked to stabilization of the humeroradial joint in a pronated posture (Rose *et al.* 1992). Collectively, these features indicate preferences for quadrupedalism on arboreal substrates and enhanced capabilities for forearm rotation. Thus far, no radial remains were included with confidence in the hypodigm of *R. turkanaensis* but OMO 2-10029 ***i)*** is similar in size to *R. turkanaensis*, ***ii)***

matches with the arboreal substrate preferences previously inferred for *R. turkanaensis*, ***iii)*** is from a time interval (upper part of Member G) that includes craniodental remains of *Rhinocolobus* and ***iv)*** is anatomically congruent with a humeral specimen close in age and attributed here to *Rhinocolobus* cf. *turkanaensis* (i.e., specimen F 500-1 from G-28). Indeed, humeral specimen F 500-1 has a deeply excavated humeral zona conoidea that could have corresponded to the bevel of the radial head of OMO 2-10029. Conclusively, our data point at a more parsimonious assignment of OMO 2-10029 to *R. turkanaensis*.

Functional interpretations and taxonomy of the femoral specimens.

Three femoral morphotypes from Usno and lower Member G were identified on size and anatomical differences. The specimen W 7-477B from the White Sands level of the Usno Formation is associated with an isolated M_3 (W 7-477A) referred to *P. mutiwa* by Leakey (1987). If this taxonomic allocation is correct, W 7-477A and -B might represent the oldest occurrence of *P. mutiwa*. To date, no securely associated craniodental and postcranial specimens were attributed to *P. mutiwa* within the corresponding time interval (3.40 Ma - 3.10 Ma). Functionally, the short and robust femoral neck of W 7-477B denote the need for its proximal femur to resist significant mechanical stress (Nakatsukasa 1994, Tallman & Cooke 2016), as also observed in leaping primates (Cooke & Tallman 2012). The acute collodiaphyseal angle of W 7-477B reflects hip motions restricted to the parasagittal plane and accords with leaping and cursorial behaviors (Ward 1993, Gebo & Sargis 1994, Fleagle & Simons 1995, Bacon 2001, Cooke & Tallman 2012). Its narrow trochanteric fossa also reflects a hip joint used preferentially in the parasagittal plane. This narrow trochanteric fossa is associated with a developed trochanteric crest and quadrate tubercle that indicates the presence of a powerful *m. quadratus femoris*, a lateral rotator of the thigh. Its developed enthesis for the ischiofemoral ligament suggests a stabilized hip joint, especially during internal rotation and hip abduction (Hidaka *et al.* 2014, Fleagle & Simons 1995). Its medially facing and enlarged lesser trochanter would have facilitated recruitment of the *m. iliopsoas* and facilitated the flexion of the thigh (Bacon, 2001). Finally, the moderate proximal projection of the greater trochanter is consistent with a mobile joint and contrasts with the restricted hip joint (and thus the highly projected greater trochanter) of terrestrial cercopithecids.

A second femoral morphotype from the lower part of Member G is represented by specimens OMO 75/N-1971-728 and OMO 50-1973-4450. These specimens are morphologically similar to KNM-ER 551 and KNM-ER 40058, two putative *Rhinocolobus* specimens from the KBS Member of Koobi Fora. OMO 75/N-1971-728 and OMO 50-1973-4450 differ from W 7-477B in having an extensive encroachment of the femoral head onto the

Deleted: ï

Deleted: er

Deleted: n

neck, a centrally-placed fovea capitis, an enlarged insertion site of the illiofemoral ligament and a larger trochanteric fossa. The articular surface of the femoral head impinging on the neck indicates that the head was well embedded into the acetabulum, probably with extensive contact during external rotation and abduction of the hip (Anemone 1990, Ward 1993, Nakatsukasa 1994). The centrally placed fovea capitis of OMO 75/N-1971-729 and OMO 50-1973-4450 also suggests habitual use of the thigh in various postures while the eccentrically placed fovea of W 7-477B is more informative of a hip usually positioned in abduction (Jenkins & Camazine 1977, Ward 1993, Nakatsukasa 1994). The shape of the trochanteric fossa impacts the recruitment of several ischio-trochanteric muscles. Deep, wide fossae, such as those in OMO 75/N-1971-729 and OMO 50-1973-4450, are indicative of versatile thigh postures and powerful recruitment of the *m. obturator externus* (Bacon 2001). The developed enthesis for the illiofemoral ligament in OMO 75/N-1971-729 and OMO 50-1973-4450 indicates a hip stabilized against frequent extension and external rotation (Hidaka *et al.* 2014). The proximal projection of the greater trochanter in these specimens is moderate and agrees with a mobility of the hip similar to most extant arboreal colobines (Harrison 1989, Nakatsukasa 1994). Conclusively, the functional picture of the hip of OMO 75/N-1971-728 and OMO 50-1973-4450 is that of a frequently abducted and externally rotated mobile joint. Taxonomically, this study supports the placement of OMO 75/N-1971-729 and OMO 50-1973-4450 in the hypodigm of *R. turkanaensis*. Our argument is strengthened by the presence of craniodental specimens of *R. turkanaensis* in the temporal frame of Shungura (2.19 Ma - 2.06 Ma) in which these specimens were recovered.

Deleted:

A third morphotype is represented by small-sized specimens from Member L (i.e., OMO 342-10298, OMO 342-10344 and OMO 342-10019; Fig.19). These specimens differ from *Co. freedmani* and *Colobus* sp. indet. from Asbole in the increased robustness of their necks and the enlargement of their entheses (i.e., illiofemoral ligament and *m. vastus lateralis*). These differences reflect greater reliance in leaping behaviors in Omo colobines. Overall, the functional anatomy and age of the proximal femora from Member L support their attribution to *Colobus*.

Functional interpretations and taxonomy of the tibial specimens.

The tibial anatomy of the Shungura colobines is known only from OMO 377-10024, a nearly complete tibia from Member L that matches extant *Colobus* in size.

Functionally, the marked concavity of its condyles would have increased the stability of its knee relative to the parasagittal plane, a characteristic seen in leaper and runner monkeys (Fleagle & Simons, 1982b). Its retroflexed proximal epiphysis indicates a knee preferentially

placed in a semi-flexed posture, as is typical of arboreal monkeys (Fleagle & Simons 1995). The angulation and spacing of the intercondylar spines are related to the rotational capacity of the knee joint, and specifically to the independent rotation of the femur on the tibia (Tardieu 1983,White & Gebo 2004). Subsequently, the widely spaced intercondylar spines of OMO 377-10024 indicate substantial knee rotation capabilities. Additionally, the mediolateral extension of its posterior intercondyloid area could be related to a developed posterior cruciate ligament, thus limiting any extensive tibial posterior translation. The distal extension of the tibial tuberosity (attachment site of the patellar ligament) impacts the lever arm of the *m. quadriceps femoris* (Frelat *et al.* 2017, Laird *et al.* 2018). The distal imprinting of the tibial tuberosity in the Omo specimen is therefore suggestive of powerful extension of the thigh.

The developed enthesis of the *m. tibialis anterior* and *posterior* located on the proximal diaphysis of OMO 377-10024 also suggest a well-developed musculature for dorsiflexion and plantarflexion of the foot. The marked mediolateral constriction of the proximal metaphysis and mid-diaphysis of OMO 377-10024 is consistent with behaviors that exert bending stresses in the parasagittal plane, such as leaping and running (Fleagle & Simons 1995).

The distal extension of the bony eminence present at the anterior border of the distal articular surface of the tibia is linked to the stability of the talocrural joint in dorsiflexion (Harrison 1989, DeSilva *et al.* 2010). The weak development of this tubercle in OMO 377-10024 implies a moderate stabilization of its talocrural joint in dorsiflexion. The malleolar robustness is an indicator of the loading regime that is applied to the ankle. A robust malleolus is related to frequent inversion of the foot, a posture of the ankle adopted during vertical climbing (DeSilva 2008). The robust malleolus of OMO 377-10024 indicates frequent ankle loading in inverted posture, likely during climbing.

OMO 377-10024 is in the size range of *Co. freedmani*, *Colobus* sp. indet from Asbole and extant Colobini (i.e., *Piliocolobus* spp. and *Colobus* spp.). It differs from *Co. freedmani* by minor morphological variations (i.e., the size of the posterior intercondyloid area, the orientation of the intercondylar septum and the entheseal development on the proximal metaphysis). Such features may translate a greater reliance on leaping for the Omo specimen compared to *Co. freedmani*. This hypothesis is in line with our functional interpretation of the Member L *Colobus* femoral morphotype.

IMPLICATIONS FOR THE EVOLUTIONARY HISTORY AND PALEOECOLOGY OF THE PLIO-PLEISTOCENE FOSSIL COLOBINES

Paracolobus mutiwa

Deleted:

Our only source of information concerning the postcranial anatomy of *Paracolobus mutiwa* comes from the associated male partial skeleton KNM-WT 16827 from the Lomekwi Member of the Nachukui Formation (Harris *et al.* 1988, Anderson 2021). Despite the description of *n* = 42 craniodental specimens spanning an extensive temporal interval (from ca. 3.6 Ma to ca. 1.9 Ma according to Leakey 1987), no postcranial specimens of *P. mutiwa* have been yet published from Usno and Shungura. Here, we provide morphological and functional arguments in favor of a taxonomic allocation of *n* = 10 specimens to the species *P. mutiwa*. Humeral, ulnar and femoral specimens with morphological resemblance to the *P. mutiwa* partial skeleton KNM-WT 16827 were found in members C, E and G of the Shungura Formation and in the White sands locality of the Usno Formation. The partial skeleton KNM-WT 16827 provided critical information on the substrate preferences of *P. mutiwa* and the previous functional analysis of Anderson (2021) hypothesized that it was mainly terrestrial based on, among the anatomical characters also preserved in the Omo specimens, a robust deltoid tuberosity, a retroflexed humeral epicondyle, a deep ulnar sigmoid notch, a prominent femoral greater trochanter and an asymmetrical astragalar trochlea. Our functional interpretation of *P. mutiwa* is more balanced and demonstrate that its elbow was likely adapted to tree climbing and overall, that its anatomy was consistent with mixed ("semi-terrestrial") locomotor substrate preferences.

The most distinct morphological aspects of the *Paracolobus* cf. *mutiwa* from the Omo are their enlarged *m. brachioradialis* enthesis (and hence enlarged lateral supracondylar crest) and their deep supratrochlear fossae, features unknown in this state of development in other colobines apart for the partial skeleton of *P. mutiwa* KNM-WT 16827. A broad and proximally developed lateral supracondylar crest was interpreted in relation to manual foraging and climbing in the papionines *Mandrillus* and *Cercocebus* (Fleagle & McGraw 2002) and climbing in fossil and extant anthropoids (Fleagle & Simons 1982, Senut *et al.* 2001, Koukoubis *et al.* 1995) and carnivores (Gardin *et al.* 2021). Given the primary role of the *m. brachioradialis* as an elbow flexor (Boland and Spigelman 2008), we interpret here the developed lateral supracondylar crest of the Omo specimens and KNM-WT 16827 as evidence for climbing behaviors instead of terrestrial quadrupedalism, as proposed by Anderson (2021). Similarly, a deep sigmoid notch would have stabilized the elbow during slow and cautious climbing. The morphology of the supratrochlear fossae and medial epicondyle also supports our functional hypothesis regarding climbing abilities. The large size of *P. mutiwa* implies osteological and behavioral adaptations to dwell in trees. Specifically, we hypothesize that *P. mutiwa* presents osteological adaptations related to enhanced abilities to maneuver and climb on vertical arboreal supports with a flexed elbow.

Deleted: s

Commented [MOU29]: Since Soromandrillus is also found in the Omo, can we be certain that these specimens belong to Pa. mutiwa rather than Soromandrillus? Some comment on why they are likely to be mutiwa rather than Soromandrillus is needed somewhere in here. Can T. brumpti be ruled out as well?

Commented [MOU30]: Can you provide an extant species with these features that is more of a climber than a terrestrial species, as you are suggesting here? Mandrills have many of these features and are quite terrestrial, for instance, so while it seems reasonable to point out that there might have been more climbing in the repertoire than previously appreciated, many of these features seem associated with more terrestrial behaviors. If you have a reference for the deep sigmoid notch being indicative of climbing, please provide it. But it has been noted previously to be associated with a stable elbow and terrestrial quadrupedalism.

While minor morphological variation is observed in *P.* cf. *mutiwa* specimens from the Omo, substantial differences in size and mass were noticed based on geometric mean comparisons and body mass inferences. These observations demonstrate the presence of a high sexual dimorphism and thus identification of presumably large male individuals (i.e., OMO 176-10006) and smaller female individuals (i.e., OMO 70-10042 and L 293-10004) according to the lower and upper range of size variation of our sample. Apart from KNM-WT 16827, no canine of *P. mutiwa* are preserved (i.e., only the lower portion of the upper canine crown is preserved in KNM-ER 3843). Thus, on the sole basis of canine dimensions, we cannot confidently assess the level of sexual dimorphism in *P. mutiwa*. According to our postcranial specimens, the degree of sexual dimorphism in *P. mutiwa* would be as high as that of *Nasalis larvatus*. Sexual dimorphism in frequencies of substrate use and locomotor behaviors is known for extant cercopithecids (e.g., described for *Cercocebus agilis* in Shah 2003, for *Rhinopithecus bieti* in Isler & Grüter 2006, and for *Rhinopithecus strykeri* in Yang *et al.* 2021). Our functional results have significant implications on this aspect as the specimen L 293-10004, which is assumed to be from a female *P.* cf. *mutiwa* individual, presents a distinct morphology from the male *P.* cf. *mutiwa* individuals. Indeed, its overall gracility, enhanced mobility of its proximal radioulnar joint, and lack of marked stabilization of the humeroulnar joint reflect a greater utilization of arboreal substrates regarding putative male ulnar specimens. Subsequently, this suggests sexual dimorphism in locomotor substrate use in conjunction with body mass differences in the fossil species *P. mutiwa*.

Rhinocolobus turkanaensis

Hypothesis regarding the locomotor repertoire and locomotor substrate use of *R. turkanaensis* were primarily based on the partial male skeleton KNM-ER 1542 (Jablonski & Leakey, 2008b), but isolated remains from Koobi Fora (Jablonski & Leakey 2008b), Hadar (Ciochon 1986, Frost & Delson 2002) and Laetoli (Harrison 2011) are also part of the hypodigm of *R. turkanaensis*. Although the taxonomic allocations of ulnar and humeral specimens of *Paracolobus* cf. *mutiwa* have been confidently demonstrated, the case is noticeably different for *R. turkanaensis* since the specimens discussed here (with the exclusion of the cf. *Rhinocolobus* sp. from Laetoli) span a time interval of ca. 600,000 years for the Omo specimens and 1.84 million years for asserted and presumed *Rhinocolobus* comparative specimens.

With regard to forearm bones, the morphotype from members C and E that we likened to *Rhinocolobus* suggests increased forearm extension and rotational capabilities compared to *P. mutiwa*. Our knowledge of the postcranial anatomy of *Rhinocolobus* comes primarily from

Deleted: i

Commented [MOU31]: Again, these are likely bettter assigned to Kuseracolobus, not Rhinocolobus. See Frost et al. (2022) in colobine book.

male specimens (Jablonski & Leakey 2008b). Our data support the hypothesis of sexual dimorphism to explain the differences between *Rhinocolobus* specimens from the Omo and Koobi Fora, as their size difference does not exceed that of *Nasalis larvatus*.

The *R.* cf. *turkanaensis* femora identified from lower Member G exhibits a morphology reminiscent to that of an isolated femur from Koobi Fora putatively identified as *Rhinocolobus* sp. (KNM-ER 551). A nearly complete radius (OMO 2-10029) from unit G-29 has anatomical characteristics in line with a frequent use of arboreal substrates and enhanced forearm mobility. Its radial head anatomy is a perfect fit with its congruent portion on the distal part of a sub-complete humerus from G-28 (F 500-1). The nearly complete humerus F 500-1 fits the morphology and size of the comparative sample of *Rhinocolobus* from Koobi Fora, particularly to KNM-ER 45611.

As for the functional anatomy and paleoecology of *Rhinocolobus*, our analysis corroborates previous studies (Table 1) and supports: ***i)*** increased arm extension capabilities and mobility of the humeroradial and glenohumeral joints, ***ii)*** preferential use of arboreal substrates, and ***iii)*** significant hip mobility.

Deleted:

Early Colobus *from Member L*

Our knowledge of the appearance of the genus *Colobus* is based on fossils spanning from the lower Pliocene of Kanam East (if we assume the stratigraphic context is correct) to the Upper Pleistocene of the Asbole deposits (Harrison 1996, Frost & Alemseged 2007). Prominently, specimens from the Koobi Fora Formation (Okote Member) and Asbole Formation, are at least 380,000 years older and up to 450,000 years younger, respectively, than the fossil colobines from Member L. Fossils from the Okote Member represent *Co. freedmani*, a species distinct from any modern species, whereas the taxonomic status of the Asbole sample is not precisely asserted (*Piliocolobus* spp. or *Colobus* spp. but excluding *Co. guereza*). In any case, no definitive assignment of cranial, dental nor postcranial fossils to *Co. guereza* has been established with certainty in the Pliocene and early Pleistocene of Africa. Molecular dating of the separation of *Co. guereza* from its sister taxa *Co. polykomos* and *Co. vellerosus* to ca. 1.60 ± 0.40 Ma (Ting, 2008) overlaps the time interval corresponding to Member L deposition (1.38 Ma - 1.05 Ma).

Numerous craniodental specimens similar in morphology and size to *Colobus* have been identified in the members K and L of the Shungura Formation (Leakey 1987). The postcranial specimens of early *Colobus* described here from Member L present unambiguous morphological adaptations for arboreal locomotor substrate preferences. Nevertheless, minor morphological differences have been demonstrated in Shungura specimens, mostly related

to higher abilities for leaping compared to *Co. freedmani*. A humerus from Konso (KGA 4-418), previously identified as an indeterminate Cercopithecidae by Frost (2014), is also hypothesized here to be a colobine similar in morphology to extant and fossil *Colobus*. Moreover, KGA 4-418 bears a close resemblance with the *Colobus* collection from Shungura. A precise taxonomic allocation is impossible based on the postcranial specimens recovered so far from Shungura, and we recognize the limitation of our comparative dataset in identifying significant postcranial differences between *Colobus* and *Piliocolobus*. Indeed, our *Piliocolobus* sample is dominated by female individuals and by populations predominantly coming from central Africa. Future studies focusing on the morphological distinction between *Colobus* and *Piliocolobus* could potentially clarify the taxonomic status of Shungura specimens.

As forest-dependent cercopithecids, contraction and expansion of forest cover as well as changes in the hydrographic system may have significantly influenced the taxonomy and distribution of early *Colobus* representatives. If we consider Koobi Fora, Asbole and Omo specimens to have different taxonomic status, then this taxonomic distinctiveness may reflect distinct forest refugia, similar to the pattern inferred from molecular data in Cercopithecini (Tosi 2008). Future studies of craniodental fossils of the small colobines from Member L may resolve the issue of the taxonomy of the earliest Shungura *Colobus* representatives.

Taxonomically indeterminate specimens from Usno and the Member B

Previously identified as a colobine (Ciochon 1993), the humerus OMO 3/O-1968-1410 has a puzzling mosaic of characters and its taxonomic assignment is treated with caution here. If we accept the colobine status of this specimen, then it provides evidence of a partly terrestrial colobine in the time frame covered by unit B-12 (ca. 2.92 Ma). The recognition of a new partially terrestrial colobine will further add to the ecomorphological diversity documented hitherto among this subfamilly (Jablonski & Leakey 2008a&b, Pallas *et al.* 2019). Until now, evidence for the ulnar anatomy of early medium-sized colobines from the late Pliocene in eastern Africa has been meager (Frost & Delson 2002, Hlusko 2006, 2007).

Ulnar specimens of a medium-sized colobine from the lower part of the Member B (P 732-1) and Usno (B-818A) demonstrate the presence of arboreal colobines during this period in the northern part of the Turkana Depression.

Taxonomically indeterminate specimens from the Member C

Intriguing postcranial specimens that differ in size and shape from *Rhinocolobus* and *Paracolobus* were identified in Member C. The morphological distinctiveness of OMO 165-

1973-608, OMO 18-1967-135 and OMO 18-1971-702 confirms taxonomic diversity among the colobine paleocommunity of Shungura Member C, a period that also includes *Rhinocolobus* and *Paracolobus*. These specimens may represent the same taxon as Colobinae gen. indet. sp. indet. known from isolated dental specimens in Member C (n = 13 specimens spanning units C-4 to C-8, and from locality OMO 18 according to Leakey 1987). This last point is strengthened by the adequacy of body masses inferred from postcranial and dental data.

In functional terms, the morphology of the humerus of the indeterminate colobine from the Member C reflects a combination of mobility and stabilization of the humeroradial and humeroulnar joint. The closest morphological similarity is with *Ce. meaveae* and with specimens from Lemudong'o conservatively assigned to *P. enkorikae* (Hlusko 2007), although the Omo specimens are larger than the latter. Considering the meager postcranial data we have for this Colobinae gen. indet. sp. indet., it seems difficult to assess taxonomic hypotheses with confidence but further comparisons with *Ce. meaveae* are needed.

Deleted: *meavae*

Deleted: *meavae*

Deleted: ?

CONCLUSION

In the present study, we described fore- and hindlimb fossils with close morphological affinities to associated postcranial specimens of *Rhinocolobus turkanaensis* and *Paracolobus mutiwa*, adding to the knowledge of the functional anatomy and paleoecology of these large extinct colobines. A diversity of size and morphologies is highlighted in our *Rhinocolobus* cf. *turkanaensis* sample while our description of isolated specimens presumably assigned to *P. mutiwa* provides valuable information on the functional aspect of the postcranial anatomy of this species, particularly in regard to its climbing abilities. Among others, we described a partial elbow of a possible *Paracolobus mutiwa* individual (L 236-1a&b), sub-complete humeri of specimens possibly belonging to *Paracolobus mutiwa* and *Rhinocolobus turkanaensis*, the second most complete radius of a large colobine and a sub-complete tibia of a colobine similar in size to *Colobus*. Evidences for enhanced foream extension capabilities were highlighted in ulnar specimens from the members C and E (*e.g.*, L 373-3 and OMO 57/4-1972-164) while climbing and leaping are characterized in specimens from Lower G (*e.g.*, OMO 222-1973-2751) and Member L (*e.g.*, OMO 342-10019), respectively. This analysis confirms the arboreal substrate preferences of *Rhinocolobus* and add new insights regarding the mixed substrate preferences of *P. mutiwa* and its climbing abilities. By documenting morphologically distinct specimens in presumed sympatry in members C, E and Lower G, the present work

also appears as a first step towards a better understanding of the niche partitioning of the early colobines. This last point is of tremendous value given the diverse Plio-Pleistocene primate paleocommunity hitherto documented within African paleoecosystems.

Acknowledgements

We are grateful to the National Museum of Ethiopia/Ethiopian Heritage Authority (ex-ARCCH, Ministry of Tourism) for allowing to access collections and perform research. We deeply thank the NME staff (T. Getachew, S. Selassie, and G. Tekle Yemanebirihan) for guidance and support with collection study. We are thankful to the curators of various institutions who allowed us to study extant specimens under their care (E. Gillisen, RMCA; J. Cuisin, MNHN; L. Costeur and F. Dammeyer, NMB; D. Berthet MHNL; C. Zollikofer and M. Ponce de León UZH-MA; J. Kibii, NMK). We thank William Kimbel and Kaye Reed for providing access to the Hadar cercopithecid fossil collection. L. Pallas is grateful to the doctoral school Theodore Monod (Faculty of Fundamental and Applied Sciences, University of Poitiers) and Groupement de Recherche (GDR) Rift for financial support. We thank the CFEE and PALEVOPRIM staff for administrative support (M. Bridonneau, A.-L. Goujon, F. Guy, C. Ménard, L. Painault, G. Reynaud, H. Seyoum, A. Solomon). We are grateful to L. Hlusko, M. Nakatsukasa, J. Braga, L. Shapiro, A. Houssaye, G. Thiery, and C. Grohé for insightful comments on an earlier version of this manuscript. We are deeply indebted to the hundreds of people who participated to the fieldwork missions of the IORE, of the OGRE and of other research programs, who managed collections and databases, who prepared specimens, who contributed to their study, who provided financial support, who helped with administrative processes, and who provided advice and moral support. The OGRE is a joint program of PALEVOPRIM, the CFEE and the EHA principally funded by the Ministry of Europe and Foreign Affairs, the National Research Agency, the Région Nouvelle-Aquitaine, CNRS INEE, PALEVOPRIM, and the Fyssen Foundation. The OGRE is extremely grateful to the EHA, the SNNPR, the South Omo Zone, the Nyangatom and Dassanetch Weredas and their people for their help and reception.

Funding

This work was principally funded by the Ministry of Europe and Foreign Affairs (Mission Paléoanthropologique dans l'Omo), the National Research Agency (HOMTECH, n° ANR-17-CE27-0005-02, OLD, n° ANR-16-CE27-0009-02), the Région Nouvelle-Aquitaine (ECCE-OMO, n° 2017-1R40219), CNRS INEE (SEEG), PALEVOPRIM, and the Fyssen Foundation.

Conflict of interest disclosure

The authors declare that they comply with the PCI rule of having no financial conflicts of interest in relation to the content of the article.

Author contributions

J.R.B led field research and new specimen acquisition, L.P., G.D., G.M., and J.R.B. participated to the conceptualization and supervision of the study; L.P. and J.R.B. participated to data curation; L.P. performed the analysis, methodology and acquired all data presented in the manuscript; L.P., G.D. and J.R.B. participated to funding acquisition; L.P. write the original draft of the manuscript with comments and revisions from G.D., G.M. and J.R.B.

Data, script, code, and supplementary information availability

Supplementary data is available at the following link: https://osf.io/27rb9/

BIBLIOGRAPHY

Anderson M. 2021. – An assessment of the postcranial skeleton of the *Paracolobus mutiwa* (Primates: Colobinae) specimen KNM-WT 16827 from Lomekwi, West Turkana, Kenya. *Journal of Human Evolution* 156: 103012. https://doi.org/10.1016/j.jhevol.2021.103012

Anemone R. 1990. – The VCL Hypothesis Revisited: Patterns of Femoral Morphology Among Quadrupedal and Saltatorial Prosimian Primates. *American Journal of Physical Anthropology* 83: 373-393. https://doi.org/10.1002/ajpa.1330830310

Bacon A.-M. 2001. – *La locomotion des primates du Miocène d'Afrique et d'Europe*. Cahiers de Paléoanthropologie, CNRS Éditions, Paris, 138 p.

Benefit B.R. 1999. – *Victoriapithecus*: the key to Old World monkey and catarrhine origins. *Evolutionary Anthropology: Issues, News, and Reviews* 7: 155-174. https://doi.org/10.1002/(SICI)1520-6505(1999)7:5<155::AID-EVAN2>3.0.CO;2-D

Bibi F., Souron A., Bocherens H., Uno K. & Boisserie J.-R. 2012. – Ecological change in the lower Omo Valley around 2.8 Ma. *Biology Letters* 9: 1-4. https://doi.org/10.1098/rsbl.2012.0890

Birchette M.G. 1981. – Postcranial remains of *Cercopithecoides*. *American Journal of Physical Anthropology* 54: 201.

Birchette M.G. 1982. – *The postcranial skeleton of Paracolobus chemeroni*. Ph.D. Dissertation, Harvard University, Harvard, 494 p.

Bismark M. 2010. – Proboscis Monkey (*Nasalis larvatus*): Bio-ecology and Conservation, *in* Gursky S. & Supriatna J. (eds), *Indonesian Primates*. Springer, New York, pp. 217-233.

Blondel C., Rowan J., Merceron G., Bibi F., Negash E., Barr W.A. & Boisserie J.-R. 2018. – Feeding ecology of Tragelaphini (Bovidae) from the Shungura Formation, Omo Valley, Ethiopia: Contribution of dental wear analyses. *Palaeogeography, Palaeoclimatology, Palaeoecology* 496: 103-120. https://doi.org/10.1016/j.palaeo.2018.01.027

Bobe R. & Leakey M.G. 2009. – Ecology of Plio-Pleistocene Mammals in the Omo—Turkana Basin and the Emergence of *Homo*, *in* Grine F.E., Fleagle J.G. & Leakey, R.E. (eds), T*he First Humans – Origin and Early Evolution of the Genus* Homo. Springer Netherlands, Dordrecht, pp. 173-184.

Boisserie J.-R., Delagnes A., Beyene Y. & Schuster M. 2010. – Reconstructing the African background to human expansions in Eurasia: New research in the Shungura Formation, Ethiopia. *Quaternary International* 223-224: 426–428. https://doi.org /10.1016/j.quaint.2009.07.013

Boisserie J.-R., Guy F., Delagnes A., Hlukso L.J., Bibi F., Beyene Y. & Guillemot C. 2008. –

New palaeoanthropological research in the Plio-Pleistocene Omo Group, Lower Omo Valley, SNNPR (Southern Nations, Nationalities and People Regions), Ethiopia. *Comptes Rendus Palevol* 7: 429-439. https://doi.org/10.1016/j.crpv.2008.07.010

Boyer D.M. & Seiffert E.R. 2013. – Patterns of astragalar fibular facet orientation in extant and fossil primates and their evolutionary implications: Fibular Facet Orientation in Primates. *American Journal of Physical Anthropology* 151: 420-447. https://doi.org/10.1002/ajpa.22283

Brown F.H. & Heinzelin J. de 1983. – The Lower Omo Basin *in* de Heinzelin J. (ed.), *The Omo Group - Archives of the International Omo Expedition*. Annales du Musée Royal de l'Afrique Centrale, Tervuren, Belgique, pp.7-21.

Cerling T.E., Levin N.E. & Passey B.H. 2011a. Stable Isotope Ecology in the Omo-Turkana Basin. *Evolutionary Anthropology: Issues, News, and Reviews* 20: 228-237. https://doi.org/10.1002/evan.20326

Cerling T.E., Wynn J.G., Andanje S.A., Bird M.I., Korir D.K., Levin N.E., Mace W., Macharia A.N., Quade J. & Remien C.H. 2011b. Woody cover and hominin environments in the past 6 million years. *Nature* 476: 51-57. https://doi.org/10.1038/nature10306

Ciochon R.L. 1993. – Evolution of the Cercopithecoid Forelimb: Phylogenetic and Functional Implications from Morphometric Analyses. *University of California Publications in Geological Sciences* 138: 1-251.

Cooke S.B. & Tallman M. 2012. – New endemic platyrrhine femur from Haiti: Description and locomotor analysis. *Journal of Human Evolution* 63: 560-567. http://dx.doi.org/10.1016/j.jhevol.2012.05.008

Delson E., Terranova C.J., Jungers W.L., Sargis E.J., Jablonski N.J. & Dechow P.C. 2000. – Body mass in Cercopithecidae (Primates, Mammalia): estimation and scaling in extinct and extant taxa. *Anthropological Papers of the American Museum of Natural History* 83: 1-159.

DeSilva J.M., Morgan M.E., Barry J.C. & Pilbeam D. 2010. – A hominoid distal tibia from the Miocene of Pakistan. *Journal of Human Evolution* 58: 147-154. https://doi.org/10.1016/j.jhevol.2009.11.002

DeSilva J.M. 2008. – *Vertical climbing adaptations in the anthropoid ankle and midfoot: implications for locomotion in Miocene catarrhines and Plio-Pleistocene hominins*. Ph.D. Dissertation, University of Michigan, Michigan, 363 p.

Drapeau M.S.M. 2004. – Functional anatomy of the olecranon process in hominoids and plio-pleistocene hominins. *American Journal of Physical Anthropology* 124: 297-314. https://doi.org/10.1002/ajpa.10359

Dunham N.T., Kane E.E. & McGraw W.S. 2017. Humeral correlates of forelimb elevation in

four West African cercopithecid monkeys. *American Journal of Physical Anthropology* 162: 337-349.

Elton S., Jansson A.-U., Meloro C., Louys J., Plummer T. & Bishop L.C. 2017. – Exploring morphological generality in the Old World monkey postcranium using an ecomorphological framework. *Journal of Anatomy* 228: 534-560. https://doi.org/10.1002/ajpa.23123

Feibel C.S., Brown F.H. & McDougall I. 1989. – Stratigraphic context of fossil hominids from the Omo Group Deposits: Northern Turkana Basin, Kenya and Ethiopia. *American Journal of Physical Anthropology* 78: 592-622. https://doi.org/10.1002/ajpa.1330780412

Fashing, P.J., 2017. – Guereza, *in* Rowe N. & Myers M. (eds), All the World's Primates. Pogonias Press, Charlestown, Rhode Island, pp. 524-527.

Fleagle J.G. & McGraw W.S. 1999. – Skeletal and dental morphology supports diphyletic origin of baboons and mandrills. *Proceedings of the National Academy of Sciences of the United States of America* 96: 1157-1161. https://doi.org/10.1073/pnas.96.3.1157

Fleagle J.G. & McGraw W.S. 2002. – Skeletal and dental morphology of African papionins: unmasking a cryptic clade. *Journal of Human Evolution* 42: 267-292. https://doi.org/10.1006/jhev.2001.0526

Fleagle J.G. & Simons E.L. 1995. – Limb Skeleton and Locomotor Adaptations of *Apidium phiomense*, an Oligocene Anthropoid from Egypt. *American Journal of Physical Anthropology* 3: 235-289. https://doi.org/10.1002/ajpa.1330970303

Fleagle J.G. & Simons E.L. 1982a. The Humerus of *Aegyptopithecus zeuxis*: A Primitive Anthropoid. *American Journal of Physical Anthropology* 59: 175-193. https://doi.org/10.1002/ajpa.1330590207

Fleagle J.G. & Simons E.L. 1982b. Skeletal Remains of *Propliopithecus chirobates* from the Egyptian Oligocene. *Folia Primatologica* 39: 161-177. https://doi.org/10.1159/000156075

Ford S.M. 1988. – Postcranial adaptations of the earliest platyrrhine. *Journal of Human Evolution* 17: 155-192. https://doi.org/10.1016/0047-2484(88)90053-X

Frost S.R. & Delson E. 2002. – Fossil Cercopithecidae from the Hadar Formation and surrounding areas of the Afar Depression, Ethiopia. *Journal of Human Evolution* 43: 687-748. https://doi.org/10.1006/jhev.2002.0603

Frost S.R. & Alemseged Z. 2007. Middle Pleistocene fossil Cercopithecidae from Asbole, Afar Region, Ethiopia. *Journal of Human Evolution* 53: 227-259. https://doi.org/10.1016/j.jhevol.2007.02.003

Frost S.R., Haile-Selassie Y. & Hlukso L.J. 2007. Cercopithecidae, *in* Haile-Selassie Y. & WoldeGabriel G. (eds), Ardipithecus kadabba*: Late Miocene Evidence from the Middle Awash, Ethiopia*. University of California Press, Berkeley, pp 135-158.

Frost S.R., Jablonski N.G. & Haile-Selassie Y. 2014. – Early Pliocene Cercopithecidae from Woranso-Mille (Central Afar, Ethiopia) and the origins of the *Theropithecus oswaldi* lineage. *Journal of Human Evolution* 76: 39-53. https://doi.org/10.1016/j.jhevol.2014.05.003

Frost S.R. 2014. – Fossil Cercopithecidae of the Konso Formation, *in* Suwa G., Beyene Y. & Asfaw B. (eds), Konso-Gardula Research Project. Vol 1. – Paleontological Collections: Background and Fossil Aves, Cercopithecidae and Suidae. The University Museum, The University of Tokyo, 47, pp. 41-72.

Gebo D.L. 1989. – Postcranial Adaptation and Evolution in Lorisidae. *Primates* 30: 347-367. https://doi.org/10.1007/BF02381259

Gebo D.L. & Sargis E.J. 1994. – Terrestrial adaptations in the postcranial skeletons of guenons. *American Journal of Physical Anthropology* 93: 341-371. https://doi.org/10.1002/ajpa.1330930306

Gebo D.L. & Chapman C.A. 1995. – Positional behavior in five sympatric Old World monkeys. *American Journal of Physical Anthropology* 97: 49-77. https://doi.org/10.1002/ajpa.1330970105

Gebo D. & Chapman C.A. 2000. – Locomotor behavior in Ugandan monkeys, in Whitehead P.F. & Jolly C.J. (eds), Old World Monkeys. Cambridge University press, pp. 480-495.

Gilbert C.C., Goble E.D. & Hill A. 2010. – Miocene Cercopithecoidea from the Tugen Hills, Kenya. *Journal of Human Evolution* 59: 465-483. https://doi.org/10.1016/j.jhevol.2010.05.005

Harris J.M., Brown F.H. & Leakey M.G. 1988. – Stratigraphy and paleontology of Pliocene and Pleistocene localities west of Lake Turkana, Kenya. *Contributions in science* 399: 1-125.

Harrison T. 1989. – New postcranial remains of *Victoriapithecus* from the middle Miocene of Kenya. *Journal of Human Evolution* 18: 3-54. https://doi.org/10.1016/0047-2484(89)90022-5

Harrison T. 2011. – Cercopithecids (Cercopithecidae, Primates), *in* Harrison T. (ed.), Paleontology and Geology of Laetoli: Human Evolution in Context. Fossil Hominins and the Associated Fauna. Springer, Dordrecht, pp. 83-140.

Hidaka E., Aoki M., Izumi T., Suzuki D. & Fujimiya M. 2014. – Ligament strain on the iliofemoral, pubofemoral, and ischiofemoral ligaments in cadaver specimens: Biomechanical measurement and anatomical observation. *Clinical Anatomy* 27: 1068-1075. https://doi.org/10.1002/ca.22425

Hlusko L.J. 2007. – A new large Pliocene colobine species (Mammalia: Primates) from Asa Issie, Ethiopia. *Geobios* 39: 57-69. https://doi.org/10.1016/j.geobios.2004.09.001

Hlusko L.J. 2007. A new Late Miocene species of *Paracolobus* and other Cercopithecoidea

(Mammalia: Primates) fossils from Lemudong'o, Kenya. *Kirtlandia, The Cleveland Museum of Natural History* 56: 72-85.

Howell F.C. & Coppens Y. 1974. – Inventory of remains of Hominidae from Pliocene/Pleistocene formations of the lower Omo basin, Ethiopia (1967-1972). *American Journal of Physical Anthropology* 40: 1-17. https://doi.org/10.1002/ajpa.1330400102

Ibáñez-Gimeno P., Galtés I., Manyosa J., Malgosa A. & Jordana X. 2014. – Analysis of the forearm rotational efficiency in extant hominoids: New insights into the functional implications of upper limb skeletal structure. *Journal of Human Evolution* 76: 165-177. https://doi.org/10.1016/j.jhevol.2014.08.004

Isler K. & Grüter C.C. 2007. – Arboreal locomotion in wild black-and-white snub-nosed monkeys (*Rhinopithecus bieti*). *Folia Primatologica* 77: 195-211.

Jablonski N.J. & Leakey M.G. 2008a. Systematic paleontology of the large colobines, *in* Jablonski N.J. & Leakey M.G. (eds), *Koobi Fora Research Project. The Fossil Monkeys, vol. 7.* California Academy of Sciences, San Francisco, pp. 31-102.

Jablonski N.J. & Leakey M.G. 2008b. Systematic paleontology of the small colobines, *in* Jablonski N.J. & Leakey M.G. (eds), *Koobi Fora Research Project. The Fossil Monkeys, vol. 7*. California Academy of Sciences, San Francisco, pp.12-30.

Jenkins F.A. & Camazine S. 1977. Hip structure and locomotion in ambulatory and cursorial carnivores. *Journal of Zoology* 181: 351-370. https://doi.org/10.1111/j.1469-7998.1977.tb03249.x

Kawabe M. & Mano T. 1972. – Ecology and behavior of the wild proboscis monkey, *Nasalis larvatus* (Wurmb), in Sabah, Malaysia. *Primates* 13: 213-227. https://doi.org/10.1007/BF01840882

Kidane T., Brown F.H. & Kidney C. 2014. – Magnetostratigraphy of the Fossil-Rich Shungura Formation, southwest Ethiopia. *Journal of African Earth Sciences* 97**:** 207-223. https://doi.org/10.1016/j.jafrearsci.2014.05.005

Kingdon J. & Groves C.P. 2013. – Subfamily COLOBINAE – Colobines: Colobus Monkeys, *in* Kingdon J., Butynski T.M. & Kalina J. (eds), *Primates, Mammals of Africa Volume II.* Bloomsbury Publishing, London, pp. 165-167.

Krentz H.B. 1993. – Postcranial anatomy of extant and extinct species of *Theropithecus*, *in* Jablonski N.G. (ed.), Theropithecus*: The Rise and Fall of a Primate Genus*. Cambridge University Press, Cambridge, pp. 383-424.

Lague M.R., Chirchir H., Green D.J., Mbua E., Harris J.W.K., Braun D.R., Griffin N.L. & Richmond B.G. 2019. – Cross-sectional properties of the humeral diaphysis of Paranthropus boisei: Implications for upper limb function. *Journal of Human Evolution* 126:

51-70. https://doi.org/10.1016/j.jhevol.2018.05.002

Laird M.F., Kozma E.E., Kwekason A. & Harrison, T. 2018. – A new fossil cercopithecid tibia from Laetoli and its implications for positional behavior and paleoecology. *Journal of Human Evolution* 118: 27-42. https://doi.org/10.1016/j.jhevol.2018.02.005

Langdon J.H. 1987. – Functional Morphology of the Miocene Hominoid Foot. *Contributions to Primatology* 22: 1-226.

Latimer B., Ohman J.C. & Lovejoy O.C. 1987. Talocrural Joint in African Hominoids: Implications for *Australopithecus afarensis*. *American Journal of Physical Anthropology* 74: 155-175. https://doi.org/10.1002/ajpa.1330740204

Leakey M.G. 1987. Colobinae (Mammalia, Primates) from the Omo Valley, Ethiopia, *in* Coppens Y. & Howell F.C. (eds), *Les faunes plio-pleïstocènes de la vallée de l'Omo (Ethiopie)*. Tome 3. Cahiers de Paléontologie, pp. 149-169.

Leakey M.G., Teaford M.F. & Ward C.V. 2003. – Cercopithecidae from Lothagam, in Leakey M.G. & Harris J.M. (eds), *Lothagam, The Dawn of Humanity in Eastern Africa*. Columbia University Press, pp. 201-248.

MaClatchy L., Gebo D., Kityo R. & Pilbeam D. 2000. – Postcranial functional morphology of Morotopithecus bishopi, with implications for the evolution of modern ape locomotion. *Journal of Human Evolution* 39: 159-183. https://doi.org/10.1006/jhev.2000.0407

MacPhee R.D.E. & Meldrum J. 2007. – Postcranial Remains of the Extinct Monkeys of the Greater Antilles, with Evidence for Semiterrestriality in *Paralouatta*. *American Museum Novitates* 3516: 1-65.

Madar S.I., Rose M.D., Kelley J., MacLatchy L. & Pilbeam D. 2002. – New Sivapithecus postcranial specimens from the Siwaliks of Pakistan. *Journal of Human Evolution* 42: 705-752. https://doi.org/10.1006/jhev.2002.0554

Martin F., Plastiras C.-A., Merceron G., Souron A. & Boisserie, J.-R. 2018. – Dietary niches of terrestrial cercopithecines from the Plio-Pleistocene Shungura Formation, Ethiopia: evidence from Dental Microwear Texture Analysis. *Scientific Reports* 8: 14052. https://doi.org/10.1038/s41598-018-32092-z

Maslin M.A. & Trauth M.H. 2009. – Plio-Pleistocene East African Pulsed Climate Variability and Its Influence on Early Human Evolution, *in* Grine F.E., Fleagle J.G. & Leakey, R.E. (eds), *The First Humans – Origin and Early Evolution of the Genus* Homo. Springer Netherlands, Dordrecht, pp. 151-158.

Matsuda I., Chapman C.A., Shi P., Chua Y., Mun S., John C. & Clauss M. Primate resting postures: constraints by foregut fermentation? *Physiological and Biochemical Zoology* 90: 383-391. https://doi.org/10.1086/691360

McDougall I. & Brown F.H. 2008. – Geochronology of the pre-KBS Tuff sequence, Omo Group, Turkana Basin. *Journal of the Geological Society* 165: 549-562.

McDougall I., Brown F.H., Vasconcelos P.M., Cohen B.E., Thiede D.S. & Buchanan M.J. 2012. – New single crystal ^{40} Ar/ ^{39} Ar ages improve time scale for deposition of the Omo Group, Omo–Turkana Basin, East Africa. *Journal of the Geological Society* 169: 213-227. https://doi.org/10.1144/0016-76492010-188

McQuinn, A. 2017. – Bengal Sacred (Hanuman) Langur, *in* Rowe N. & Myers M. (eds), *All the World's Primates*. Pogonias Press, Charlestown, Rhode Island, pp. 578-579.

Nakatsukasa M. 1994. – Morphology of the humerus and femur in African mangabeys and guenons: functional adaptation and implications for the evolution of positional behavior. *African Study Monographs* 21: 1-61.

Nakatsukasa M., Mbua E., Sawada Y., Sakai T., Nakaya H., Yano W. & Kunimatsu Y. 2010. – Earliest colobine skeletons from Nakali, Kenya. *American Journal of Physical Anthropology* 143: 365-382. https://doi.org/10.1002/ajpa.21327

Pallas L., Daver G., Mackaye H.T., Likius A., Vignaud P. & Guy F. 2019. – A window into the early evolutionary history of Cercopithecidae: Late Miocene evidence from Chad, Central Africa. *Journal of Human Evolution* 132: 61-79. https://doi.org/10.1016/j.jhevol.2019.03.013

Patel B.A. 2005. – The hominoid proximal radius: re-interpreting locomotor behaviors in early hominins. *Journal of Human Evolution* 48: 415-432. https://doi.org/10.1016/j.jhevol.2005.01.001

Patel B.A., Ruff C.B., Simons E.L.R. & Organ J.M. 2013. – Humeral Cross-Sectional Shape in Suspensory Primates and Sloths: Long Bone Cross-Sectional Shape. *The Anatomical Record* 296: 545-557. https://doi.org/10.1002/ar.22669

Polk J.D. 2002. – Adaptive and phylogenetic influences on musculoskeletal design in cercopithecine primates. *Journal of Experimental Biology* 205: 3399-3412. https://doi.org/10.1242/jeb.205.21.3399

R Core Team. 2018. *R: A language and environment for statistical computing*. R Foundation for Statistical Computing, Vienna, Austria. URL https://www.R-project.org/.

Rahman M., Jaman F., Khatun T., Alam M., Kayum R. & Uddin M. 2015. – Substrate utilization by Bengal Sacred Langur *Semnopithecus entellus* (Dufresne, 1797) in Jessore, Bangladesh: effect of resource type on feeding in urban and rural groups. *International Journal of Pure and Applied Zoology* 3: 162-172.

Reed K.E. & Russak S.M. 2009. – Tracking Ecological Change in Relation to the Emergence of *Homo* Near the Plio-Pleistocene Boundary, *in* Grine F.E., Fleagle J.G. & Leakey R.E.

(eds), The First Humans – Origin and Early Evolution of the Genus Homo. Springer Netherlands, Dordrecht, pp. 159-171.

Richmond B.G., Fleagle J.G., Kappelman J., & Swisher III, C. C. 1998. First hominoid from the Miocene of Ethiopia and the evolution of the catarrhine elbow. *American Journal of Physical Anthropology* 105 : 257-277. https://doi.org/10.1002/(SICI)1096-8644(199803)105:3<257::AID-AJPA1>3.0.CO;2-P

Ripley S. 1967. The leaping of langurs: A problem in the study of locomotor adaptation. *American Journal of Physical Anthropology* 26: 149-170. https://doi.org/10.1002/ajpa.1330260206

Rose M.D. 1979. – Positional behavior of natural populations: some quantitative results of a field study of *Colobus guereza* and *Cercopithecus aethiops*, *in* Morbeck M.E., Preuschoft H. & Gomberg N. (eds), *Environment, Behavior and Morphology: Dynamic Interactions in Primates*. Gustav Fisher, New York, pp. 95-117.

Rose M.D. 1983. – Miocene Hominoid Postcranial Morphology: Monkey-like, Ape-like, Neither, or Both? *in* Ciochon R.L. & Corruccini R.S. (eds), *New Interpretations of Ape and Human Ancestry*. Springer US, Boston, MA, pp. 405-417.

Rose M.D. 1988. – Another look at the anthropoid elbow. *Journal of Human Evolution* 17: 193-224. https://doi.org/10.1016/0047-2484(88)90054-1

Rose M.D. 1989. – New postcranial specimens of catarrhines from the Middle Miocene Chinji Formation, Pakistan: descriptions and a discussion of proximal humeral functional morphology in anthropoids. *Journal of Human Evolution* 18: 131-162. https://doi.org/10.1016/0047-2484(89)90067-5

Rose M.D., Leakey M.G., Leakey R.E.F. & Walker A.C. 1992. – Postcranial specimens of *Simiolus enjiessi* and other primitive catarrhines from the early Miocene of Lake Turkana, Kenya. *Journal of Human Evolution* 22: 171-237. https://doi.org/10.1016/S0047-2484(05)80006-5

Rose M.D., Nakano Y. & Ishida H. 1997. – *Kenyapithecus* postcranial specimens from Nachola, Kenya. *African Study Monographs* 24: 3-57. https://doi.org/10.14989/68384

Rowan J., Martini P., Likius A., Merceron G. & Boisserie J.-R. 2018. – New Pliocene remains of *Camelus grattardi* (Mammalia, Camelidae) from the Shungura Formation, Lower Omo Valley, Ethiopia, and the evolution of African camels. *Historical Biology* 31: 1-12. https://doi.org/10.1080/08912963.2017.1423485

Ruff C.B. 2003. – Long bone articular and diaphyseal structure in Old World monkeys and apes. II: Estimation of body mass. *American Journal of Physical Anthropology* 120: 16-37. https://doi.org/10.1002/ajpa.10118

Schmitt D. 1998. – Forelimb mechanics during arboreal and terrestrial quadrupedalism in Old World Monkeys, *in* Strasser E., Fleagle J.G., Rosenberger A.L. & McHenry H.M. (eds), *Primate Locomotion*. Springer US, Boston, pp. 175-200.

Schmitt D. 2003. – Mediolateral reaction forces and forelimb anatomy in quadrupedal primates: implications for interpreting locomotor behavior in fossil primates. *Journal of Human Evolution* 44: 47-58. https://doi.org/10.1016/S0047-2484(02)00165-3

Schultz M. 1986. The forelimb of the Colobinae, *in* Swindler R. (ed), *Comparative Primate Biology Vol. 1 Systematics, Evolution, and Anatomy.* Alan R. Liss., New Yorl, pp. 559-569.

Simpson S.W., Levin N.E., Quade J., Rogers M.J. & Semaw S. 2019. – *Ardipithecus ramidus* postcrania from the Gona Project area, Afar Regional State, Ethiopia. *Journal of Human Evolution* 129: 1-45. https://doi.org/10.1016/j.jhevol.2018.12.005

Souron A., Balasse M. & Boisserie, J.-R. 2012. – Intra-tooth isotopic profiles of canines from extant Hippopotamus amphibius and late Pliocene hippopotamids (Shungura Formation, Ethiopia): Insights into the seasonality of diet and climate. *Palaeogeography, Palaeoclimatology, Palaeoecology* 342-343: 97-110. https://doi.org/10.1016/j.palaeo.2012.05.007

Strasser E. 1988. – Pedal evidence for the origin and diversification of cercopithecid clades. *Journal of Human Evolution* 17: 225-245. https://doi.org/10.1016/0047-2484(88)90055-3

Su D.F. & Jablonski N.G. 2009. – Locomotor Behavior and Skeletal Morphology of the Odd-Nosed Monkeys. *Folia Primatologica* 80: 189-219.

Swedell L. & Chowdhury S. 2017. – Hamadryas Baboon *in* Rowe N. & Myers M. (eds), All the World's Primates. Pogonias Press, Charlestown, Rhode Island, pp. 436-437.

Takano T., Nakatsukasa M., Kunimatsu Y., Nakano Y., Ogihara N. & Ishida H. 2018. – Forelimb long bones of *Nacholapithecus* (KNM-BG 35250) from the middle Miocene in Nachola, northern Kenya. *Anthropological Science* 126: 135-149. https://doi.org/10.1537/ase.181022

Tallman M. & Cooke S.B. 2017. – New endemic platyrrhine humerus from Haiti and the evolution of the Greater Antillean platyrrhines. *Journal of Human Evolution* 91: 144-167. https://doi.org/10.1016/j.jhevol.2015.10.010

Tardieu C. 1983. – L'articulation du genou des primates catarhiniens et hominides fossiles. Implications phylogenetique et taxinomique. *Bulletin et Mémoires de la Société d'Anthroplogie de Paris* 10: 355-372.

Ting N. 2001. – *A functional analysis of the hip and thigh of* Paracolobus chemeroni *and* Paracolobus mutiwa. M.A. Dissertation, University of Missouri, Missouri, 79 p.

Ting N. 2008. – Mitochondrial relationships and divergence dates of the African colobines:

evidence of Miocene origins for the living colobus monkeys. *Journal of Human Evolution* 55: 312-325. https://doi.org/10.1016/j.jhevol.2008.02.011

Tosi A.J. 2008. – Forest monkeys and Pleistocene refugia: a phylogeographic window onto the disjunct distribution of the *Chlorocebus lhoesti* species group. *Zoological Journal of the Linnean Society* 154: 408-418. https://doi.org/10.1111/j.1096-3642.2008.00419.x

Ward C.V. 1993. – Partial Skeleton of *Proconsul nyanzae* from Mfangano Island, Kenya. *American Journal of Physical Anthropology* 90: 77-111. https://doi.org/10.1002/ajpa.1330900106

White J.L. & Gebo, D.L. 2004. – Unique proximal tibial morphology in strepsirrhine primates. *American Journal of Primatology* 64: 293-308. https://doi.org/10.1002/ajp.20079

White T.D., Ambrose S.H., Suwa G., Su D.F., DeGusta D., Bernor R.L., Boisserie J.-R., Brunet M., Delson E., Frost S., Garcia N., Giaourtsakis I.X., Haile-Selassie Y., Howell F.C., Lehmann T., Likius A., Pehlevan,C., Saegusa H., Semprebon G., Teaford M. & Vrba E. 2009. – Macrovertebrate Paleontology and the Pliocene Habitat of *Ardipithecus ramidus*. *Science* 326: 67-67, 87-93. https://doi.org/10.1126/science.1175822

Yang Y., Youlatos D., Behie A. M., Belbeisi R. A., Huang Z., Tian Y., Wang B., Zhou L., Xiao W. 2021. – Positional behavior and canopy use of black snub-nosed monkeys *Rhinopithecus strykeri* in the Gaoligong Mountains, Yunnan, China. *Current Zoology* 68: 401-409. https://doi.org/10.1093/cz/zoab071

Yapuncich G.S., Feng H.J., Dunn R.H., Seiffert E.R. & Boyer D.M. 2019. – Vertical support use and primate origins. *Scientific Reports* 9: 1-10. https://doi.org/10.1038/s41598-019-48651-x

Youlatos D. & Koufos G.D. 2010. – Locomotor evolution of *Mesopithecus* (Primates: Colobinae) from Greece: evidence from selected astragalar characters. *Primates* 51: 23–35. https://doi.org/10.1007/s10329-009-0161-2

Youlatos D., Couette S. & Koufos G.D. 2012. – A functional multivariate analysis of Mesopithecus (Primates: Colobinae) humeri from the Turolian of Greece. *Journal of Human Evolution* 63: 219-230. https://doi.org/10.1016/j.jhevol.2012.05.007

Yeager C.P., Booratana R. & Groves C.P. 2017. – Proboscis Monkey in Rowe N. & Myers M. (eds), *All the World's Primates*. Pogonias Press, Charlestown, Rhode Island, pp. 630-631.